SPACE DIVISION

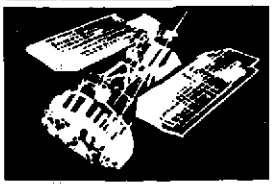
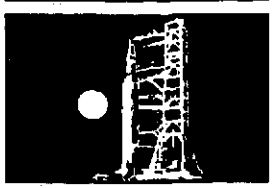
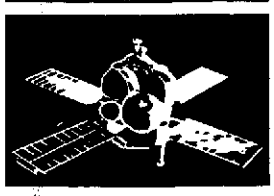

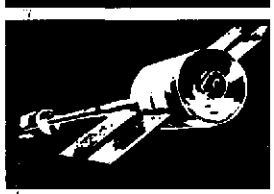

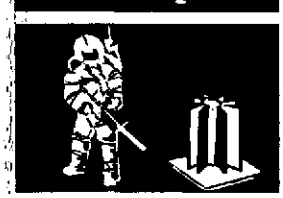
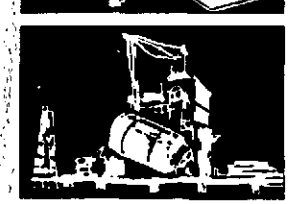

CRYSTAL GROWTH IN FUSED SOLVENT SYSTEMS

BY D.R. ULRICH, B.A. NOVAL, K.E. SPEAR,
W.B. WHITE AND E.C. HENRY

CONTRACT NAS 8-28114

CONTROL NUMBER DCN-1-1-50-13670-(IF)

PREPARED FOR THE

NATIONAL AERONAUTICS AND SPACE ADMINISTRATION
MARSHALL SPACE FLIGHT CENTER
HUNTSVILLE, ALABAMA 35812

GENERAL ELECTRIC

CRYSTAL GROWTH IN FUSED SOLVENT SYSTEMS

D. R. Ulrich, B. A. Noval, K. E. Spear,
W. B. White and E. C. Henry

FINAL REPORT

November 1974

Contract NAS 8-28114

Control Number DCN-1-1-50-13670-(1F)

Prepared for the

National Aeronautics and Space Administration
Marshall Space Flight Center
Huntsville, Alabama 35812

Prepared by

General Electric Company
Space Division
Space Sciences Laboratory
P. O. Box 8555
Philadelphia, Pennsylvania 19101

This report was prepared by the Space Sciences Laboratory of the General Electric Company under Contract NAS 8-28114, "Study of Crystal Growth in Fused Solvent Systems," for the George C. Marshall Space Flight Center of the National Aeronautics and Space Administration.

TABLE OF CONTENTS

LIST OF FIGURES

LIST OF TABLES

FOREWORD

This report was prepared by a team of General Electric Space Sciences Laboratory and Pennsylvania State University Materials Research Laboratory staff personnel. The research was carried out under the supervision of Mr. R. Ruff, Contract Monitor, of the Space Sciences Laboratory, George C. Marshall Space Flight Center of the National Aeronautics and Space Administration and Dr. Donald R. Ulrich, Principal Investigator, of the General Electric Company Space Sciences Laboratory, Valley Forge Space Technology Center.

The authors are respectively:

Dr. Donald R. Ulrich, Group Leader, Electronic Materials, General Electric Company, Space Sciences Laboratory

Dr. Barry A. Noval, Material Scientist, General Electric Company, Space Sciences Laboratory

Dr. William B. White, Professor of Geochemistry, Materials Research Laboratory, Pennsylvania State University

Dr. Karl E. Spear, Assistant Professor of Solid State Science, Materials Research Laboratory, Pennsylvania State University

Dr. E. C. Henry, Corporate Consultant, General Electric Company

Scientific collaborators at the General Electric Space Sciences Laboratory were Dr. E. Feingold, Mr. T. A. Harris, Mr. M. Birenbaum, Mr. R. W. Gunnett, Mrs. B. Faust and Dr. G. Bethke.

Acknowledgement is extended to Dr. S. Tehon of the General Electric Electronics Laboratory, Syracuse, New York, for his discussions and collaboration relative to surface wave acoustic materials and devices.

At Pennsylvania State University, acknowledgement is extended to R. L. Mohler, for his role in conducting the experiments, Dr. J. F. Balascio, who provided two TGS crystals, Professor L. E. Cross for the use of his dielectric measurement apparatus, and Mrs. Carol King, who assisted with the crystal growth.

SUMMARY

Space Processing of electronic crystals appears desirable for producing crystals important to the development of technically interesting advanced devices. Leading materials in this category are the electronic oxide crystals for surface wave acoustic and electro-optic use such as bismuth germanate, lead germanate, and lithium niobate.

The scope of this study over the past two years has been to develop the technical understanding of the solution growth of oxide crystals in space, to identify compositions which can benefit by production with this technique in space, to investigate the relative effects of convection and diffusion on solution growth, and to define the requirements for a Shuttle-Space Lab. solution growth of crystals experiment. The Skylab experiments, which centered on the growth of well-understood semiconductor crystals, supported this view and showed that the low-g environment of space resulted in crystals of enhanced size and perfection.

Higher perfection is required in the oxide crystals than can be obtained from the currently used Czochralski technique of vertically pulling from seeded, low viscosity pure melts, or from seeded, low viscosity fused salts. Pulling in space may still not overcome the setting up of the thermal and mechanical stresses giving rise to compositional non-uniformity and optical inhomogeneities.

As an alternative technique, the slow growth of these crystals from a seeded glass solvent of high viscosity is being investigated on the premise that the high viscosity minimizes the convective and temperature variations and therefore the rythmic feeding of the solute to the seed. It is expected that growth proceeds by slow diffusion and that one might expect further improvements in space. In the absence of planned space experiments of long duration for the next few years, the high viscosity of glass solvents permits us to approximate seeded growth under space conditions.

In view of a current difference of opinion as to where ceramic oxide bulk single crystals and thin film structures fit relative to the production of surface acoustic wave, electrooptical and other electronic devices, a comparison was made of both materials. For the low-volume,

specialty applications which call for the unique properties inherent to the oxidic compositions, the conditions for the effective coupling of the surface waves with the unique (piezoelectric) crystallographic axis can only be met with bulk crystals. Film forms result in low electro-mechanical coupling coefficient and high acoustic insertion loss since the conditions are not satisfied as of today. Much improvement is required in the optical quality and crystallinity of thin films for optical waveguides before they will surpass the reactive-type bulk crystal modulator.

The two compounds selected for study were bismuth germanate, $Bi_{12}Ge0_{20}$ and lead germanate, $Pb_5Ge_30_{11}$. There are good technical and practical resons for doing so. The compounds have high value and gravity-sensitive properties, but it is not easy to grow them with fused salt techniques. High quality crystals of $Pb_5Ge_30_{11}$ have not been grown with Czochralski techniques either.

There may be a more immediate and higher chance of success of growing large crystals with other compositions, but the stakes are lower and the physical and solid state properties are not as exciting or as sensitive for evaluation relative to space grown crystals.

The significant achievement during this reporting period has been the successful nucleation of bismuth germanate from the fused solvent on a high quality seed and the growth of respectable regions of single crystal of the same orientation as the seed. The single crystal regions grown from the seeded high viscosity solvent showed no large scale nonuniformities characteristically observed with seeded melt or fused salt growth. Surface roughness was minimal except near glass occlusions which arose during growth under non-ideal conditions. Defining the characteristics of the growth has enabled us to devise a program for the elimination of the defects. Comparison of $Bi_{12}GeO_{20}$ crystals grown from the melt with those grown from the glass solvent showed striations in the former, but not the latter, showing that the higher viscosity dampens the thermal vibrations. Considerable effort was devoted to solvent development, to the determination of the relation between spontaneous nucleation and solution composition, seeded growth experiments and crystal perfection characterization.

Priority has been placed on the growth of $Bi_{12}GeO_{20}$ for surface wave acoustic substrates. However, the growth of $Pb_5Ge_3O_{11}$ from seeded fused solvents, which was identified last year as a promising electrooptic crystal for future devices, has also been pursued. While not as thoroughly researched as $Bi_{12}GeO_{20}$, solvents have been

developed which show $Pb_5Ge_3O_{11}$ as the primary phase of crystallization during spontaneous nucleation or seeded growth. To date the crystallization has been random in the viscous solvent rather than by nucleation on the seed. Work has centered on the adjustment of viscosity and the relationship for the spontaneous appearance of crystals as controlled by the addition of Al_2O_3 to the lead borate solvent. Use of $Pb_5Ge_3O_{11}$-SiO_2, with emphasis on the isomorphous compound $Pb_5Ge_2SiO_{11}$, has been examined as an alternative solvent since SiO_2 increases viscosity while decreasing the rate of viscosity change with temperature.

The sub-contract work at Pennsylvania State University has focused down to the characterization of volume defects as a function of growth by laser light scattering ultramicroscopy and dielectric loss in triglycine sulfate (TGS). Volume defects (500 Å to 5 μcm) were observed which are not generally visible to optical examination. Increasing perfection appears to be a matter of decreasing size of volume defects rather than a decrease in their number. There is a qualitative correlation between the dielectric loss and the size and number of volume imperfections.

As a final section of this report, the important requirements for solution crystal growth of systems identified in the past two years have been collected. The requirements have been analyzed to determine which are practical and compatible on a space flight experiment. The section has detailed the benefits and the relative difficulty of meeting the individual requirements.

I. INTRODUCTION

The electronic, acoustic and optical systems which will be coming into use in the early 1980's will be designed around advanced and emerging technologies which today are in the conceptual or research stage. They will utilize materials having unique optical, acoustic, and electrical properties in the performance of their functions. Semiconductor crystals are playing the predominant materials role today to meet the requirements of present and near-future solid state systems. Exemplified by silicon, they have become a commodity product.

While semiconductor crystals are expected to meet the materials needs of new products through either the preparation of new compounds or the improved processing of present compositions, they cannot meet all of the demands simply because inherently they do not have the requisite properties to do so.

It is the ceramic oxide crystals which will fulfill many of these demands because, by their nature, they have acoustic, optical and electrical properties which are unique and different. Oxidic crystals have been around for a long time. They have been researched and produced for many years, but, with the exception of quartz, none have received any concentrated effort. However, the long range future needs of advanced technology have brought them to the forefront of materials science along with semiconductors. They can be grown in useable sizes and acceptable qualities. However, they often fall short of their

theoretical or engineering figures of merit because imperfections have been introduced or size restrictions imposed during the growth process.

The primary sources of the imperfections are due to gravity-induced sedimentation and convection in the growth solutions. Growing of these crystals in the low-g environment of space may markedly improve them to the extent that they will be worth more to the users than it costs to provide them. The scope of this study over the past two years has been to develop the technical understanding of the solution growth of oxide crystals in space, to identify compositions which can benefit by production with this technique in space, to investigate the relative effects of convection and diffusion on solution growth, and to define the requirements for a Shuttle-Space laboratory solution growth of crystals experiment.

The Skylab crystal growth experiments have clearly demonstrated that pronounced improvement in single crystal size and perfection can be attained from processing in the microgravity of space. The experiments centered on the growth of semiconductors whose imperfections as a result of the growth process are well characterized.

Leading oxidic crystals are those for electro-optic and surface wave acoustic use. Examples are bismuth germanate, lithium niobate, and lead germanate. While it is recognized that completely new oxidic or inorganic compositions may be identified in the future, current research for the preparation of Shuttle-

Spacelab experiments is centered on the aforementioned crystals and a solvent for growing them.

Currently, there is a difference of opinion as to where ceramic oxide bulk single crystals and thin film structures fit relative to the production of surface wave acoustic, electrooptic, and other electronic devices. High volume production of electronic devices makes use of thin film structures because of the ease of producing circuits at low cost. However, for low volume, specialty applications, i.e., surface wave acoustic devices, the unique intrinsic properties of compositions such as lithium niobate (high electromechanical coupling coefficient) and bismuth germanate (moderate coupling coefficient, low acoustic velocity) call for the use of bulk single crystals rather than piezoelectric polycrystalline films.

Bulk crystals which have high intrinsic coupling coefficients generally have high acoustic insertion loss in film form since the piezoelectric or unique crystallographic axis is not parallel to the direction of surface wave propagation and the conduction does not exist for effective coupling. In addition, transducer loss is high in thin film structures which introduces lower electromechanical coupling coefficients. This means that films cannot operate with any reasonable bandwidth in the zero insertion loss region, while bulk single crystals can have zero insertion loss from narrow to moderately wide bandwidths.

These crystals generally are grown by the Czochralski technique of vertically pulling from the seeded pure crystal melt of low viscosity. Higher perfection is required than can be obtained by pulling from the pure, low viscosity melt because of the stresses introduced during the pulling operation. In electrooptic crystals these stresses result in minor variations in the index of refraction and the birefringence which reduce electrooptic and nonlinear optic activity. Crystals for surface wave acoustic devices require the same high degree of perfection as electro-optic crystals. Czochralski pulling in space from a low viscosity melt may still not overcome the setting up of the thermal and mechanical stresses.

The growth on earth from seeded low viscosity fused salts rather than from the stoichiometric melt is characterized by the occurrence of defects which are a consequence of the presence of the earth's gravitational field. That is, gravity driven convection results in thermal fluctuations during growth and are responsible for the familiar appearance of growth striations, representative of compositional and optical non-uniformity.

Our approach has been to grow crystals by the seeding of a highly viscous solution, namely a glass or fused solvent, on the premise that the high viscosity would minimize the convective and temperature variations. This reduces the rythmic feeding of the solute to the seed, and permits growth to proceed by the slow diffusion of the solutions to the seed. It is expected that one might expect further improvements in space using this technique.

In the absence of planned space experiments of long duration for the next few years, we should conduct terrestrial experiments using techniques which approach space conditions. The high viscosity of glass solvents and the corresponding decrease in convective flow permits us to approximate seeded growth under space conditions. Contrary to this, the low viscosity of fused salts are much further away from duplicating or approaching space conditions.

The two compositions selected for study on the basis of technical importance, gravity-sensitive properties, high value, and apparent compatibility with the seeded fused solvent technique are bismuth germanate, $Bi_{12}GeO_{20}$ and lead germanate, $Pb_5Ge_3O_{11}$. Both compositions have melting points under 1000°C and are compatible with present space processing equipment so that they can quickly be converted from the earth to space mode if the opportunity arises.

The growth of these crystals presents quite a challenge. There are good technical and practical reasons for doing so, but on top of this, it is difficult to grow either composition with conventional fused salt techniques; the Czochralski growth of $Pb_5Ge_3O_{11}$ has resulted in multi-crystalline growth. There may be a more immediate and higher chance of success of growing larger crystals with other compositions, but the stakes are lower and the physical and solid state properties are not as exciting, or as sensitive for

evaluation relative to space grown crystals. It is intended that the sensitive electrooptic and acoustic properties of $Pb_5Ge_3O_{11}$ and $Bi_{12}GeO_{20}$ (as well as the ferroelectric and piezoelectric properties, respectively, in correlation with the structural properties) be used to establish standards against which space grown crystals can be compared.

The significant achievement during this reporting period has been the successful nucleation of $Bi_{12}GeO_{20}$ on a high quality seed and the growth of respectable regions of single crystal of the same orientation as the seed. The regions have been characterized by Laue x-ray techniques, microscopic examination, laser optical rotation measurements, microprobe analyses, emission spectroscopy, and other techniques to verify single crystal growth of the same orientation and of similar stoichiometry.

Examinations were conducted to compare the single crystal regions grown. The single crystal regions grown from the seeded high viscosity solvent showed no large scale, gross nonuniformities characteristically observed with seeded melt or fused salt growth. Surface roughness was minimal except near glass occlusions, which arose during growth under non-ideal conditions. Defining the characteristics of the growth has enabled us to devise a program for the elimination of the defects. Comparison of $Bi_{12}GeO_{20}$ crystals grown from the melt with those grown from seeded glass solvent showed that a number of growth striations or bands are observed in the former but are absent in the latter. This indicates that the viscous glass solvent dampen the thermal vibrations which give rise to periodic compositional changes.

Now that the feasibility of the seeded growth of $Bi_{12}GeO_{20}$ from a highly viscous glass solvent has been demonstrated, a two-pronged effort should follow. First, realizing that considerable resources were spent this year in solvent development, determination of the relation between spontaneous nucleation and solution composition, seeded growth experiments and crystal perfection characterization, work should now be done to optimize in depth all the variables which have been defined to design this succesful experiment. These include refinement of the solvent system, detailed determination and completion of the study of solubility characteristics, and determination of the precise temperature and thermal control requirements which will result in the growth of crystals of optimized size and perfection. For example, the results of programmed control experiments with cooling rates down to $0.2^{o}C$ per hour as opposed to $2^{o}C$ per hour should be examined. A furnace should now be designed and constructed which will minimize any convective currents which may arise in the glass due to a horizontal temperature gradient and may not be completely dampened by the viscosity. While the successful solution consisted of 80 w/o of $Bi_{12}GeO_{20}$ solute dissolved in 20 w/o solvent ($.75Bi_2O_3 \cdot 0.5Al_2O_3 \cdot 1.0B_2O_3$), the ratio of $Bi_2O_3 \cdot Al_2O_3 \cdot B_2O_3$ should be "fine tuned" so as to completely inhibit undesirable spontaneous nucleation while at the same time permitting maximum growth on the seed.

Second, we propose that a Sounding Rocket Flight Experiment be conducted on $Bi_{12}GeO_{20}$-containing solvents. This would provide some data points on the nucleation and crystallization characteristics of the fused solvent system under low-gravity conditions. An experiment has been outlined for this purpose.

During the first year of study lead germanate, $Pb_5Ge_3O_{11}$, had been identified as a new ferroelectric crystal having large electrooptic and nonlinear optic constants as desirable switching properties for future electrooptic device applications. While this composition has not been as thoroughly researched as $Bi_{12}GeO_{20}$, solvents have been developed which show the $Pb_5Ge_3O_{11}$ as the primary phase of crystallization during spontaneous nucleation or seeded growth. To date, the crystallization has been random in the viscous solvent rather than by nucleation on the seed. Immediate work has centered on the adjustment of the Al_2O_3 in the $PbO \cdot 2B_2O_3$ solvent which has increased viscosity, inhibited spontaneous nucleation and stabilized the glass in the seed area, thereby providing conditions suitable for achieving crystal growth nucleated by the seed.

The use of the $Pb_5Ge_3O_{11}$-SiO_2 glass system has been investigated as a possible substitute for the $PbO \cdot Al_2O_3 \cdot B_2O_3$ or $PbO \cdot B_2O_3$ fused solvent systems for the seeded growth of $Pb_5Ge_3O_{11}$. SiO_2 increases the viscosity of the solvent and decreases the rate of change of viscosity with temperature. Since the ferroelectric $Pb_5Ge_2SiO_{11}$ is an isomorphous

compound of $Pb_5Ge_3O_{11}$ it was considered that this may be a suitable solvent for a $Pb_5Ge_3O_{11}$ seed. Along with $Pb_5Ge_{1.8}Si_{1.2}O_{11}$, it was examined by the glass-ceramic technique. The crystallization of the glass was studied by differential thermal analysis and the optical-rotation and dielectric constant-temperature profiles were determined.

Over the past two years research has been sponsored under subcontract to the Materials Research Laboratory, Pennsylvania State University to investigate characterization techniques for comparing differences between earth-grown and space-grown crystals in a quantitative manner.

Triglycine sulfate (TGS) was chosen as a model compound for this work. This is an aqueous solution, low temperature grown crystal. Volume defects as a function of growth were characterized by Raman spectroscopy, laser light scattering ultramicroscopy and dielectric loss. These very small defects (500 Å to 5 μcm) were studied by special techniques since they are not generally visible to optical examination. Increasing perfection appears to be a matter of decreasing size of volume defects rather than a decrease in their number. There is a qualitative correlation between the dielectric loss and the size and number of volume imperfections.

As a third task, an experimental study on ceramic oxide crystals needing solution temperatures higher than 1000°C was initiated. This class of materials needs to be evaluated since the Shuttle-Spacelab capabilities will not be as restricted as those of Skylab. Solvent work was initiated on compositions for the growth of $KTaO_3$-$KNbO_3$ mixed crystals, specifically, $KTa_{0.65}Nb_{0.35}O_3$. In view of the seeded growth knowledge learned from the nucleation and growth of $Bi_{12}GeO_{20}$, the reexamination of the growth of $LiNbO_3$ from fused solvents at higher temperatures should be considered under this task.

As a final section of this report, the important requirements for solution crystal growth of systems identified in the past two years have been collected. The requirements have been analyzed to determine which are possible and compatible on a space flight experiment. The section has detailed the benefits and the relative difficulty of meeting the individual requirements. The experiment which is practical and comparible for a space flight is the slow cooling of $Bi_{12}GeO_{20}$ from a seeded fused solvent.

II. BISMUTH GERMANATE

Bismuth germanate, $Bi_{12}Ge0_{20}$, is one of the best crystal candidates for surface wave acoustic delay lines and has been identified as a candidate for space processing. With its low velocity of propagation and short wavelength it has a long delay; its velocity is 1.6×10^5 cm/sec as compared to 3.5×10^5 for $LiNb0_3$ [1]. However, growth ridges interfere with the propagation of high-frequency surface waves. Because of mechanical damage and imperfections introduced even during grinding and lapping, polished surfaces do not transmit a signal as undistorted as that expected from an equally, large, flat natural surface. It can be grown at relatively low temperatures (melting point is 935°C) and rates (1/2°C per minute). Bismuth germanate crystals have been grown in the Space Sciences Laboratory by nucleation of a crystal on the bead of a thermocouple inserted in the melt and then slowly pulled vertically. While substantial growth was obtained it was primarily multi-crystalline. The growth perfection of this material is limited by convective effects in the melt. Considerable effort was made to find a suitable glass solvent of relatively high viscosity with which to grow $Bi_{12}Ge0_{20}$ crystals in order to greatly reduce the number of convection related defects.

---

(1) Appl. Phys. Letters, Vol. 9, No. 8, October 15, 1964, pp. 290-91, E. G. Spencer, P. V. Lenzo, A. A. Ballman.

A. Solvent Criteria

Laudise [2] has prepared a list of the requirements of a good solvent for molten salt growth, which would apply to glass solvents almost equally as well. These are:

1. That the solute is the stable solid phase at growth conditions.

2. Solute solubility of 10-50%.

3. An appreciable temperature coefficient of solubility ($\sim$1 wt %/10°) so that slow cooling is practical.

4. Low volatility (covered or welded crucibles will relax this requirement).

5. Unreactivity with platinum (other crucible materials could relax this requirement, but few other materials have been found practical).

6. Low solvent solubility in the grown crystals (a common ion between crystal and solvent is helpful in repressing solvent contamination).

7. Good-quality growth at reasonable rates in the solvent.

It is suggested that increased solute solubilities ranging upwards from 50% be required of glass solvents as a consequence of significantly higher viscosity of the solution. Material transport is appreciably reduced in viscous molten glass; therefore, higher growth temperatures as well as operating near the limit of saturation are both necessary for achieving practical growth rates. Since the degree of solubility also increases with temperature it is most desirable to employ a glass solvent with

(2) Laudise, R.A. in "The Art and Science of Growing Crystals" Wiley, N.Y., 1963, p. 295.

the highest obtainable solute solubility. This also permits an expanded growth range enabling a choice of conditions which may differ depending upon a particular need for growth of high perfection crystals, for growth of a preferred habit and orientation or for large sized crystals grown at rapid rates.

B. Solvent Development

The area of flux growth of single crystals has been dominated primarily by the utilization of molten salts such as PbO, PbF_2, KF and Li_2O-MoO_3. Only isolated examples of glass solvent growth are discovered in the literature and these include YIG from $BaO \cdot 6B_2O_3$ [3] and (Ba, Pb) TiO_3 from $BaO \cdot B_2O_3$-$PbO \cdot B_2O_3$ [4]. For growth of $Bi_{12}GeO_{20}$ single crystals, it was believed that the choice of $Bi_2O_3 \cdot 2B_2O_3$ as a glass solvent could satisfy many of the desired criteria.

1. $Bi_2O_3 \cdot 2B_2O_3$ Glass Solvent

For purposes of evaluation the following compositions were prepared and their nucleation behavior characterized:

FF-90	30 w/o $Bi_{12}GeO_{20}$ - 70% $Bi_2O_3 \cdot 2B_2O_3$
FF-88	40 w/o $Bi_{12}GeO_{20}$ - 60% $Bi_2O_3 \cdot 2B_2O_3$
FF-92	50 w/o $Bi_{12}GeO_{20}$ - 50% $Bi_2O_3 \cdot 2B_2O_3$
FF-78	60 w/o $Bi_{12}GeO_{20}$ - 40% $Bi_2O_3 \cdot 2B_2O_3$
FF-77	80 w/o $Bi_{12}GeO_{20}$ - 20% $Bi_2O_3 \cdot 2B_2O_3$
FF-76	90 w/o $Bi_{12}GeO_{20}$ - 10% $Bi_2O_3 \cdot 2B_2O_3$

(3). Laudise, R.A., in "The Art and Science of Growing Crystals". Wiley, N.Y., 1963, pp. 252.

(4). Perry, F.W., in "Crystal Growth", Ed. by H. S. Peiser, Pergamon, N.Y., 1967, pp. 483-487.

The results are shown in Table 1.

TABLE 1

NUCLEATION BEHAVIOR OF $Bi_{12}GeO_{20}$ FROM Bi_2O_3 GLASS SOLVENT

Composition	Observations
FF-90	No crystals on cooling from 725°C down to 570°C
FF-88	Crystal observed at 595°C on surface-viscosity very high
FF-92	Surface covered with crystals at 608°C
FF-78	Displayed a region of rapid change in viscosity, but also a region in which viscosity was unchanging.
FF-77	Experienced rapid crystallization as melt was cooled.
FF-76	Experienced rapid crystallization as melt was cooled.

Seeded crystal growth experiments were conducted with FF-92 one of the more promising of the compositions studied. The seed crystal employed in all of the $Bi_{12}GeO_{20}$ growth studies was of very high quality, obtained from Crystal Technology Inc., and oriented along the (110) direction. A single crystal bar, 1/4 x 1/4 x 1 inch, as received was cut with a thin bladed diamond saw to produce smaller bars 1/10 x 1/10 x 1/2 inch for use

as seeds. An evaluation of the extent of crystallization that occurred at 610°C, 625°C and 650°C was made. Insertion of a preheated seed into the melt resulted in appreciable growth after only 5 to 10 minutes at the lower temperatures. At 650°C no growth was detected after 1 1/2 hours and rounding of corners and edges indicated the seed to be close to equilibrium with the melt.

A portion of the growth at 610°C was studied by x-ray diffraction and microprobe analysis. The x-ray diffraction data are shown in Table 2.

A comparison of observed "d" spacings and intensities with reported ASTM[5] data for $Bi_{12}GeO_{20}$ indicates that:

1) the major phase to be $Bi_{12}GeO_{20}$ and another unknown phase to be present in large concentration

2) high angle diffraction lines with "d" spacings of 1.212 Å, 1.195 Å and 1.179 Å reported in the ASTM card for $Bi_{12}GeO_{20}$ based on a publication by Bernstein[6] to have intensity values of 100 are found to be much weaker for material grown in glass solvent. It was first believed that the reduced intensity values signified the presence of a $12Bi_2O_3 \cdot B_2O_3$ compound as reported by Levin[7]. This phase is represented as having a similar body centered cubic unit cell and value of lattice constant (for $Bi_{12}GeO_{20}$ a_o = 10.1455 Å [8]; for $12Bi_2O_3$ a_o = 10.124 Å) with however substantially reduced intensities for the high angle diffraction lines. During study of the high quality $Bi_{12}GeO_{20}$

---

(5). ASTM card #20-168.
(6). Bernstein, J.L., J. Crystal Growth 1, 1, 45-46.
(7). Levin, E. M., McDaniel, C.L., J. Amer. Ceram. Soc. 45, 8, pg. 355-360 (1962).
(8). Abrahams, S.C., Jamieson, P.B., Bernstein, J.L., J. Chem. Phys. 47, 10, pg. 4034-4041 (1967).

TABLE 2. X-RAY DIFFRACTION FOR FF-92 (50 w/o $Bi_{12}Ge0_{20}$-50 w/o $Bi_2B_4O_9$)

FF-92		ASTM card #20-168 also reference: Bernstein, J. Crystal Growth, 1, 1, 45-46		Crystal Technology $Bi_{12}Ge0_{20}$ seed crystal		Solid State Product $6Bi_2O_3 + GeO_2$	
d	I/I_o	d	I/I_o	d	I/I_o	d	I/I_o
10.048	12						
9.071	15						
7.872	7						
6.228	15						
6.176	8						
5.567	12						
4.671	12			5.075	4	5.07	5
3.978 (sh)	43					4.14	7
3.922	100						
3.410	17	3.57	30	3.584	27	3.581	33
3.326	27						
3.278	25						
3.235	28	3.20	100	3.210	100	3.203	100
3.106	100+						
2.979	9			3.001	5	3.000	7
2.940	25	2.922	40	2.928	29	2.927	36
2.757	12						
2.698	9	2.702	90	2.707	78	2.707	88
2.678	9						
2.622	11						
2.550	33	2.569	5				
2.522	11			2.534	4	2.345	6
2.499	8						
2.466	9						
2.417	8	2.384	10	2.390	12	2.389	14
2.342	28						
2.313	13	2.265	10	2.267	10	2.266	15
2.143	22	2.158	20	2.162	19	2.162	24
2.030	30	2.066	20	2.070	13	2.070	19
1.976	25						
1.965	25	1.986	40	1.989	18	1.989	23
1.923	40			1.925	2	1.926	6
1.897	13						
1.870	17						
1.852 (sh)	17	1.852	30	1.851	8	1.851	12
1.842	26						
1.813	22					1.791	3
1.755	10	1.738	80	1.739	34	1.740	53
1.658	4	1.690	50	1.691	22	1.691	19
1.635	13	1.644	70	1.646	30	1.646	33
1.621	22						
1.608 (sh)	17						
1.560	37	1.564	10	1.565	5	1.565	7
1.546	17	1.529	10	1.530	4	1.530	5
1.503	13	1.495	70	1.496	20	1.495	22
1.473	7	1.484	10				
1.458	8						
1.455	8						
1.434	10	1.434	60	1.434	12	1.434	12
1.427	5						
1.410	8	1.416	10				
1.405	6						
1.389	7					1.399	3
1.381	8	1.379	60	1.379	4		
1.372	8					1.380	8
1.352	6	1.355	20				
1.313	6	1.332	50			1.355	5
1.270	5	1.288	40	1.288	4		
1.232	8	1.231	30			1.288	7
1.209	15	1.212	100	1.212	13	1.230	4
1.205	17					1.213	17
1.200	7						
1.197	5	1.195	100	1.195	11	1.195	17
1.187	6	1.179	100	1.179	9	1.179	13
1.167	6						

seed crystal used in the crystal growth experiments by means of the x-ray diffractometer it was observed that these same high angle diffraction lines were of comparable low intensity as those in crystallized growth from a glass solvent. This was further confirmed for $Bi_{12}GeO_{20}$ prepared by solid state reaction of Bi_2O_3 with GeO_2 at 760°C for 17 hours. Therefore it is concluded that the information in the ASTM card relating to intensities of high angle lines is in question and that the main phase precipitating out is $Bi_{12}GeO_{20}$. The unidentified strong lines bear some resemblance to other reported bismuth borate phases*. The diffraction data for the $Bi_{12}GeO_{20}$ seed crystal and for the product resulting from solid state reaction of Bi_2O_3 and GeO_2 are presented for comparison with data for the phase crystallizing from glass solvent as well as that given in the ASTM card for $Bi_{12}GeO_{20}$.

2. $Bi_2O_3 \cdot x Al_2O_3 \cdot (2-x) B_2O_3$ Glass Solvent.

Another glass former, Al_2O_3, was partially substituted for B_2O_3 in the glass composition for these reasons:

a) to adjust viscosity of the solution
b) to inhibit spontaneous nucleation
c) to improve crystallization behavior during seeded growth
d) to inhibit formation of a bismuth borate compound.

During prior studies of crystallization of glass-ceramics at the Space Sciences Laboratory it was noted that the addition of a half mole of Al_2O_3 to $PbO \cdot 2B_2O_3$ glass significantly improved the viscosity and surface tension relationship upon which the successful drawing of fibers depends. Because of similarities that exist in conditions required for growth of

* Pertinent to this observation is that microprobe examination of the growth on the seed indicates a deficiency of Ge in the vicinity of the seed, which could be accounted for by the presence of a bismuth borate compound.

crystals and for fiberization it was believed that besides nucleating the proper phase it could provide improved crystallization as well.

The compositions incorporating Al_2O_3 additions which were prepared and evaluated to some degree are:

FF-79 60 w/o $Bi_{12}GeO_{20}$ - 40 w/o $Bi_2O_3 \cdot 0.5Al_2O_3 \cdot 2B_2O_3$

FF-93 60 w/o $Bi_{12}GeO_{20}$ - 40 w/o $Bi_2O_3 \cdot 0.5Al_2O_3 \cdot B_2O_3$

FF-94 40 w/o $Bi_{12}GeO_{20}$ - 60 w/o $Bi_2O_3 \cdot 0.5Al_2O_3 \cdot B_2O_3$

FF-95 50 w/o $Bi_{12}GeO_{20}$ - 50 w/o $Bi_2O_3 \cdot 0.5Al_2O_3 \cdot B_2O_3$

FF-96 70 w/o $Bi_{12}GeO_{20}$ - 30 w/o $.75Bi_2O_3 \cdot 0.5Al_2O_3 \cdot B_2O_3$

FF-97 70 w/o $Bi_{12}GeO_{20}$ - 30 w/o $Bi_2O_3 \cdot 0.5Al_2O_3 \cdot 0.5B_2O_3$

FF-98 80 w/o $Bi_{12}GeO_{20}$ - 20 w/o $.75Bi_2O_3 \cdot 0.5Al_2O_3 \cdot B_2O_3$

FF-99 85 w/o $Bi_{12}GeO_{20}$ - 15 w/o $.75Bi_2O_3 \cdot 0.5Al_2O_3 \cdot 0.5B_2O_3$

FF-100 95 w/o $Bi_{12}GeO_{20}$ - 5 w/o $.75Bi_2O_3 \cdot 0.5Al_2O_3 \cdot 0.5B_2O_3$

FF-101 90 w/o $Bi_{12}GeO_{20}$ - 10 w/o $.75Bi_2O_3 \cdot 0.5Al_2O_3 \cdot 0.5B_2O_3$

The nucleation behavior and solubility data where determined are summarized in Table 3.

TABLE 3

NUCLEATION BEHAVIOR AND SOLUBILITY OF $Bi_{12}GeO_{20}$ FROM BISMUTH ALUMINOBORATE GLASS SOLVENT

Composition	Nucleation Behavior	Solubility
FF-93	Spontaneous nucleation from 763°C to 784°C	not measured
FF-79	No detectable nucleation	not measured
FF-94	Spontaneous nucleation at 740°C to 745°C	not measured
FF-95	Spontaneous nucleation at 765°C	not measured
FF-96	Not determined	70.7 w/o $Bi_{12}GeO_{20}$ at 750°C
FF-98	Spontaneous nucleation at 762°C - 770°C	79.5 w/o $Bi_{12}GeO_{20}$ at 770°C 79.7 w/o $Bi_{12}GeO_{20}$ at 785°C
FF-99	Not determined	Unsaturated at 810°C
FF-100	Spontaneous nucleation at 810°C	not measured

The solubility measurements entailed the insertion of a preweighed $Bi_{12}GeO_{20}$ seed crystal into the melt and a hold of several hours at the given temperature. The measured weight change reflects the degree of solubility under the experimental conditions employed. Because of possible incorporation of entrapped glass or of spontaneously nucleated material such measurements may be lacking in accuracy. Variations in the amount of accompanying glass could explain the apparent discrepancy in values

obtained in measurements at 770°C and 785°C. However, in spite of possible errors, useful information was derived that was helpful in determining suitable growth conditions.

With regard to variations in temperature of spontaneous nucleation in compositions FF-94, FF-95, and FF-93, the temperature is found to rise with increasing concentration of $Bi_{12}GeO_{20}$ as expected. In compositions FF-96, FF-98, FF-99, FF-100 and FF-101 there are higher percentages of $Bi_{12}GeO_{20}$ and less Bi_2O_3 (.75 mole) in the glass. Incompleteness of data makes comparisons difficult but FF-98 (80 w/o $Bi_{12}GeO_{20}$) with one mole of Bi_2O_3 in the glass exhibits a similar nucleation temperature to FF-93 (60 w/o $Bi_{12}GeO_{20}$) with .75 mole of Bi_2O_3. The absence of observed nucleation in FF-79 requires further substantiation.

Differential Thermal Analysis (DTA) thermograms were obtained for glass frit of compositions FF-79, FF-93, FF-97, and FF-96. The results are presented in Table 4 and the traces given in Figure 1.

TABLE 4

DIFFERENTIAL THERMAL ANALYSIS (DTA) THERMOGRAM RESULTS FOR $Bi_{12}GeO_{20}$ BY GLASS SOLVENT

Composition	Exotherms	Endotherms
79	Shoulder: 440°C Major: 480°C 2nd Major: 552°C	395°C
93	Major: 415°C Minor: 495°C 2nd Major: 552°C	375°C, 545°C, 565°C
97	Major: 465°C Minor: 515°C	390°C, 565°C, 597°C
96	Shoulder: 410°C Major: 428°C Minor: 520, 535, 553	368°C, 557°C

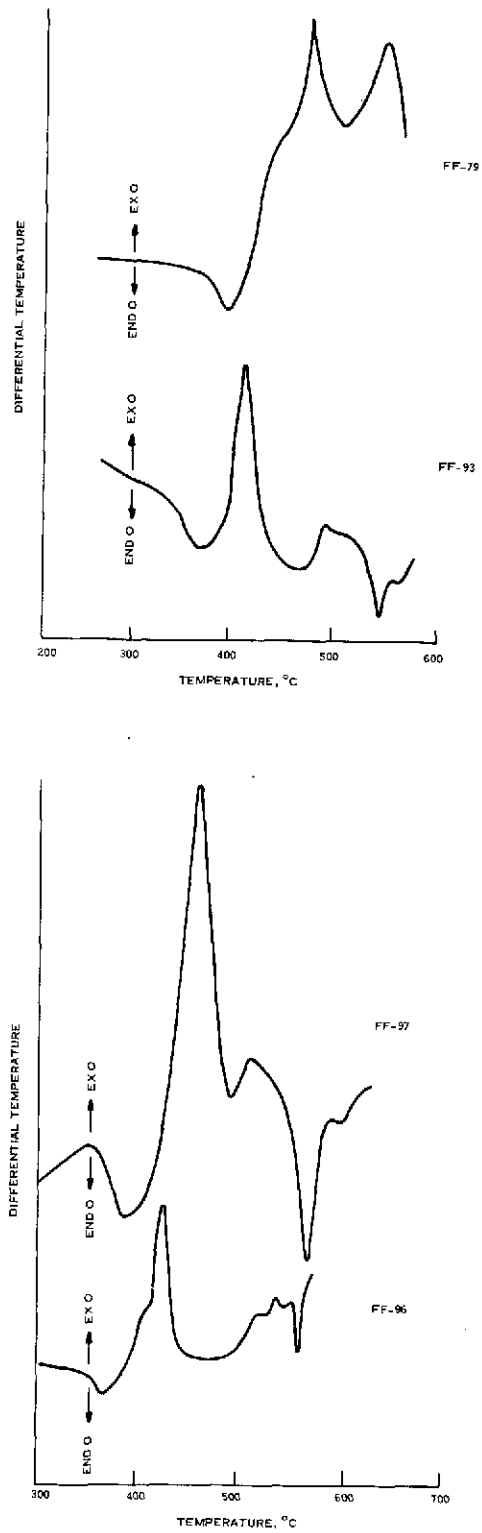

Figure 1. Differential Thermal Analysis (DTA) Thermograms for $Bi_{12}Ge0_{20}$ in Glass Solvent. (A) Composition FF-79; (B) Composition FF-93; (C) Composition FF-97, (D) Composition FF-96.

The thermograms are all fairly complex with indications of more than one phase crystallizing during heat treatment. The glass phase was modified to determine if crystallization could be limited to only one phase and DTA thermograms were used to identify trends which would indicate the direction compositional changes should take. Only for FF-97 does the thermogram reveal a minor exotherm of rather weak intensity indicating that further reductions in B_2O_3 content might result in elimination of this exotherm entirely.

The temperatures at which the major exotherm and endotherms appear are highest for FF-79 with 2 moles of B_2O_3 in the glass but are not a minimum at the lowest B_2O_3 content of .5 moles perhaps due partly to an increase in $Bi_{12}GeO_{20}$ concentration from 60 to 70 w/o. Reducing the number of moles of Bi_2O_3 from one to .75 may counteract the increased $Bi_{12}GeO_{20}$ content in FF-96 and result in similar temperatures for the location of exotherms as in FF-93.

The maximum detail in the thermograms such as resolution of shoulders on major peaks is achieved by heating slowly at 5° per minute. The presence of these shoulders could represent incorporation of B_2O_3 or Al_2O_3 or both in solid solution with $Bi_{12}GeO_{20}$ so that shifts in temperature of crystallization could occur with change in composition. The same would

apply to endotherms representing melting behavior. Minor peaks which occur at temperatures far enough removed from the major exotherms probably represent unrelated secondary phases, such as the glass, which are precipitating out.

X-ray diffraction results: To be able to better interpret the crystallization behavior represented by thermal energy changes exhibited in DTA thermograms, samples were annealed at temperatures coincident with these changes and then the phases developed were studied by means of x-ray powder diffraction technique. The composition FF-93 was annealed for 7 days at 390°C or just above the first large endotherm at 375°C; also for 18 hours at 470°C which is at the completion of the major exotherm which peaks at 415°C; and finally for 18 hours at 580°C, which is above the temperatures at which two minor exotherms and endotherms appear. The diffraction patterns for these samples were then compared to try to determine the phase changes that occurred as a result of annealing at different temperatures. The data are shown in Tables 5, 6 and 7.

TABLE 5

X-RAY DIFFRACTION DATA FOR FF-93 ANNEALED AT 390°C, 7 DAYS

FF-93		18-244 β Bi_2O_3		16-654 δ -Bi_2O_3		GeO_2 tetragonal	
d	I/I_o	d	I/I_o	d	I/I_b	d	I/I_o
3.05	S	3.14	100	3.27	100	3.108	100
2.69	M	2.78	20	2.83	45	2.399	60
1.91	M	2.694	30	2.00	65	2.199	15
		1.941	40			2.106	13
1.73	VVW	1.918	20	1.71	70	1.967	5
		1.76	10				
		1.68	40				
1.64	M-S	1.64	50	1.63	18	1.620	50
1.56	W	1.58	30			1.555	17
1.48	VVVW	1.48	5	1.42	10	1.43	9
		1.40	10				
		1.36	20	1.30	25	1.39	11
1.246		1.32	10				
1.22	VVVW	1.27	70	1.27	20	1.304	20
1.12	VVVW	1.255	40	1.16	18	1.300	17
		1.25	40	1.09	16		
		1.23	40	.957	18		
		1.22	40				
		1.18	10				

Presented along with the values of "d" spacing and intensities for annealed FF-93 are listed patterns from the ASTM card index. These seem to have the closest correspondence to FF-93 and yet there are significant differences for each of the Bi_2O_3 phases as well as for GeO_2 which does not permit positive identification of the developed phase in FF-93 annealed at 390°C.

For FF-93 annealed at 470°C for 18 hours there is good agreement in "d" spacing and intensity.

TABLE 6

X-RAY DIFFRACTION DATA FOR FF-93 ANNEALED AT 470°C, 18 HOURS. FRIT GROUND INTO POWDER

FF-93			$Bi_{12}GeO_{20}$ seed		14-699 α-Bi_2O_3	
d	I/I_o		d	I/I_o	d	I/I_o
			5.075	4		
4.4756	4	-			4.498	4
4.1601	4	-			4.084	4
3.5984	15		3.584	27	3.622	8
3.4713	5	-			3.456	20
3.3200	9	-			3.310	35
3.2177	90		3.210	100	3.253	100
3.1238	70	-	3.001	5	3.184	25
2.9359	21		2.928	29		
2.7692	12	-				
2.7176	60		2.707	78	2.708	40
2.5383	7		2.534	4	2.693	40
2.394	8		2.390	12	2.559	16
2.					2.532	10
2.2684	8		2.267	10	2.499	8
2.165	10		2.162	20	2.429	6
2.0732	9		2.070	13	2.390	14
1.9918	12		1.989	18	2.244	6
1.8775	5		1.925	2	2.176	6
1.8538	7		1.851	8	2.154	6
1.7403	27		1.739	34	2.132	8
					1.958	25
1.6923	13		1.691	22	1.878	10
1.6475	22		1.646	30	1.872	18
1.5642	7		1.565	5		
1.4977	12		1.530	4		
			1.495	20		
1.4921	11					
1.4351	5		1.434	12		
1.3821	7		1.379	4		
1.2895	5		1.288	4		
1.2130	9		1.212	13		

TABLE 7

X-RAY DIFFRACTION DATA FOR FF-93 ANNEALED AT 580°C, 18 HOURS. FRIT GROUND INTO POWDER

FF-93			Diffraction Trace, C_aK_α $Bi_{12}GeO_{20}$ seed pattern	
		I/I_o	d	I/I_o
15.96	5.548	8	5.075	4
(22.25	3.992	7		
(22.40	3.965	9		
22.84	3.8902	11		
24.82	3.584	19	3.584	27
26.16	3.4035	5		
26.78	3.326	9		
27.72	3.2154	84	3.210	100
28.74	3.1036	31		
29.16(sh)	3.0598	9		
29.66	3.0094	7		
30.44	2.934	21	2.928	29
31.34	2.8518	5 1/2		
32.93	2.7176	56	2.707	78
35.30	2.5404	7	2.534	4
35.54	2.5238	7		
36.00	2.4926	7		
36.52	2.4583	6		
37.54	2.3938	8	2.390	12
39.66	2.2706	9	2.267	10
41.70	2.1641	13	2.162	20
43.64	2.0723	11	2.070	13
45.48	1.9926	15		
45.60	1.9877	14	1.989	18
45.90	1.9754	9		
47.10	1.9278	7	1.925	2
48.60	1.8717	7		
49.16	1.8517	12	1.851	8
49.44	1.8419	10		
50.22	1.8151	7		
52.56	1.7397	30	1.739	34
54.18	1.6914	18	1.691	22
55.82	1.6455	24	1.646	30
61.98	1.4959	13	1.530	4
			1.496	20
64.90	1.4355	8	1.434	12
67.76	1.3817	6	1.379	4
73.40	1.2888	4	1.288	4

TABLE 8

"d" SPACING VALUES FOR ANNEALED FF-93 WHICH DO NOT CORRESPOND TO $Bi_{12}Ge0_{20}$ PATTERN

390°C		470°C		580°C C	
d Å	I/I_o	d Å	I/I_o	d Å	I/I_o
				5.548	8
		4.47	4	3.99	7
				3.965	9
		4.16	4	3.89	11
		3.47	5	3.40	5
		3.32	9	3.326	9
3.05	S				
2.68	M	3.12	70	3.103	31
1.91	M	1.877		3.059	9
1.73				3.009	7
1.64	MS			2.852	5
1.56				2.524	7
1.48				2.493	6
1.246				2.458	
				1.975	9
				1.928	7
1.22				1.872	7
1.12				1.815	

values for the majority of lines with the pattern for $Bi_{12}GeO_{20}$ seed crystal. There are strong lines of another phase present as well. The strongest line of this additional phase at 3.124 Å may correspond to the 3.05 Å strong line observed after the 390°C anneal. The other weak lines seem to fit the α-Bi_2O_3 pattern (ASTM card 14-699).

Finally, in regard to the diffraction data for FF-93 annealed at 580°C for 18 hours given in Table 7, just as in the case of the 470°C annealed sample there is a good correlation with $Bi_{12}GeO_{20}$ in regard to "d" spacing and intensity values. In addition there are more lines that are not accounted for by the $Bi_{12}GeO_{20}$ pattern than in the 470°C annealing. The "d" spacing and intensities of lines which do not fit the $Bi_{12}GeO_{20}$ pattern as a function of annealing temperature are presented in Table 8.

C. Crystal Growth Studies

1. Crystal Growth Experiments

As a means of defining the variables required for design of a zero-gravity single crystal growth experiment, crystallization studies involving seeded growth from glass solvents were initiated. Seeded growth in comparison with spontaneous nucleation can provide control over orientation, growth rate, perfection and doping.

Three classes of seeded growth are possible:

1) Growth by slow cooling in the presence of a seed

2) Growth on a seed where supersaturation is caused by solvent evaporation

3) Growth on a seed in the cool part of a system, while excess solute is in contact with the solvent in a higher temperature region. This is referred to as thermal gradient or Kruger-Finke growth.

The principal advantage of methods (1) and (2) is that no dissolution step is required and that the diffusion path can be shorter. Both of these methods have been employed in the present studies.

Method 2 was employed concurrently with solubility determinations. Crystal growth was obtained when the seed was introduced under conditions approaching supersaturation with temperature being maintained constant.

Method 1 was utilized after data had been acquired on solubility as a function of temperature. The seed was inserted at a temperature which was 10-15^{o}C higher than that for onset of spontaneous nucleation. Programmed slow cooling by means of a cam was then initiated. The temperature span adopted was selected because it would provide abundant growth. However this might require modification to achieve a higher degree of perfection. The amount of glass solvent occlusion is directly related to the difference between cooling schedule and crystal growth rates. This is a consequence of the inability of the solvent to diffuse away from the vicinity of the crystal; nutrient material diffusing across the concentration gradient would trap solvent specie during growth. Therefore a thorough evaluation of the crystal is required in order to make the necessary adjustment in growth parameters. An outline of the growth experiments performed and the results are presented in Table 9.

TABLE 9

CRYSTALLIZATION EXPERIMENTS FOR $Bi_{12}GeO_{20}$ IN GLASS SOLVENTS

Composition	Growth Conditions	Weight of Growth	Growth Characteristics
FF-78-4	610°C, 10 min.	Not determined, but fairly substantial	Mass accreted on seed, microprobe shows Ge deficiency near seed.
FF-92	590°C, 5 min.	9.3 gm.	Mass accreted on seed, severe cracking, was weakly crystalline
FF-93-1	775°C, 45 min.	Not determined, but fairly substantial	Laue shows some single crystallinity with different orientation fro seed; glass occlusions
FF-96-3A	745°C-750°C, 3 3/4 hours.	3.0 gm.	Laue shows some single crystallinity with different orientation fro seed; glass occlusions
-G7	757°C, 4 hr.	2.05 gm.	Yellowish white cubes randomly nucleating in ceramic-like matrix
FF-98-1	769°C, 3 hr.	2.45 g	Fairly high degree of crystallinity
-2A, 2B	785°C, 4 hr.	.64 g	
-3A	795°C 767°C, 14 hrs.	4.8 g	Highly crystalline, well developed faces. Limited nucleation by seed, glass occlusions.
FF-100-1C	816°C, 3 1/2 hr.		Couldn't free seed and growth, entire solution had solidified.

2. Growth Perfection

Crystallization experiments performed at constant temperature produced growths of rather minimal crystallinity primarily by accretion of material on the seed. This is seen in Figures 2 and 3, respectively, for the constant temperature growth of FF-78-4 and FF-92 where the glass composition consists of $Bi_2O_3 \cdot 2B_2O_3$. There are distinctive features associated with the FF-78 growth which can be observed in Figure 4 At the high magnifications of 330 X employed growth regions can be seen which are arranged in parallel fashion but oriented differently in some type of glassy matrix.

The same restricted crystallinity is obtained for growths from glass solvents which include Al_2O_3 along with B_2O_3 and Bi_2O_3 as in Figure 5 depicting 775°C constant temperature growth of composition FF-93-1. When crystallization was more extensive it apparently was the result of heterogeneous nucleation by either supporting platinum wires, the walls of the crucible or by impurities. Spontaneously nucleated crystalline material grown in the vicinity of platinum wire in a glass matrix of FF-96-3A is shown in Figure 6 Another instance of random nucleation is the development of rectangular shaped crystals about .3 - .4 mm on a side far from the locale of the seed during 769°C growth of FF-98-1. This is observed in Figure 7.

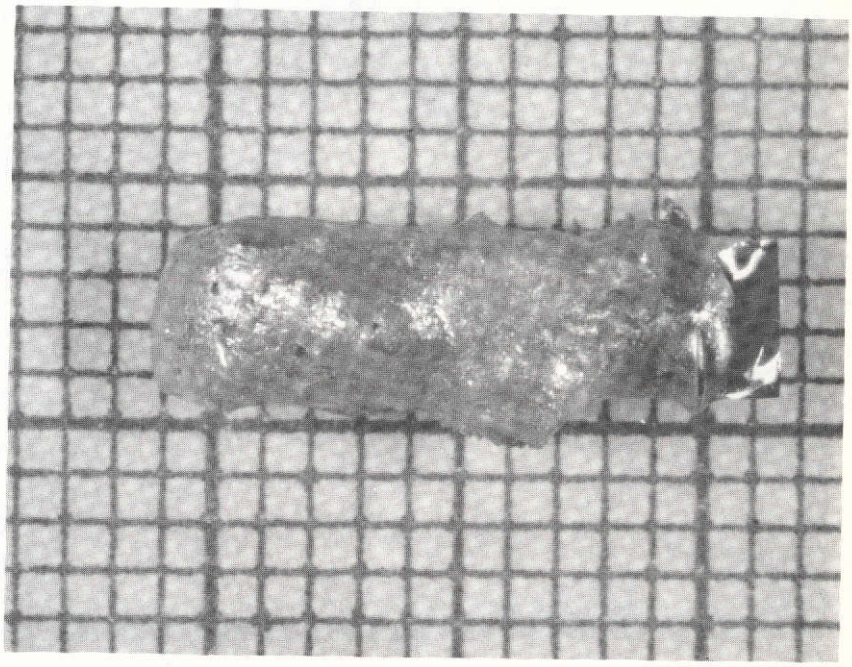

2.5 X

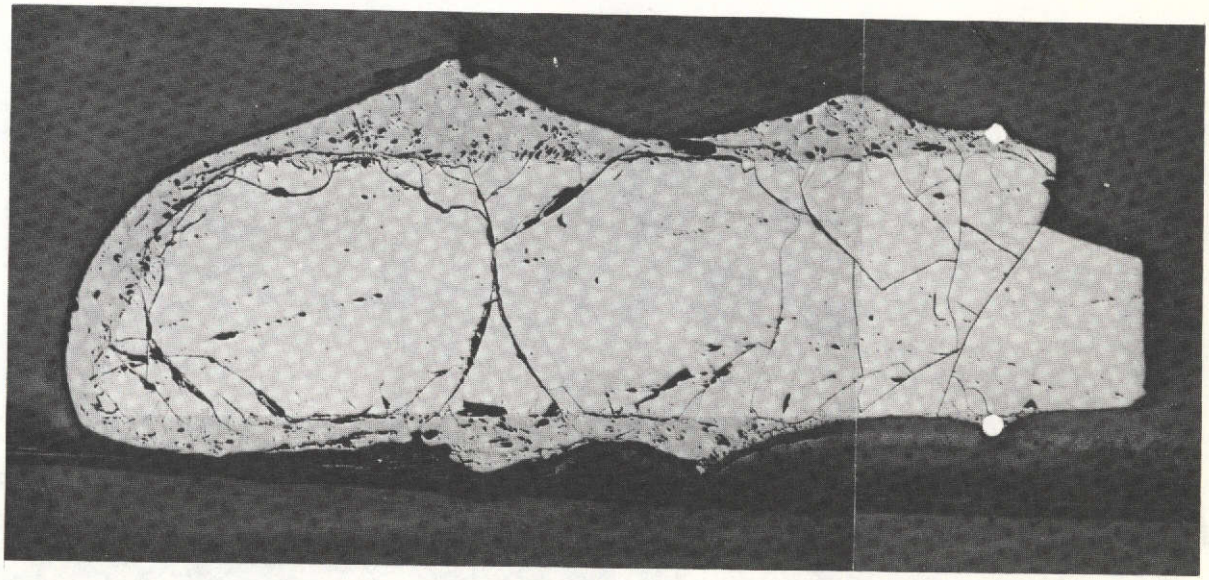

12 X

Figure 2. Accretion of Material on Seed during Attempted Growth of FF-78-4 at 610°C.

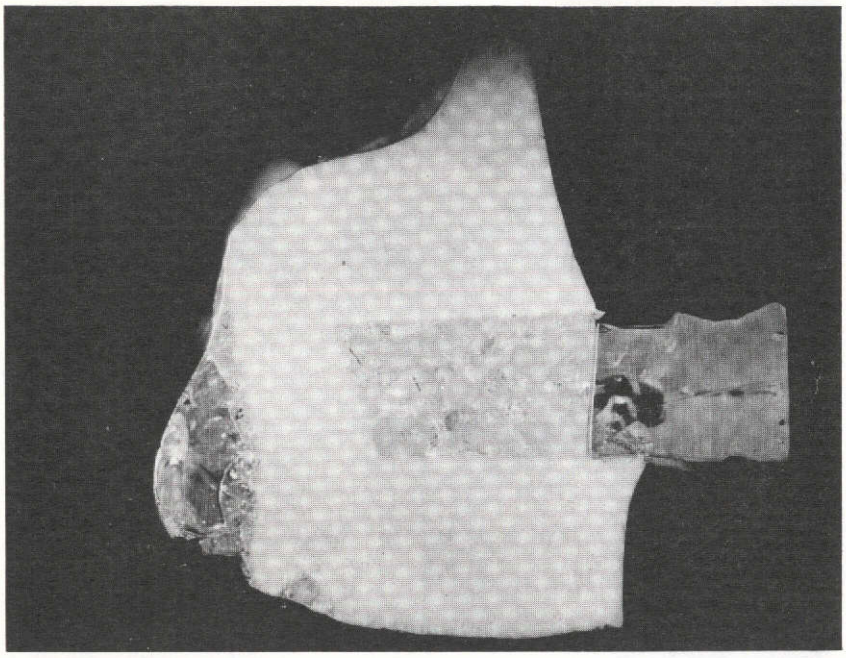

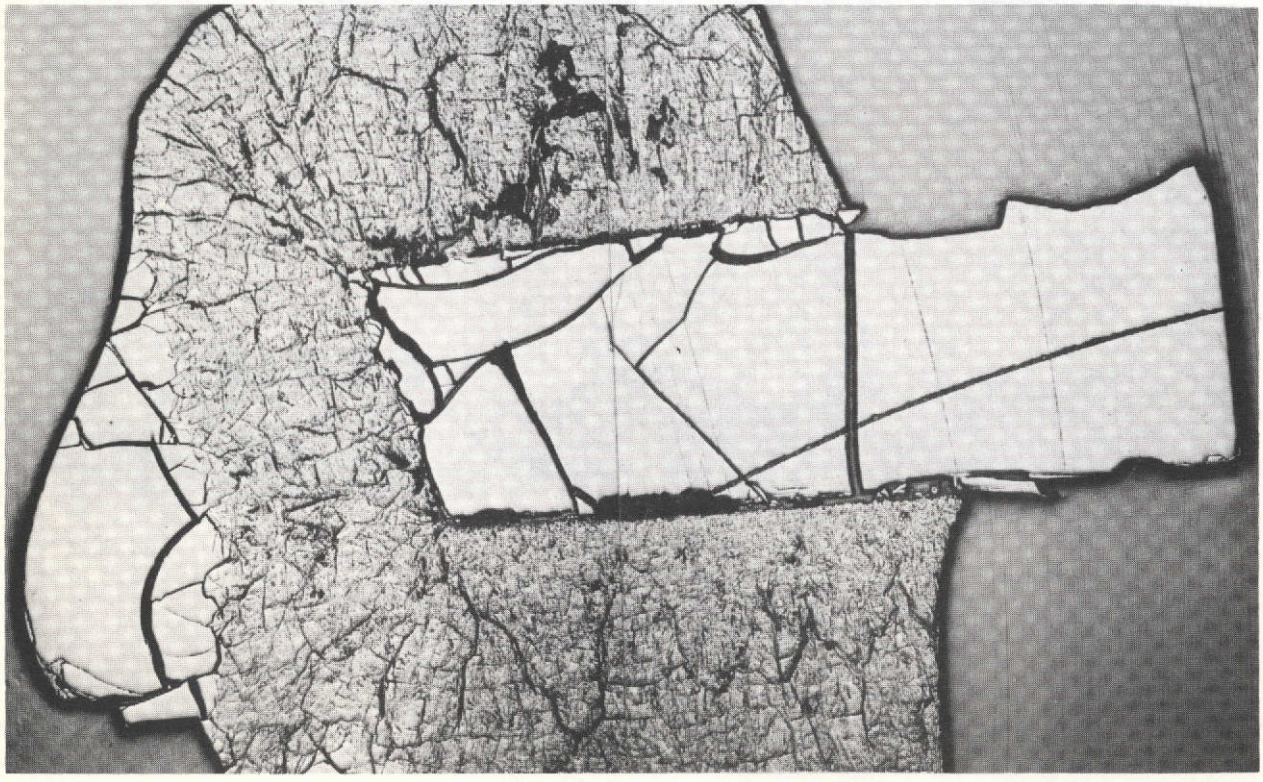

Figure 3. Accretion of Material on Seed during Attempted Growth of FF-92 at 590°C.

Seed Growth

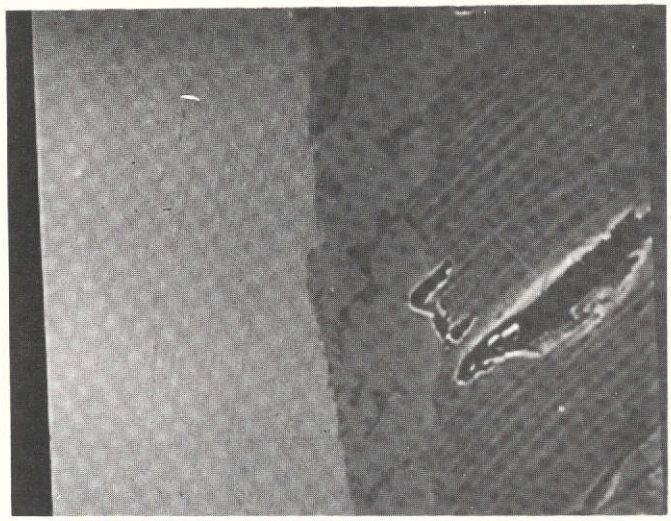

330 X

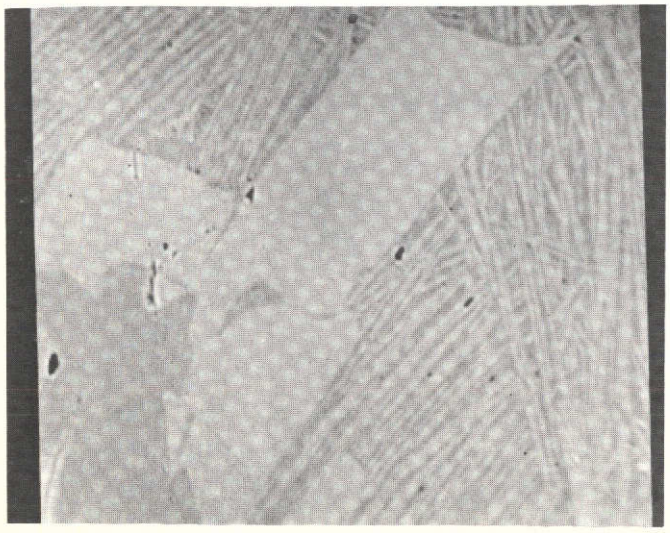

330 X

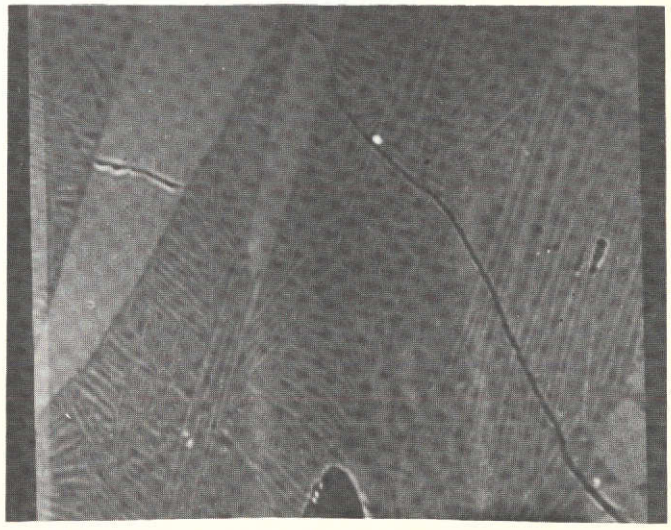

330 X

Figure 4. Parallel Oriented Growth Regions during Growth of FF-78.

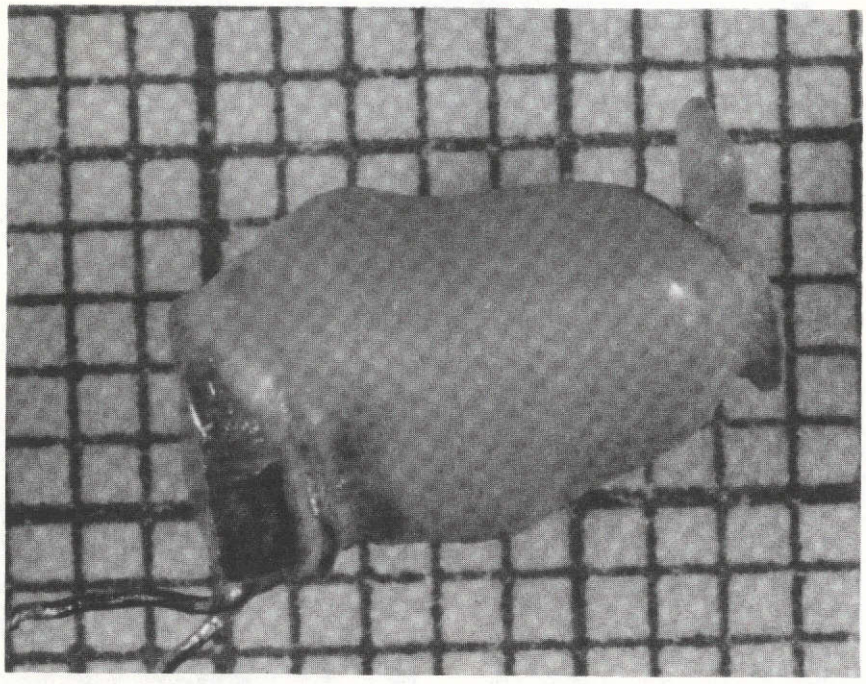

3.75 X

Figure 5. Growing Having Limited Crystallinity, FF-93-1 at 775°C.

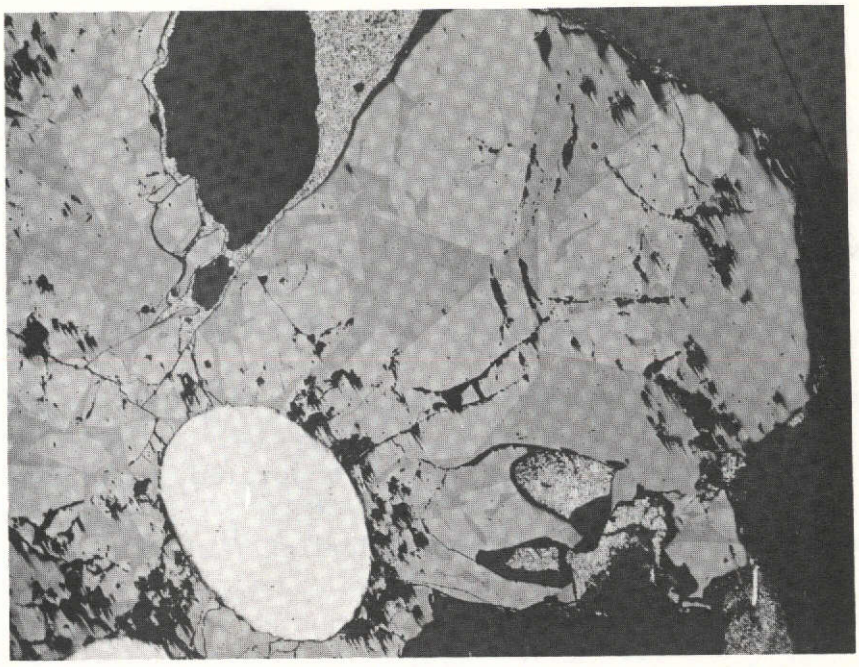

50 X

Figure 6. Spontaneously Nucleated Growth Near Platinum Wire in FF-96-3A.

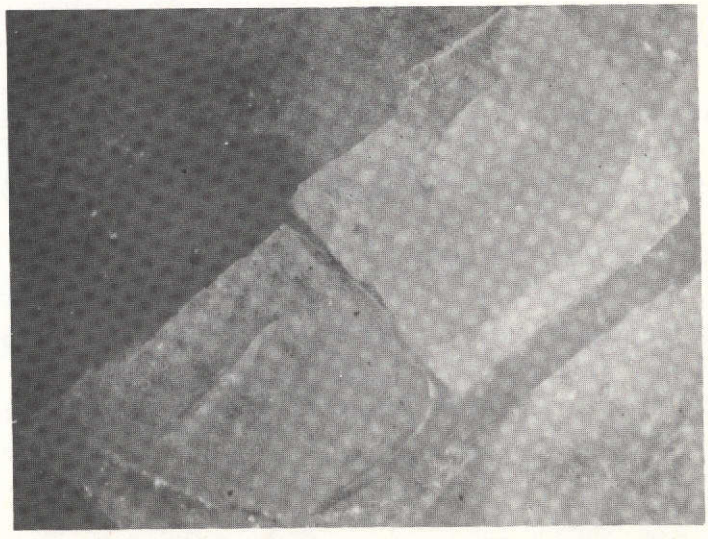

125 X

Figure 7. Development of Well-Formed Crystals Randomly Nucleated During 769°C Growth of FF-98-1.

The constant temperature growth of FF-98-1 over a period of three hours was exceptional in regard to the large amount of crystallization that was developed. An approximately cubic habit with fairly well-developed surface features was exhibited as seen in Figure 8A and Figure 8B Some glassy accreted material was also incorporated. Observation of the seed-growth interface at higher magnification (125 X) revealed the growth to be discontinuous and probably not nucleated by the seed. This is shown in Figure 9A and Figure 9B.

In order to help identify the crystalline material that grew on the seed, a small crystal was separated and studied by the Debye-Sherrer x-ray powder diffraction technique. The data is presented in Table 10, along with x-ray diffraction data for $Bi_{12}GeO_{20}$ seed crystal for comparison.

There obviously is excellent agreement with respect to "d" spacing values as well as intensity data. Therefore it can be concluded that the phase which crystallizes from a solution of 80 w/o $Bi_{12}GeO_{20}$ - 20 w/o $.75Bi_2O_3 \cdot 0.5Al_2O_3 \cdot B_2O_3$ (FF-98) is $Bi_{12}GeO_{20}$.

The most abundant growth occurred during programmed slow cooling experiments in which the temperature was lowered at a rate of $2^{\circ}C$ per hour. For composition FF-98-3A slowly cooled from $795^{\circ}C$ to $767^{\circ}C$ in a 50 cc platinum crucible the growth amounted to 5 gm using a 100 gm charge. A rectangular shaped habit with well developed faces was displayed. While most of the growth appeared contiguous with the seed, some apparent

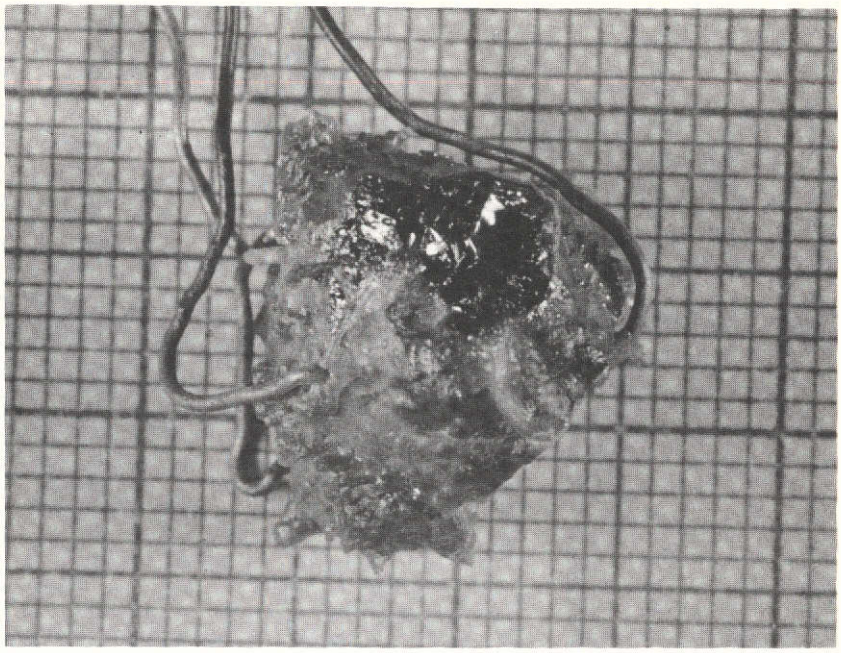

A

1.65 X

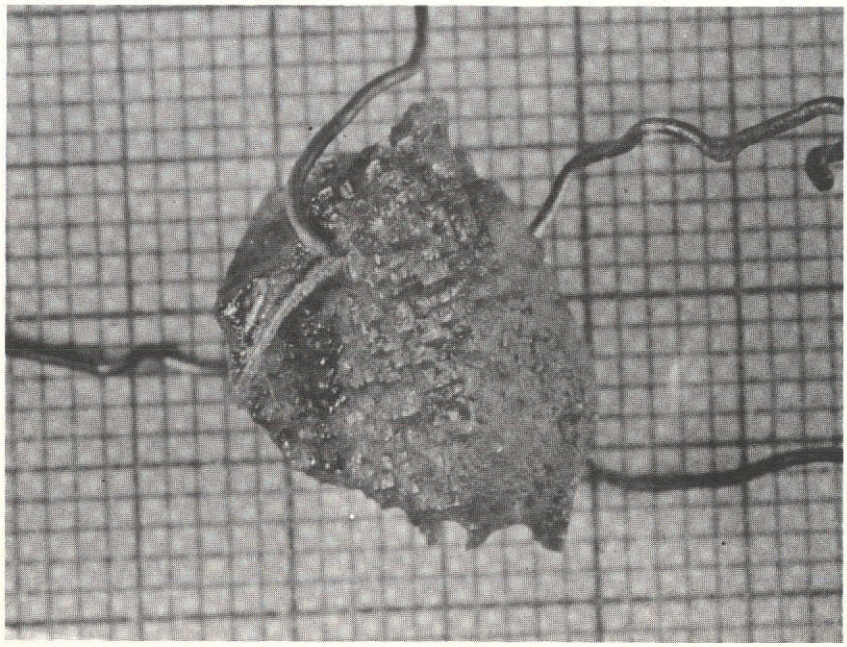

B

1.57 X

Figure 8. Surface Features and Habit for FF-98-1 Growth at 769°C for Three Hours.

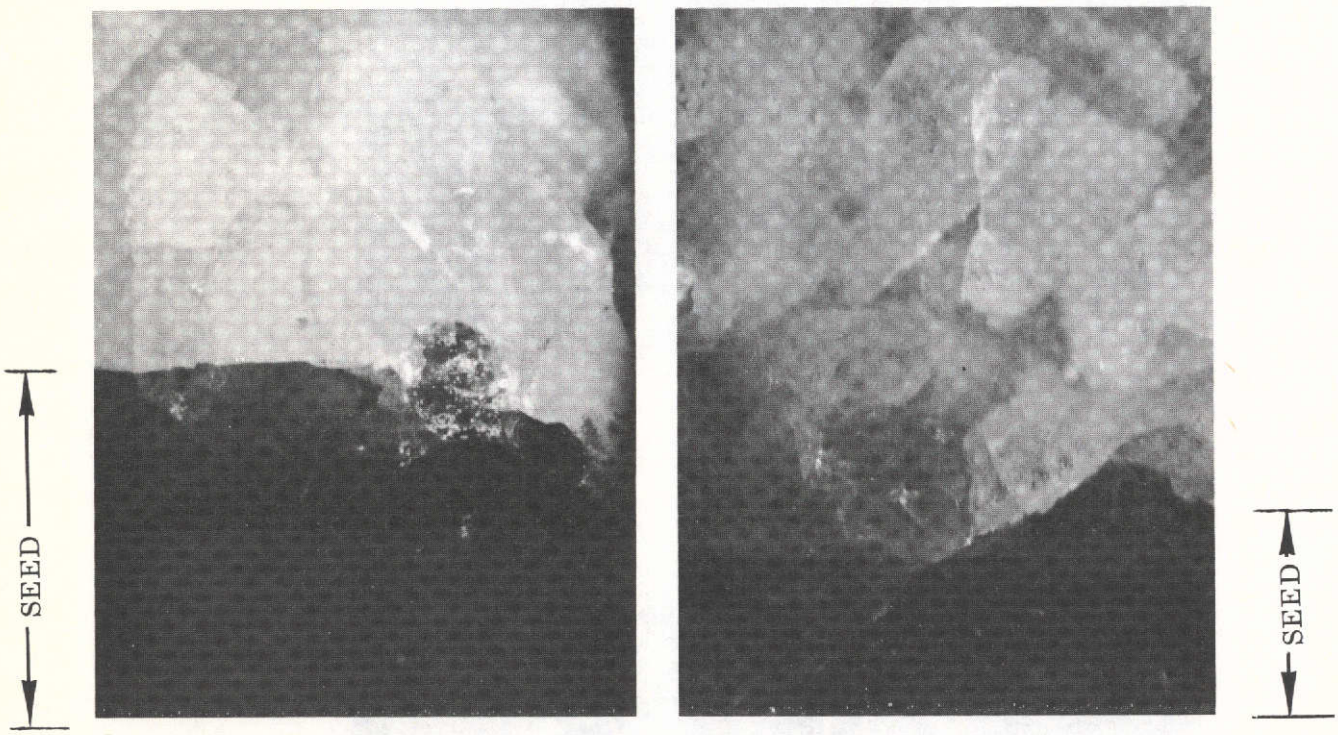

A (125 X)

B (75 X)

Figure 9. Microscopic Observation of Seed-Growth Interface for FF-98-1 Growth at 769°C for Three Hours. (Seed appears black in Figure.)

TABLE 10

X-RAY DIFFRACTION DATA FOR FF-98-1A CRYSTAL GROWTH AT 769°C FOR 3 HOURS

FF-98-1A		$Bi_{12}GeO_{20}$ seed crystal		FF-98-1A		$Bi_{12}GeO_{20}$ seed crystal	
d	I/I0	d	I/I0	d	I/I0	d	I/I0
3.52	VW	3.53	MW	.992	VVVW	.990	VVW
	S	-3.22	VVW				
3.18	S	3.16	VS	.982	VVVW	.982	VW
-2.92	VVW			.964	W	.972	VVW
						.964	W
2.88	VVW	2.89	W	.947	VVW	.948	VVW
2.67	S	2.68	S	.931	VW	.940	VVW
						.932	VW
2.36	VVVW	2.51	VW			.924	
		2.37	W	.917	VW		VVW
						.917	VW
2.23	VVVW	2.24	W	.902	VVW	.902	W
2.13	VW	2.14	VW	.888	VVW	.888	W
2.05	VW	2.05	MW	.882	VVW	.882	VW
1.97	VW	1.96	M	.875	VVW	.974	W
1.84	VW	1.84	W	.872	VVW		
1.72	M	1.73	S	.863	VVW	.862	VVW
1.68	W-M	1.68	M	.850	VVW	.850	VW
1.64	M	1.63	MS	-.845	VVW		
1.56	VVVW	1.56	W				
1.52	VVVW	1.53	W				
1.49	W	1.488	MS	.839	M	.838	W-M
1.458	VVVW	1.46	VW				
1.43	VVVW	1.43	MW	.827	VVW	.827	VW
	VVVW	-1.40	VW			.824	VVW
1.38		1.375	W	.816	VVW	.816	VVW
1.33	VVVW	1.33	VVW	.806	VVW	.806	VVW
1.284	VVW	1.284	W	.797	VVW	.797	VVW
1.244	VW	1.246	W	.792	VVW	.792	VVW
	M	1.23	VVW				
1.208		1.214	MS	.787	S	.787	W-M
1.193	M-W	1.19	MS	.785	VVW	.785	W-M
1.176	M-W	1.172	MS	.778	S	.778	W-M
1.144	VW	1.148	W	.776	W	.776	W-M
1.118	VVVW	1.118	VW				
1.104	VVVW	1.11	VW				
1.093	VVW	1.09	W				
1.066	VW	1.065	W				
1.043	VVVW	1.042	VVW				
1.023	M	1.023	MW				

nucleation by the supporting platinum wire was observed. There was also some glass solvent adhering to the surface of the crystal. Various aspects of the growth are seen in Figure 10A, B, C, and D.

In order to characterize the effect of the seed on the growth of the crystal, a cross-sectional cut passing through seed and growth and nearly perpendicular to the (110) seed direction was made. After mounting and polishing, the specimen was subjected to microscopic and back reflection Laue x-ray diffraction study.

A photograph of the cross-section at 11 X magnification is given in Figure 11A. The seed location is marked by a faint dark shadow of almost square outline in the lower center portion. A back reflection Laue x-ray diffraction study of the growth was performed in which the x-ray beam was translated systematically in the horizontal direction at a point approximately two thirds of the way up the seed. Other selected areas in the growth were probed as well. The following was determined:

1) crystallinity exists over practically the entire growth
2) nucleation of the growth by the seed has occurred
3) there are several different crystallographic orientations observed in various regions of the growth.

While single crystal Laue photographs were obtained in almost all areas probed, this doesn't preclude the presence of minor glass occlusions since

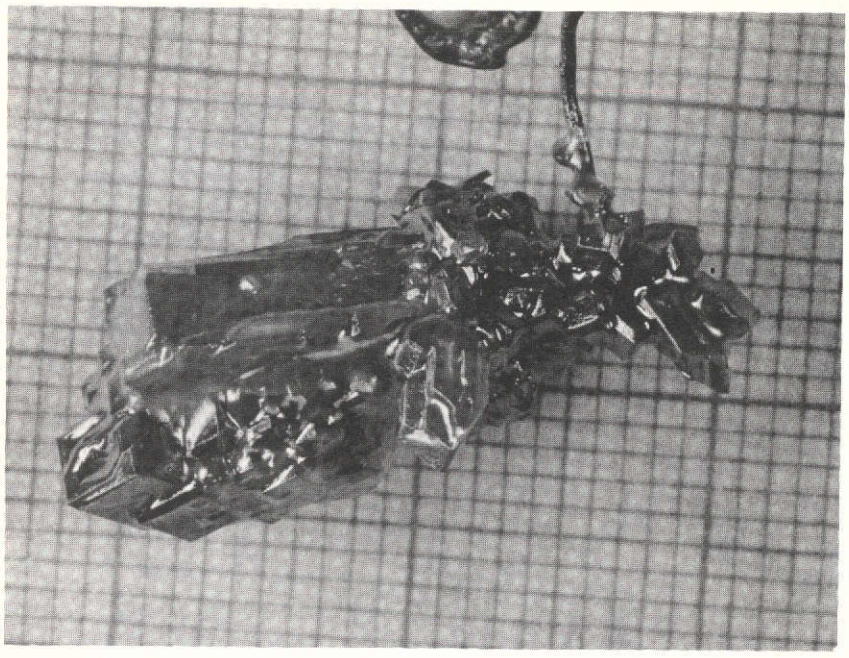

A (1.54 X)

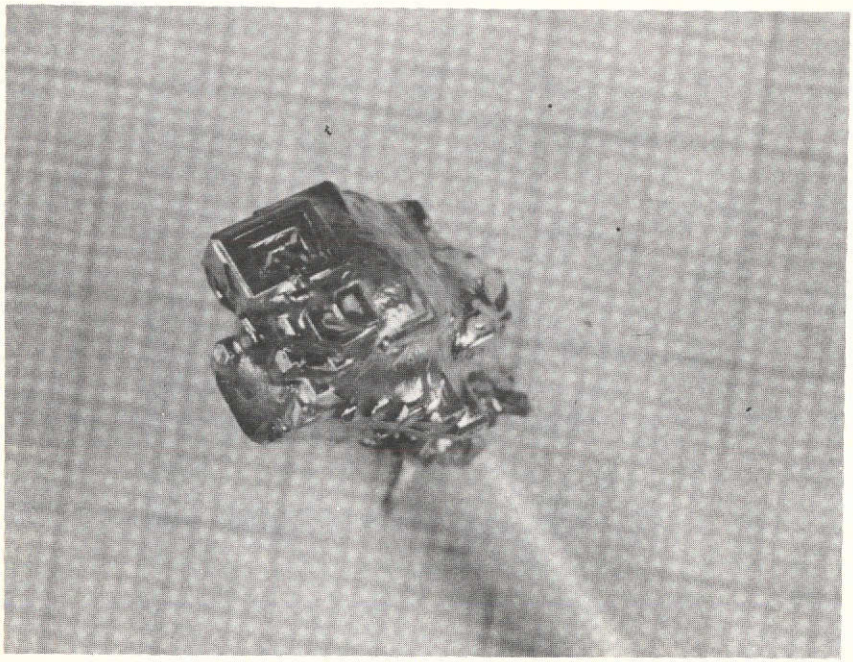

B (1.12X)

Figure 10. Morphology of $Bi_{12}Ge0_{20}$ Seeded Growth Developed in FF-98-3A Slowly Cooled at 2°C per Hour from 795°C to 767°C.

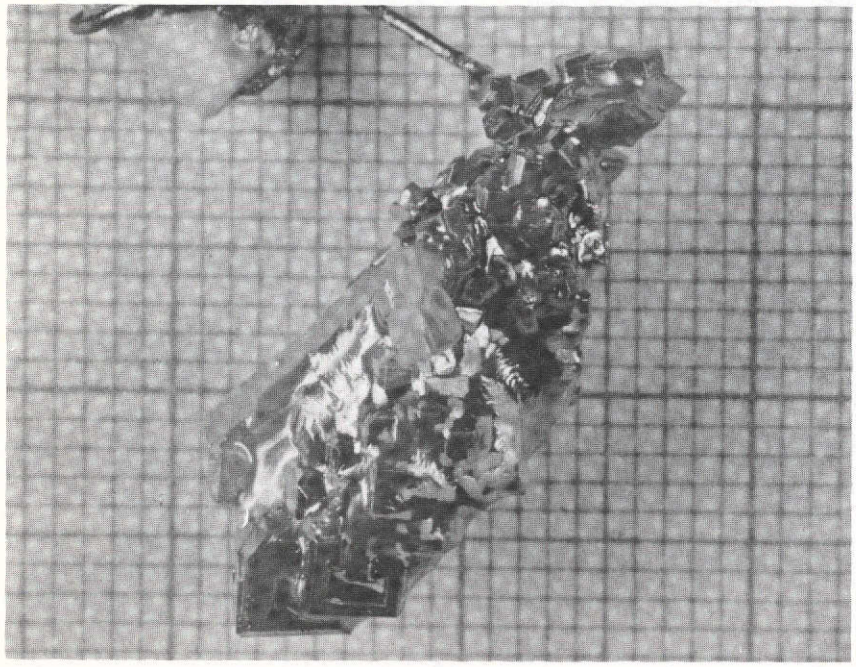

C (1.5X)

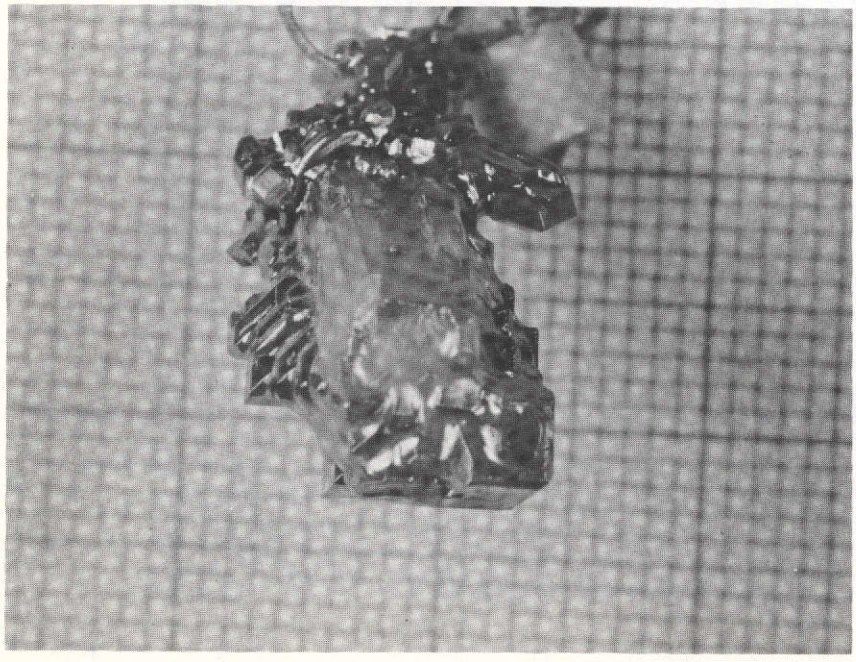

D (1.35X)

Figure 10 (Cont.)

Note: In the early constant temperature runs, a platinum basket supported the seed (Figure 8). A platinum wire wrapped around one end of the seed was later used (Figure 10). While there was evidence of spurious nucleation in the solution in direct contact with the platinum support wire, the growth morphology and microprobe analysis shows that single crystal growth contiguous with the seed took place on the major part of the seed.

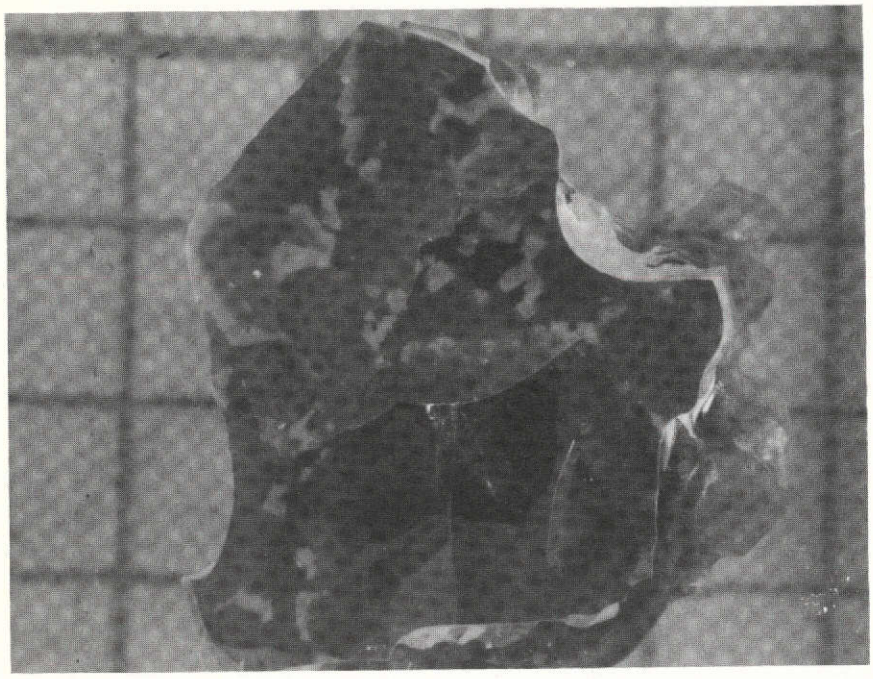

A

9.2X

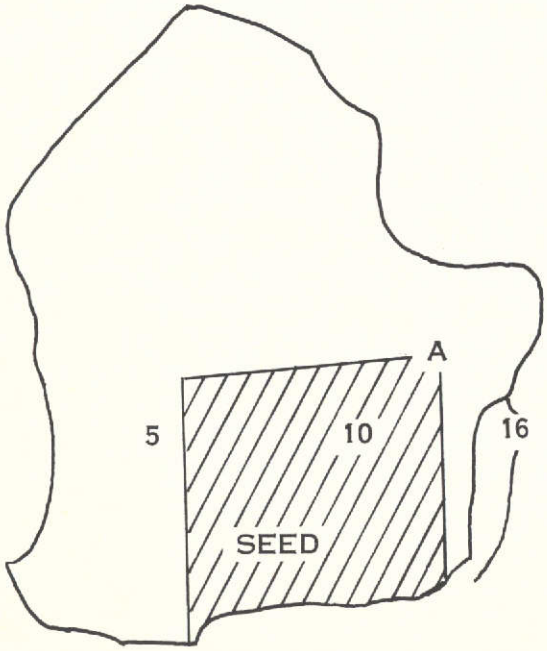

B

Figure 11. Transverse Section Through Seed and Growth of FF-98-3A - (Close to (110) plane)

the large beam diameter of .015 inches could easily result in overlap of such areas and still provide evidence of crystallinity. The most significant finding was that the same crystallographic orientation as existed in the seed was observed in the growth at a distance of slightly more than 0.030 inches from a seed edge and about 0.015 inches from the opposite edge. Several different orientations were discovered as selected locations in the growth were probed. The seed does not give the expected (110) Laue pattern because the cross-section cut was slightly directed otherwise.

Laue patterns representing locations within the growth on either side of the seed crystal along with a pattern of the seed itself for comparison (locations 5, 10, 16 in Figure 11B) are presented in Figure 12.

The more frequently observed defects associated with growth from a solvent have been identified in the growth of composition FF-98-3A. These include solvent occlusion and hopper growth. In addition cracks resulting from thermal shock are extensive. In some areas the cracks are filled with glass indicating these to have originated at the time of insertion of the seed while in others they appear as voids which suggest formation upon removal from the melt.

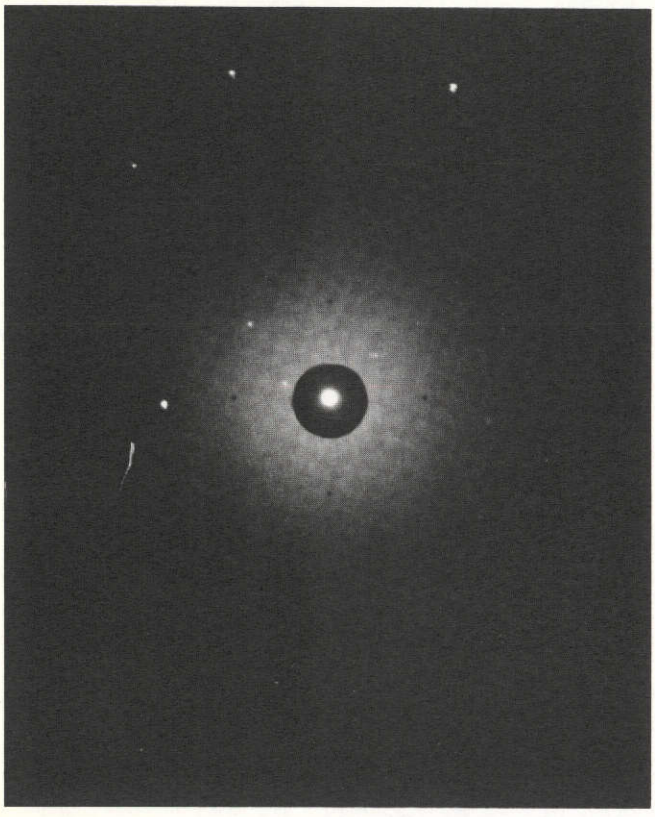

(location 5, Fig. 11)

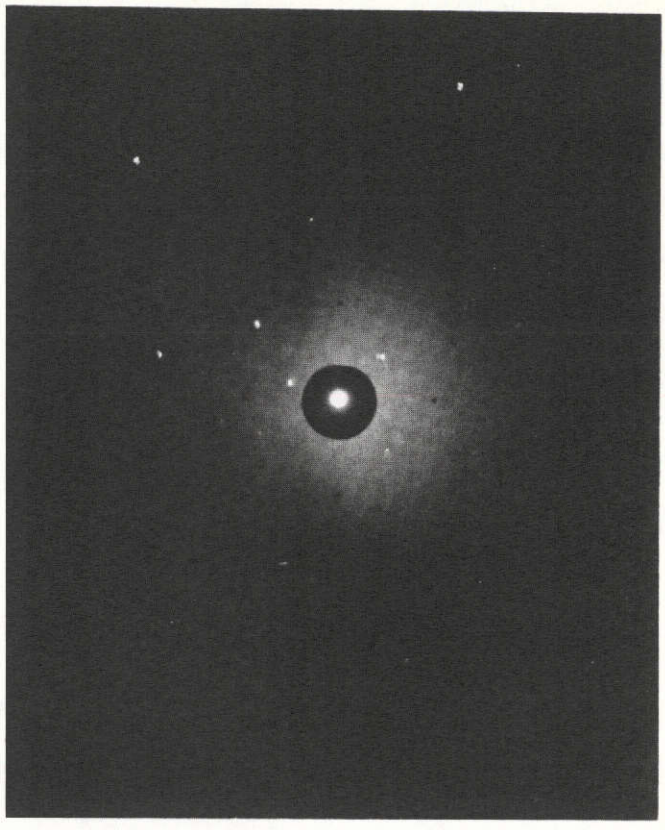

(location 16, Fig. 11)

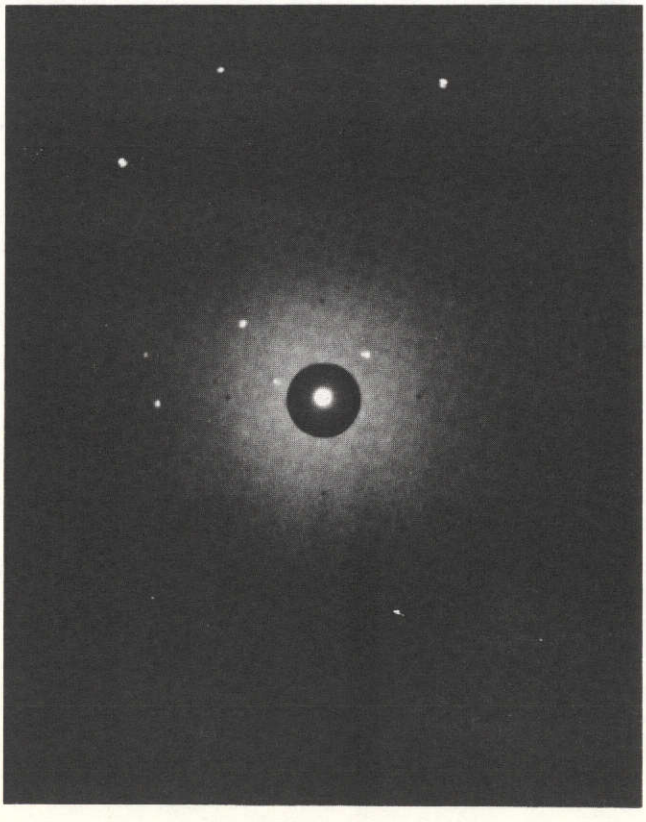

(location 10, Fig. 11)

Figure 12. Comparison of Laue X-ray Patterns of Growth Regions with that of Seed for FF-98-3A (Locations 5, 10 and 16 in Figure 11B).

Microscopic examination of the crystal growth of composition FF-98-3A in the vicinity of the seed was used to determine if nucleation by the seed had taken place. At one edge of the seed there was 0.010 inches of growth which appears to be contiguous with the seed. In another location about 0.020 inches of growth appears to have been nucleated by the seed.

Finally, a large almost square shaped area of the same orientation as the seed appears to have been nucleated at the corner of the seed. This area is from .050 inches to .060 inches on a side and appears as the largest region of nucleated growth. The extensive crack development and glass occlusions are prominent in this region. The evidence from microscopic examination confirms what has been previously found by Laue x-ray diffraction study.

Photographs of the areas which have been examined for evidence of nucleation by the seed are given in Figure 13A and Figure 13B (location A in Figure 11B).

3. Solvent Incorporation in Growth

Of prime importance in assessing the suitability of the solute-solvent system is a determination of the degree of glass solvent incorporation in the crystal. It must also be distinguished whether solvent is physically trapped because growth has proceeded under non-ideal conditions (such as excessively rapid growth), or if solvent constituents have chemically substituted by entering into solid solution. A combination of electron microprobe and emission spectrographic analysis has provided useful information relating to this question.

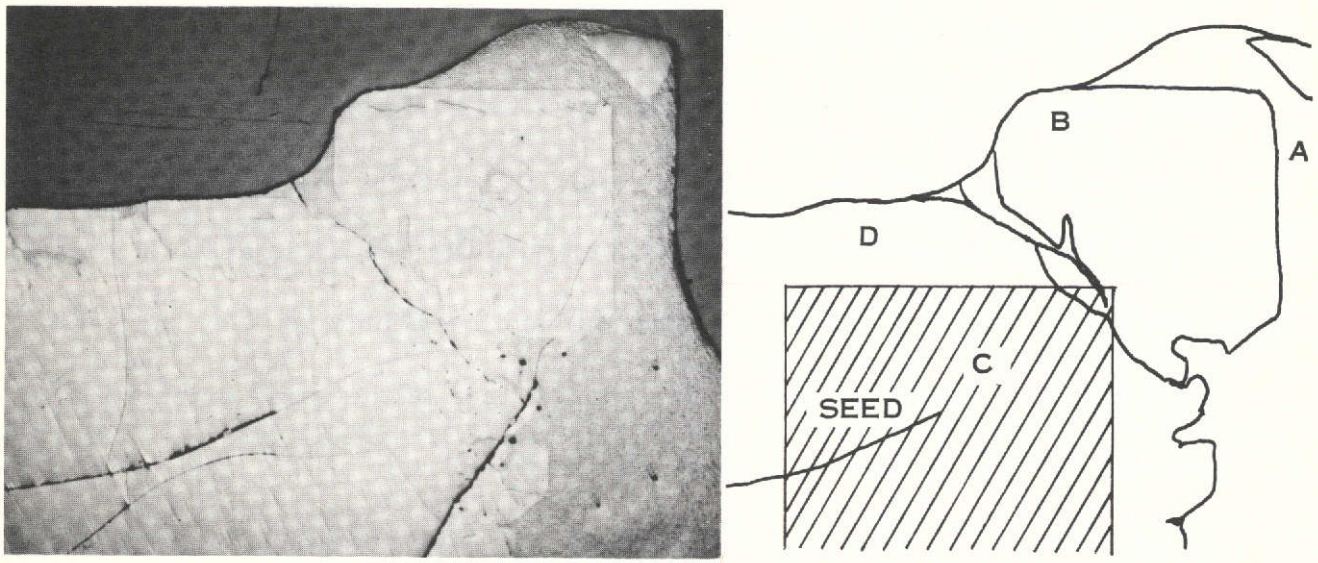

27X

A

(SEED
DARK
SHADOW)

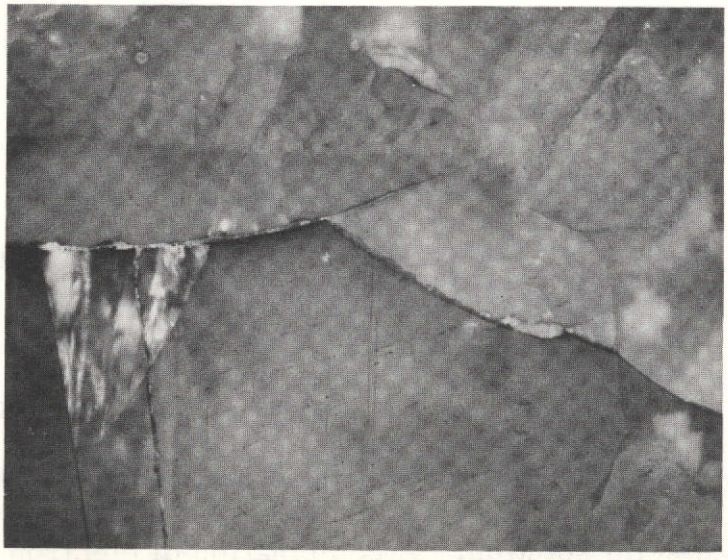

B

54X

Figure 13. Microscopic Examination of Growth Near Growth-Seed Interface for FF-98-3A (Location A in Figure 11B).

Pictorial representations of the concentration of glass and crystalline species at selected locations within the growth as determined by electron microprobe analysis are shown in several accompanying figures. For example in Figure 14 the Ge concentration in the vicinity of the seed is presented in the growth of composition FF-78 using $Bi_2O_3 \cdot 2B_2O_3$ glass.

The high density of spots in an area apart from the seed indicates that Ge has segregated and further evidence of this is the existence of a region adjacent to the seed which is depleted of Ge. There was a similar but somewhat smaller depletion of Ge near the seed in growth of composition FF-92 as seen in Figure 15. Bi_2O_3, being a common constituent of both the crystal and glass phase, should be rather uniformly distributed and this has been observed.

While boron concentration was not determinable by this technique, it was possible to analyze for aluminum. Therefore the distribution of the glass phase in which Al was incorporated, could be obtained. For composition FF-96-3A having Bi_2O_3, B_2O_3 and Al_2O_3 in the glass phase the location of the seed boundary after growth could not be readily determined during microprobe examination (Figure 16). Scanning was restricted to the vicinity of a platinum wire (white oval in Figure 6) which was used to support the seed. Lighter colored areas have the highest Ge concentration and only a negligible amount of Al. These probably come closest in

Growth Seed

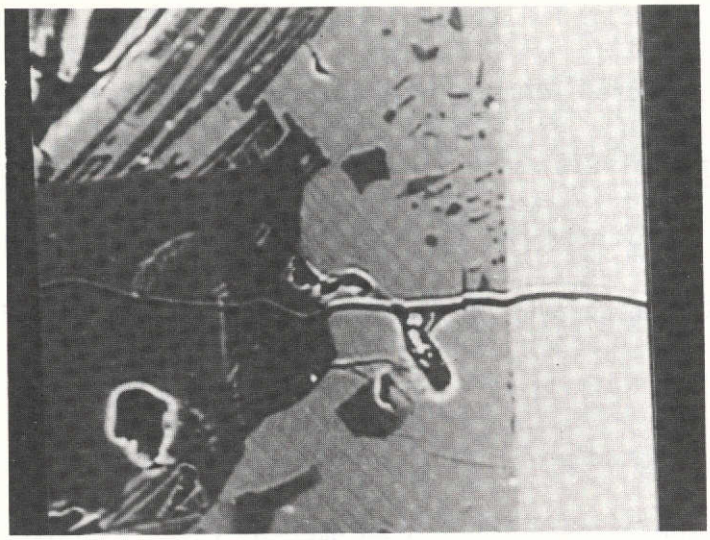

400 X

Growth Seed

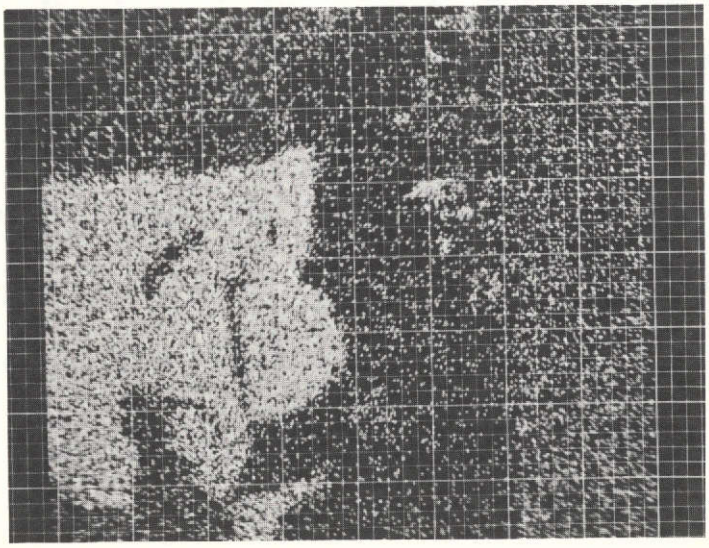

Figure 14. Microprobe Determination of Ge Distribution in Vicinity of Seed for FF-78.

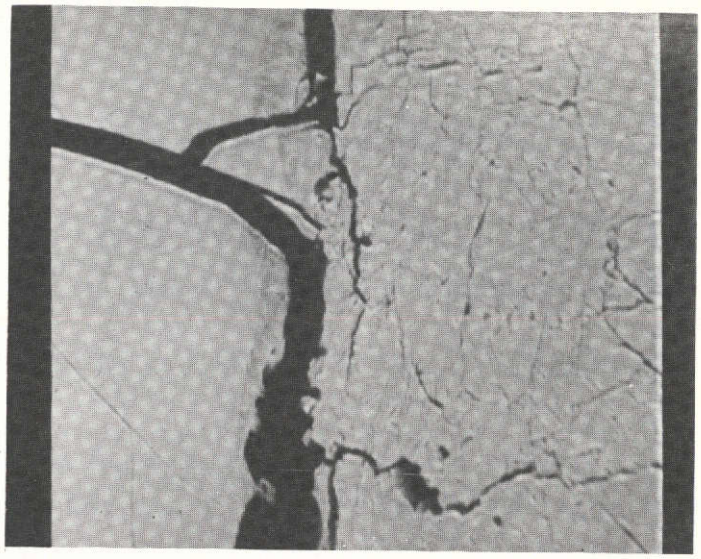

260X

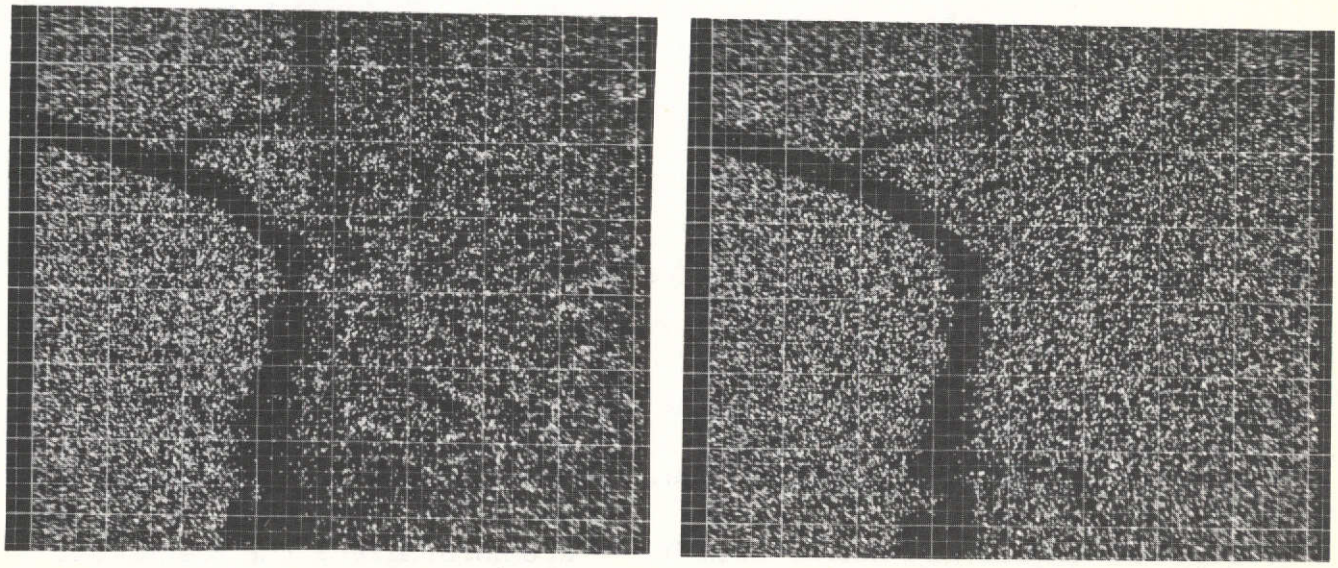

Seed Growth

Ge

Seed Growth

Bi

Figure 15. Microprobe Determination of Ge and Bi in FF-92 Growth.

composition to the seed. In Figures 16a and 16b the darker grey areas are deficient in Ge and have a somewhat higher Al content indicating some glassy character to this portion of the growth. Lastly there are black colored regions in which Ge appears to be absent and Al is present in very high concentration. A surprising result of the scan shown in Figure 16c is the small amount of both Ge and Bi in the black colored area with only Al present in abundance. These apparently represent collections of entrapped glass having a predominance of Al_2O_3 -B_2O_3 content with only a small concentration of network modifier present. These regions of trapped glass are extensive.

The growth of composition FF-98-3A, was also thoroughly studied by means of the microprobe as well as by emission spectroscopy to determine the extent of compositional uniformity. The region examined was one in which there was microscopic evidence for nucleation by the seed. This region in which glass, seed, and crystal #1 and #2 are found is indicated in Figure 13. Ge and Al relative intensities were normalized. The results are shown in Table 11.

TABLE 11

	Region	Relative Intensities Ge	Al
A.	Glass	.40	1.0
B.	Crystal #1	.68	.07
C.	Seed	1.0	.006
D.	Crystal #2	.84	.006

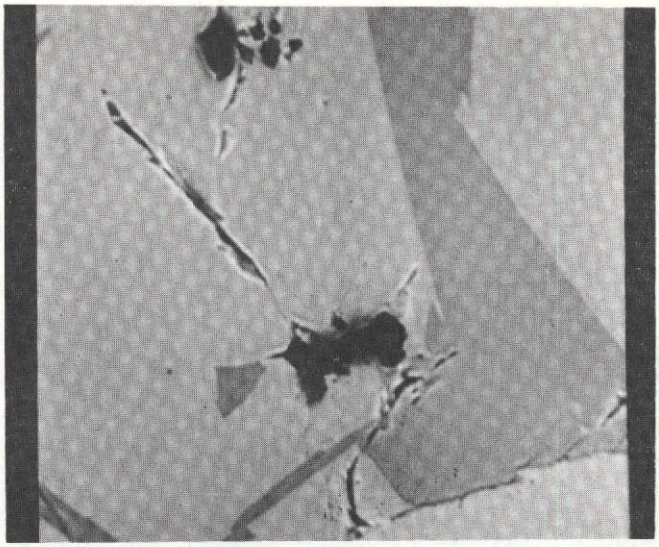

280 X

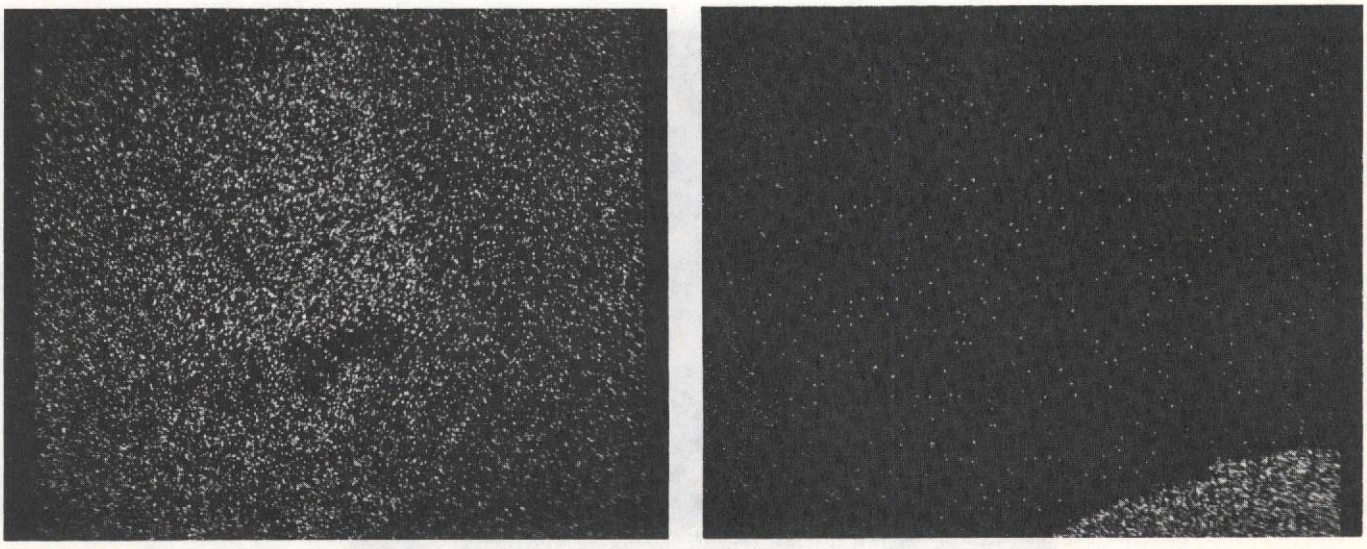

Ge

Pt

Figure 16a

Figure 16. Microprobe Determination of Ge, Al and Bi for FF-96-3A in (a - b - c) Vicinity of Platinum Supporting Wire.

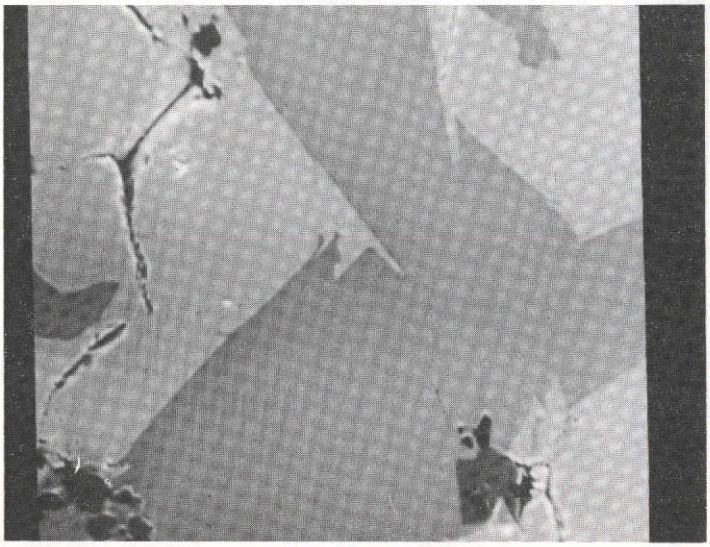

270 X

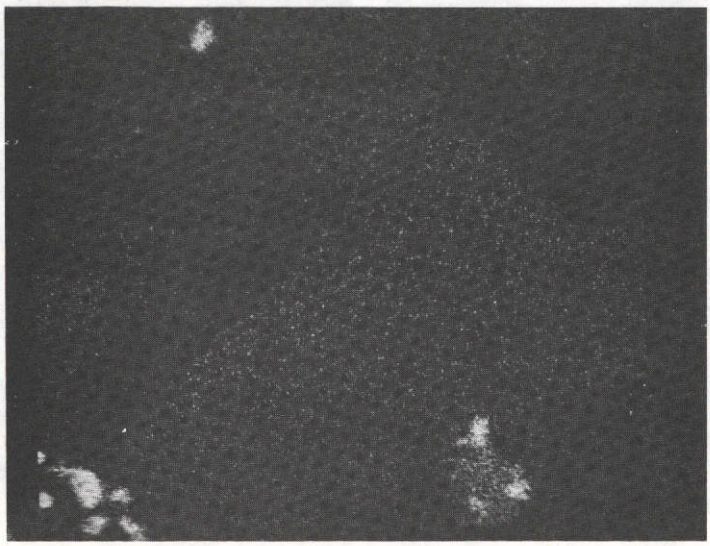

Al

Figure 16b

270 X

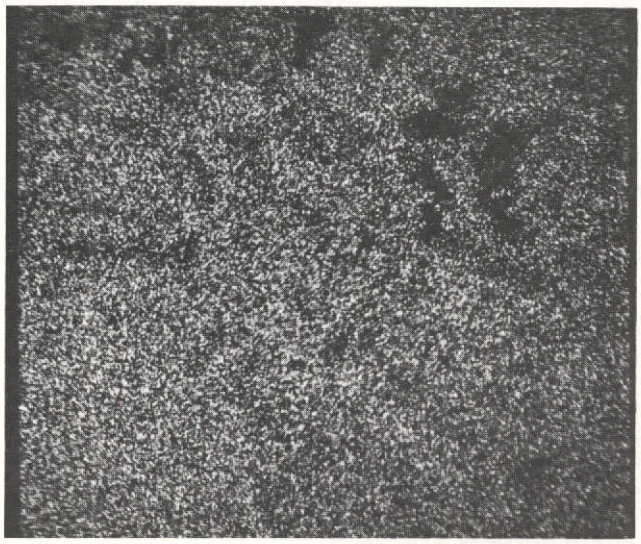

Bi

Al

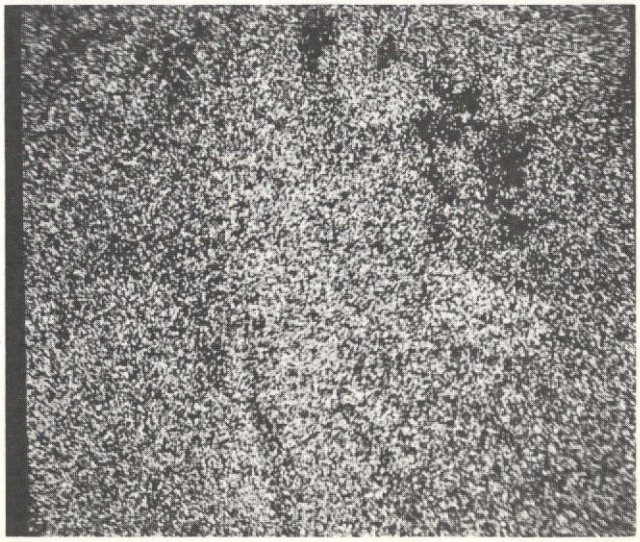

Ge

Figure 16c

It is noted that the Ge content in the crystals is variable and doesn't quite achieve the level measured in the seed. Such compositional variations could account for differences in orientation observed throughout the growth. Al content, however, can be extremely low in the crystal or very high in the glass.

Photographs showing the compositional distributions within the growth are given in Figure 17 a, b, c and d.

Because of the inability of the microprobe to provide concentration data for boron, emission spectroscopy was utilized for this purpose. A small crystal from the portion of the growth of FF-98-3A in the vicinity of the supporting platinum wire was given a 15 second etch in dilute HCl to remove surface glass, then crushed and ground to a fine powder. The sample was then studied by spectroscopic analysis. The results are given in Table 12.

Table 12. Emission Spectroscopic Analysis of FF-98-3A

Al	1800 ppm
B	1500 ppm
Ge	2 - 3%
	(only approximation).

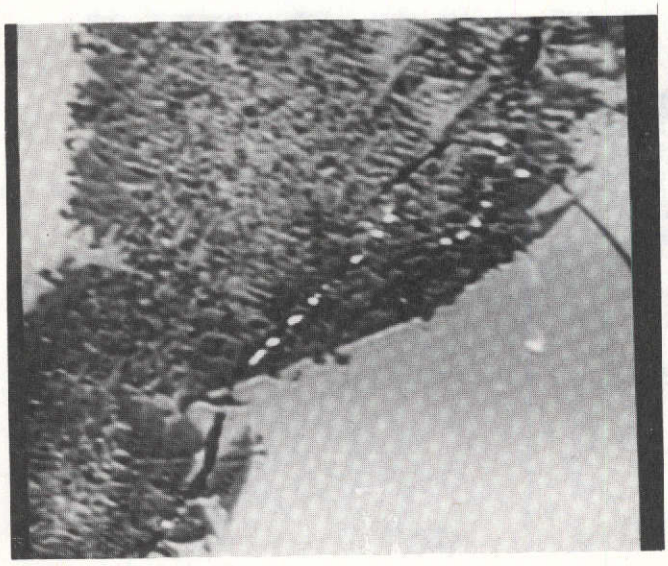

280 X

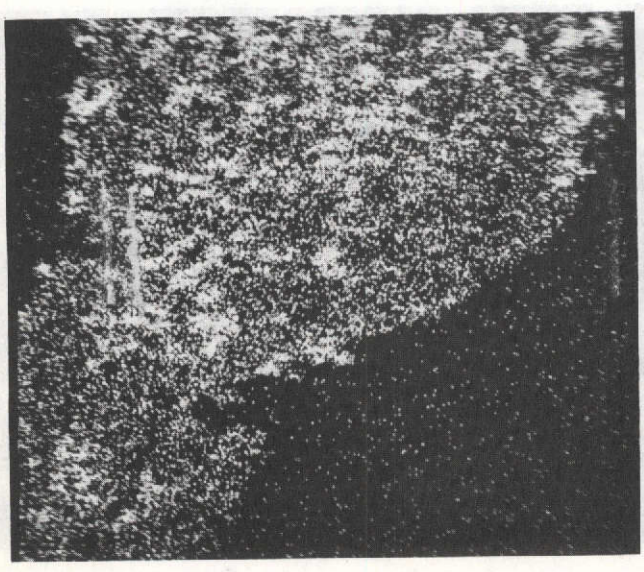

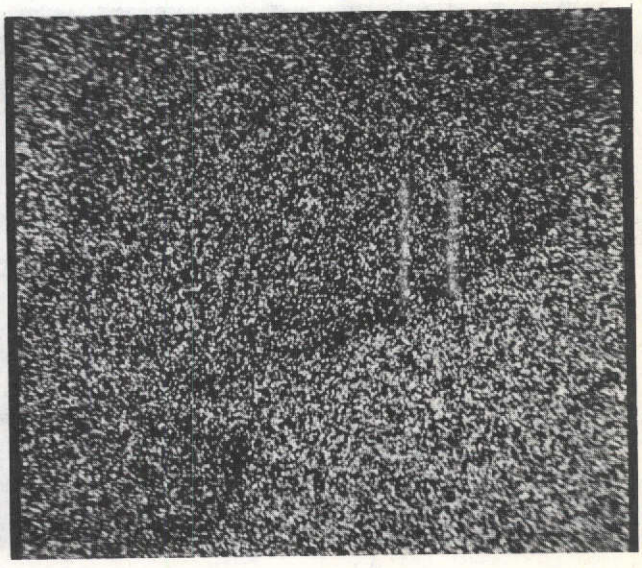

Al

Ge

Figure 17a

Figure 17. Compositional Distributions Obtained from Microprobe Analysis (a-b-c-d) within FF-98-3A Growth Region.

GLASS

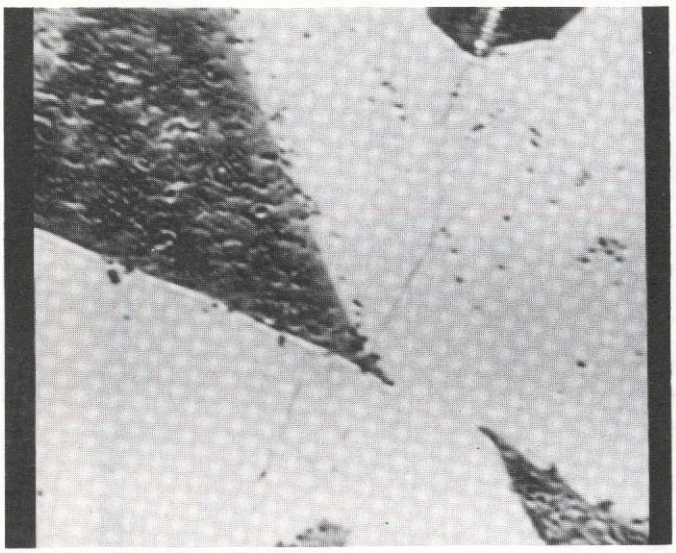

280 X

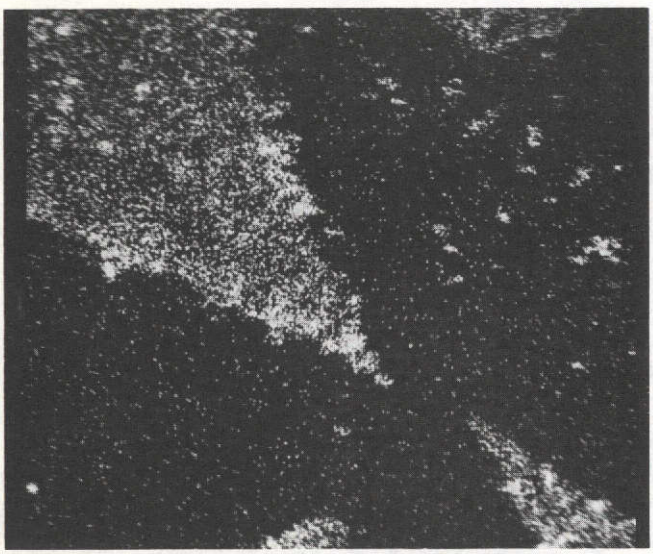

Al

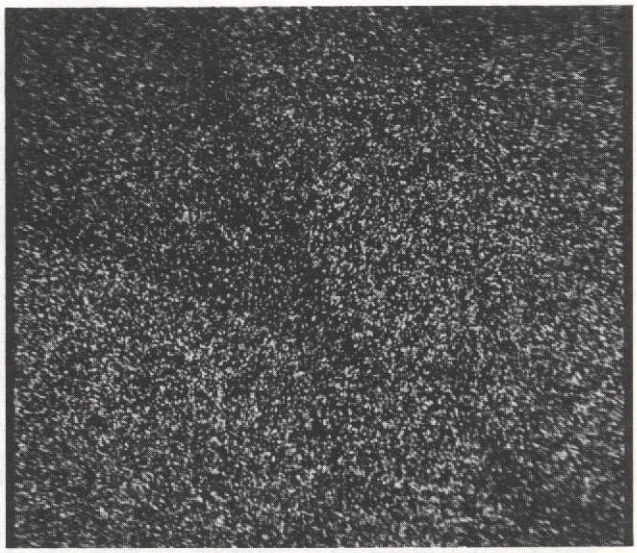

Ge

Figure 17b

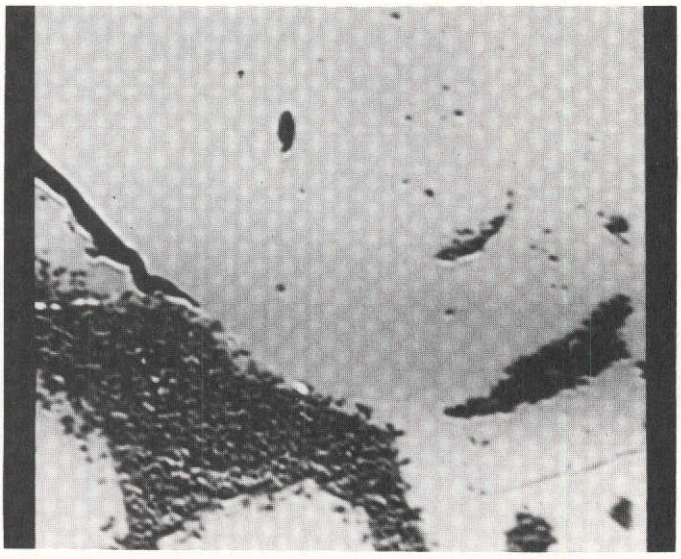

280 X

Al

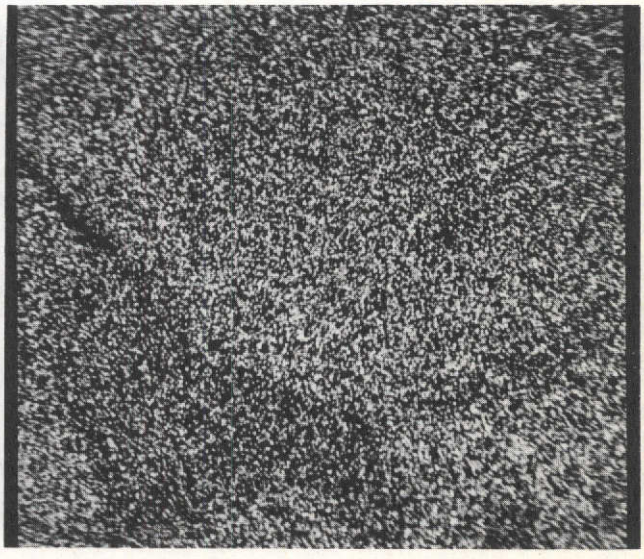

Ge

Figure 17c

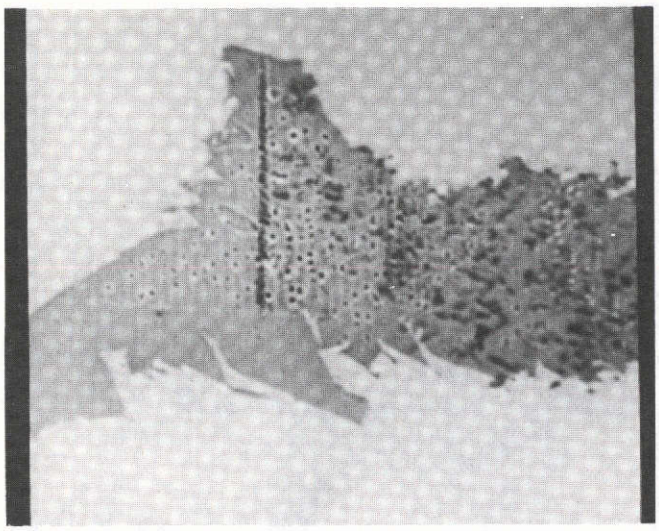

280 X

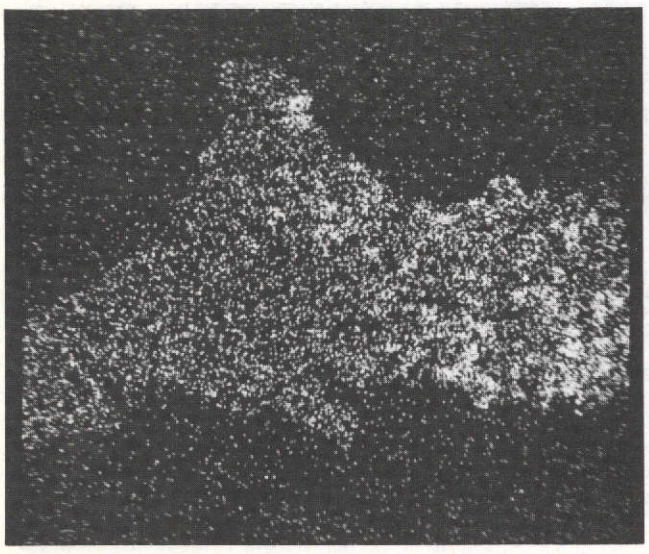

Al

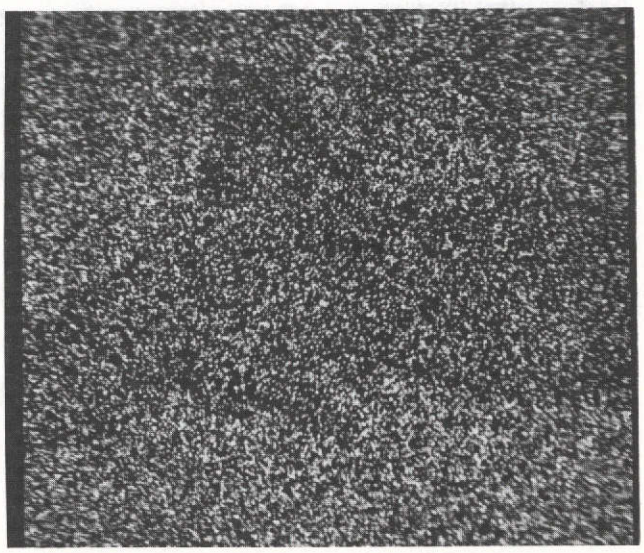

Ge

Figure 17d

Although an attempt to dissolve surface glass was made, it is not known if it was completely successful. Therefore a small fraction of the Al and B measured concentrations could still reflect a surface concentration. As shown in Table 12, the amount of Al and B in the crystal is quite low, amounting to less than .2% for each analyzed. It is expected that further optimization of the growth parameters should result in a substantial reduction in their respective concentrations.

4. Measurement of Optical Rotation

A thin polished section, about 60 mil in thickness, which included seed and surrounding growth was evaluated by means of optical rotation measurements. A He-Ne CW laser of 6330 $\mathring{A}$ wave length was employed. The extent of rotation of plane polarized light by the $Bi_{12}GeO_{20}$ seed was measured, as $+25^{\circ}$.* In the region of imperfect growth, which included entrapped glass, almost complete depolarization of the incident light occurred preventing any meaningful results from being obtained.

An attempt was made to measure optical rotation of a well-developed crystal which had grown near the platinum wire support. After preparing a thin polished section, it was discovered that depolarization was not as great and that a general nulling of the background could be achieved. Because the null was not sufficiently sharp, absolute values were not obtainable but good repeatability existed. The values obtained ranged from $+5^{\circ}$ to $+15^{\circ}$ * depending on location. The somewhat reduced values of optical rotation for the growth compared to the seed probably

*Angular Displacement not Normalized for Thickness

reflect composition variations such as deficiency of Ge and glass incorporation.

5. Etching Studies of $Bi_{12}GeO_{20}$ and $0.75Bi_2O_3 \cdot 0.5Al_2O_3 \cdot B_2O_3$ Glass

The comparative reactivities of $Bi_{12}GeO_{20}$ and the glass composition $0.75\ Bi_2O_3 \cdot 0.5Al_2O_3 \cdot B_2O_3$ (FF-96) employed in $Bi_{12}GeO_{20}$ crystal growth toward various chemical reagents has been determined with a view to effecting a chemical separation of the crystal from the physically incorporated glass. The glass was poured in a fluid state at 1100°C through steel rollers. Phase separation was evident as well as a large temperature coefficient of viscosity which resulted in the melt setting up rapidly. Nevertheless amber colored glass ribbon was obtained. Specimens of the glass and $Bi_{12}GeO_{20}$ crystals were immersed in hot (70°C) concentrated acidic and basic solutions for various lengths of time.

It was found that HNO_3 and HCl solutions readily dissolved all specimens. There was no apparent reaction with hot glacial acetic acid even after a 24 hour exposure. A solution of H_3PO_4 produced a white adherent coating over most of the glass surface after 24 hours with no apparent attack of $Bi_{12}GeO_{20}$. Hot aqueous NaOH solution (50% by weight) transformed the surface of the glass within 20 minutes to a yellow powdery

material, which could be readily removed by agitation in an ultrasonic bath. The comparable $Bi_{12}GeO_{20}$ sample experienced no weight loss after a similar duration exposure as well as after 24 hour immersion. Since hot concentrated alkali seemed best suited to selective removal of glass in combination with $Bi_{12}GeO_{20}$ it was tested on material taken from the concentrated fused solvent system - 70 w/o $Bi_{12}GeO_{20}$ - 30 w/o $0.75Bi_2O_3 \cdot 0.5Al_2O_3 \cdot B_2O_3$ composition (FF-96) on a platinum wire loop. While an overall lighter color was produced in the immersed sample it remained quite hard and only vigorous scraping with a sharp instrument could dislodge material from the surface. The larger concentration of $Bi_{12}GeO_{20}$ in intimate contact with the glass probably served to anchor whatever glass had reacted, as well as to act as a barrier to attack of subsurface glass. In conclusion, a satisfactory etchant was not found.

D. Results of Studies of $Bi_{12}GeO_{20}$ Seeded Growth

It is possible to conclude from studies of seeded growth of $Bi_{12}GeO_{20}$ from viscous glass solvents the following:

(1) $Bi_2O_3 \cdot 2\text{-}xB_2O_3 \cdot xAl_2O_3$ is a more satisfactory solvent than $Bi_2O_3 \cdot 2B_2O_3$ for growth of $Bi_{12}GeO_{20}$ because it provides for reduced segregation of Ge near seed-growth interface, enhanced crystallinity and because of the improved viscosity-temperature relationship which results in a more expanded growth range.

2) The phases which recrystallize upon low temperature heat treatment during DTA study appear to be Bi_2O_3 or GeO_2 which are stabilized as glasses during rapid quenching from the melt.

3) During seeded crystal growth by slow cooling from elevated temperatures the only phase detected is $Bi_{12}GeO_{20}$.

4) Microprobe analysis in combination with emission spectroscopy is a very useful tool for detecting variations in stoichiometry which may exist in the crystal.

5) Utilizing an 80 w/o $Bi_{12}GeO_{20}$-20 w/o $.75Bi_2O_3 \cdot 5Al_2O_3 \cdot B_2O_3$ composition with a $2^{\circ}C$/hr. cooling rate in the range of $795^{\circ}C$ to $767^{\circ}C$ provided $Bi_{12}GeO_{20}$ crystal growth which has been nucleated by the seed crystal.

6) Imperfections typical of solvent growth under non-ideal conditions have been identified and include the presence of occluded glass, hopper growth, deviations from stoichiometry which increase with distance from the seed, as well as a multiplicity of crystallographic orientations in the crystal.

E. Comparison of Growth in Viscous Glass Solvent with that from Melt and Relation to Convectionless Growth in Space

Microscopic examination of $Bi_{12}GeO_{20}$ single crystals grown from the melt by Czrochalski technique has been carried out with a view of determining the nature and number of convection related defects which are present for comparison with imperfections appearing in crystals of $Bi_{12}GeO_{20}$ grown from a viscous glass solvent, in which case convection is substantially reduced. Since in each instance the growth parameters were not optimized the number of defects was quite large. A considerable number of growth striations or bands can be observed in Figure 18, which represents a chemically etched (1:20 HCl:H_2O by vol.) section of $Bi_{12}GeO_{20}$ crystal pulled vertically from the melt. Striations are parallel bands that show up as local index changes, color changes, or birefringence changes in the crystal. They are generally parallel to crystal faces and represent changes in composition of the crystal. These can be either compositional changes of major components or of trace impurities. The frequency of the striations corresponds approximately with the observed period for temperature fluctuation during growth [9]. Precise temperature control is the way it is usually minimized.

In the $Bi_{12}GeO_{20}$ crystal grown from glass solvent, segregation, glass occlusion and random nucleation have been detected (see Figure 11). These are believed to be the result of too rapid a cooling rate during growth as well as temperature non-uniformity in the region of the crystal. However there is no evidence for the presence of growth strations, indicating that

27 X

Figure 18. Striations Observed in $Bi_{12}Ge0_{20}$ Crystal Grown from Melt by Czochralski Method. (Compare with Figure 11A Showing Absence of Striations in $Bi_{12}Ge0_{20}$ Grown from Glass Solvent.)

although compositional variations do occur as shown by microprobe analysis, the viscous glass solvent apparently dampens the thermal vibrations which give rise to periodic compositional changes. Since the microgravity environment of space would largely eliminate the existence of convection related defects during crystal growth, it is reasonable to assume that as in the case of growth in a viscous solvent there would be an absence of growth striations.

---

(9) A. B. Chase and W. R. Wilcox, J. Am. Ceram. Soc. 50, 332, (1967)

F. FUTURE WORK ON $Bi_{12}GeO_{20}$

It is suggested that problems associated with variable Ge content in the growth and presence of extensive glass entrapment regions could be largely eliminated by growing with a much lower rate of slow cooling than the present $2^{\circ}C/hr$ *. Proper precautions should be taken to eliminate temperature gradients within the melt, as well as temperature fluctuations which could cause premature solidification in regions further from the seed. In addition, the glass composition which appears to give the simplest DTA pattern should be examined as a means of minimizing non-stoichiometry in the crystal. Studies to develop a suitable discriminating etch which would enable microscopic observation of growth related defects such as dislocation networks and impurity clusters should be pursued as well.

---

* Perry [4] has indicated for growth of $(BaPb)TiO_2$ crystals from a $BaO \cdot PbO \cdot B_2O_3$ glass that a slow cooling rate about $0.2^{\circ}C/hr$. gave the most perfect crystals.

III. LEAD GERMANATE

$Pb_5Ge_3O_{11}$ is a congruent melting ferroelectric compound which displays considerable optical activity[1,2]. It has important applications in devices such as light switches, light modulators and second harmonic generators. The optical rotary power along the ferroelectric "c" axis can undergo a change in sense by the reversal of the spontaneous polarization below the Curie temperature at 177°C. It has been shown to belong to a trigonal crystal class, the measured constants of the hexagonal unit cell at room temperature being $a = 10.251$ Å and $C = 10.685$ Å. It has been selected as a candidate for space processing; switching time variability due to crystal inhomogeneities should be substantially reduced as a result of growth in the microgravity environment of space.

$Pb_5Ge_3O_{11}$ crystals were previously grown in the Space Sciences Laboratory from the melt by a Czochralski technique in which nucleation was initiated on a thermocouple bead. Crystals up to 10 mm in length and 25 mm^2 cross section were produced with the predominant growth direction being the $\langle 100 \rangle$. The ferroelectric Curie temperature was measured and found to be between 172°C - 179°C, which is in close agreement with other reported values for this crystal. These crystals served as seed material in studies of crystallization from glass solvents.

---

(1) H. Iwasaki and K. Sugii, Appl. Phys. Lett. 19, 92 (1971)
(2) T. Yamada, H. Iwasaki and N. Niizeki, J. Appl. Phys. 43, 771 (1972).

A. Solvent Development

Earlier studies focused on developing a solvent which was chemically compatible, had a high solubility for lead germanate and had sufficiently high viscosity to reduce convective related growth defects. Use was made of the common-ion principle to reduce possible solvent contamination of the crystal. Initial results based on studies of devitrification of a glass-ceramic indicated that $PbO \cdot 2B_2O_3$ would be a suitable solvent for growth of $Pb_5Ge_3O_{11}$ single crystals. Because of improved viscosity and surface tension resulting from addition of Al_2O_3 to the glass composition, the nucleation and crystallization properties of compositions incorporating Al_2O_3 additions were also studied. The following compositions were studied:

FF-74	80 w/o $Pb_5Ge_3O_{11}$ - 20 w/o $PbO \cdot 2B_2O_3$
FF-75	90 w/o $Pb_5Ge_3O_{11}$ - 10 w/o $PbO \cdot 2B_2O_3$
FF-102	80 w/o $Pb_5Ge_3O_{11}$ - 20 w/o $PbO \cdot 0.5Al_2O_3 \cdot 1.5B_2O_3$
FF-103	90 w/o $Pb_5Ge_3O_{11}$ - 10 w/o $PbO \cdot 0.2Al_2O_3 \cdot 1.8B_2O_3$
FF-104	80 w/o $Pb_5Ge_3O_{11}$ - 20 w/o $PbO \cdot 0.2Al_2O_3 \cdot 1.8B_2O_3$
FF-105	87 w/o $Pb_5Ge_3O_{11}$ - 13 w/o $PbO \cdot 0.2Al_2O_3 \cdot 1.8B_2O_3$

A summary of the results of seeded growth runs is presented in Table 13.

TABLE 13.

$Pb_5Ge_3O_{11}$ CRYSTAL GROWTH EXPERIMENTS

Composition	Nucleation Condition	Growth Conditions	Wt. of Growth	Growth Characteristics
FF-74-5	Limited nucleation at about 606°C	612°C, 17 hr.	2.57 g	Growth appears as yellow and glass-like. Seed appeared to have dissolved.
FF-74-6	Same	617°C, 15 hr.	.2916 g	Dendrites, as long as 3/16", formed as well as green-white mass; seed appeared to have dissolved.
FF-75-1e	At 630°C over most of surface. 654°C no surface nucleation.	654°C, 14 hr.	.1405 g	Pale yellow in color, glass-like; at high mag. observed hexagonal crystals in glass matrix; seed appeared to have dissolved.
FF-75-2A	Nucleation observed just below 640°C	640°C, 22 1/2 hr.	.1159 g	Yellow glass-like material fills space between platinum wires, seed appeared to have dissolved; dendrites observed growing out of glass toward surface of melt, as well as on wire.
FF-102-1A	No nucleation down to 506°C	555°C, 18 hr.	.4141 g	Appeared as if growth on seed had occurred; but not very crystalline.
FF-102-1B	Same	610°C, 15 hr.	.2198 g	Greenish-yellow, glassy in appearance, appeared to be growth on seed
FF-102-1C	Same	609°C, 15 hr. no seed, only pt. wire		Glass on wire, Laue showed amorphous pattern

TABLE 13 (Cont.)

Composition	Nucleation Condition	Growth Conditions	Wt. of Growth	Growth Characteristics
FF-103-1A	Nucleation at about 590°C	597°C, 13 1/2 hr.	.5864 g	Entire melt had solidified, couldn't remove seed; took up in temp. about 20°C and removed seed. Yellow-brown growth on seed had well-developed faces on sides away from seed. Also yellow-white glassy material.
FF-104-1A	No nucleation observed during melting and cool down			
FF-105-2A		585°C → 578°C using cam (2°/hr.)	--	Most of melt had solidified, couldn't remove seed.
FF-105-2B		624°C → 618°C using cam (2°/hr.) cam had shut off after 3 hour held at 618°C, 11 hr.	.78 g	Tip of seed was glassy with rounded sides and edges Yellow-white growth on seed, many large dendrites in vicinity of wire.

B. Characterizing Crystal Growth

Microscopic examination of the growth was undertaken. Photographs of interesting features such as the presence of hexagonal shaped crystals in a glass matrix, FF-75-1e, (Figure 19) as well as dendritic formations (Figure 20) are presented. One dendrite almost 3/16" inches in length from FF-74-6 was observed to have extensive pitting and strain.

Debye-Scherrer x-ray powder diffraction studies were carried out on representative growths to determine the degree of crystallinity and to identify the phase present. The most important observation was that in every case the x-ray diffraction pattern was weak indicating the presence of only a small amount of crystalline material. The faintness of the x-ray diffraction patterns made positive identification difficult. The data obtained for several of the growths is given in Table 14.

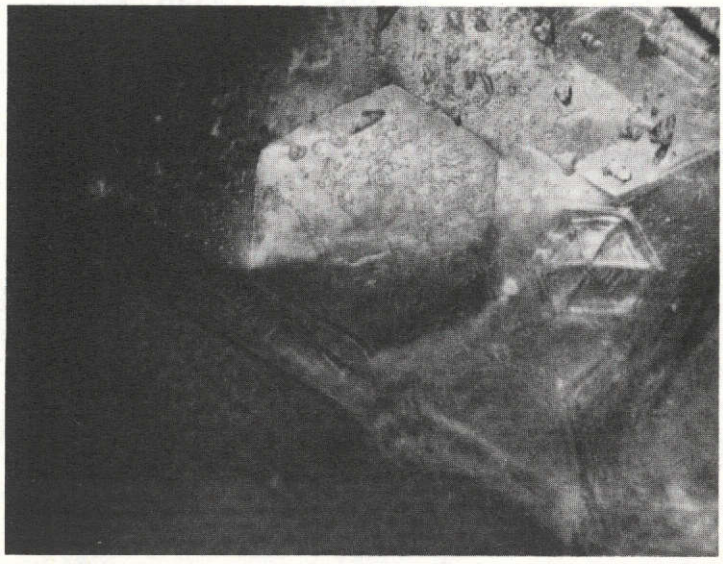

120 X

Figure 19. Presence of Hexagonal Shaped Crystals in a Glass Matrix, FF-75-1e. (Refer to Table 13 for Nucleation and Growth Conditions.

Figure 20a. Dendritic Growth FF-74-6

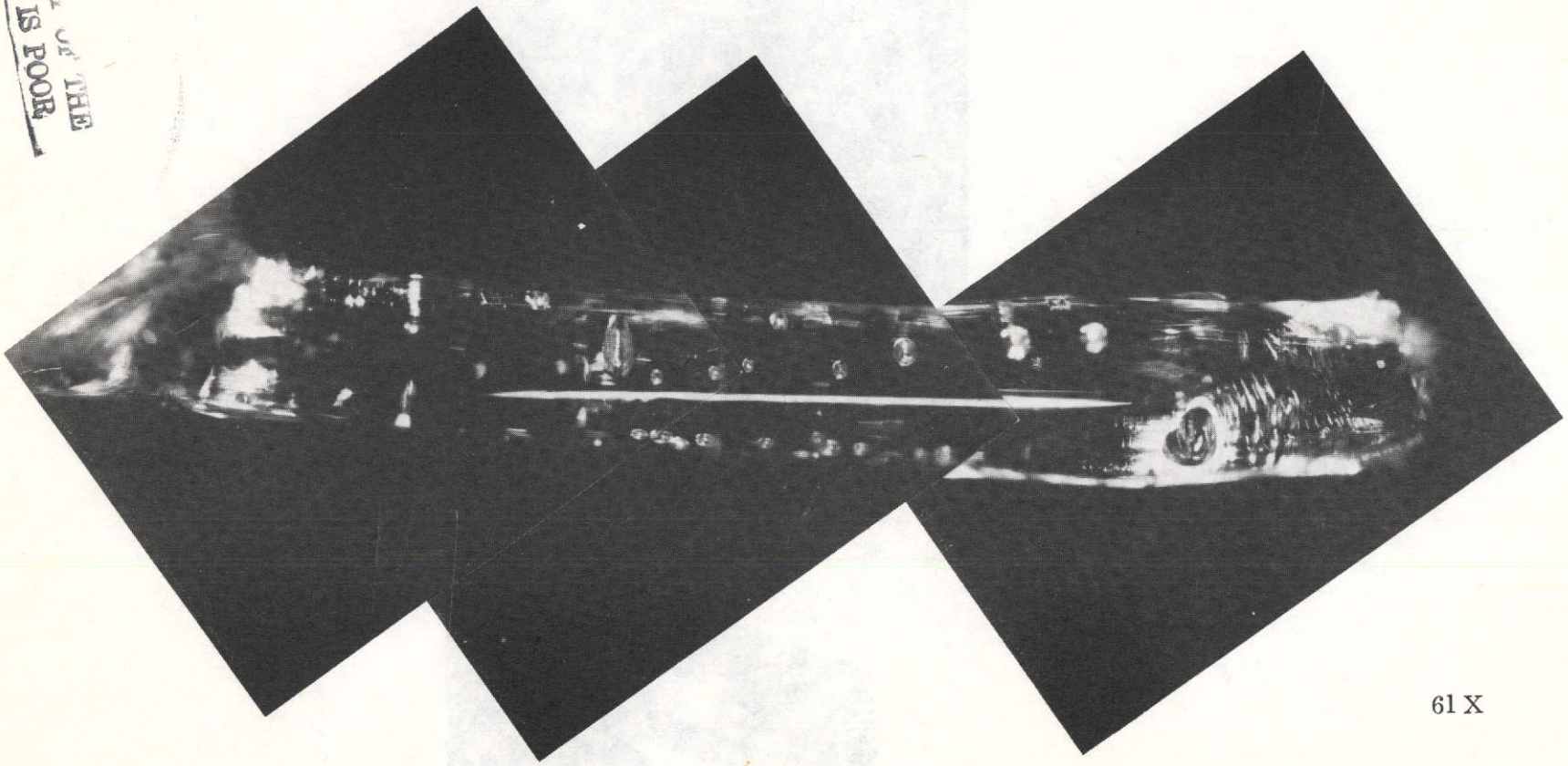

61 X

Figure 20. Presence of Dendritic Formations in FF-74-6. (Refer to Table 13 for Nucleation and Growth Conditions.)

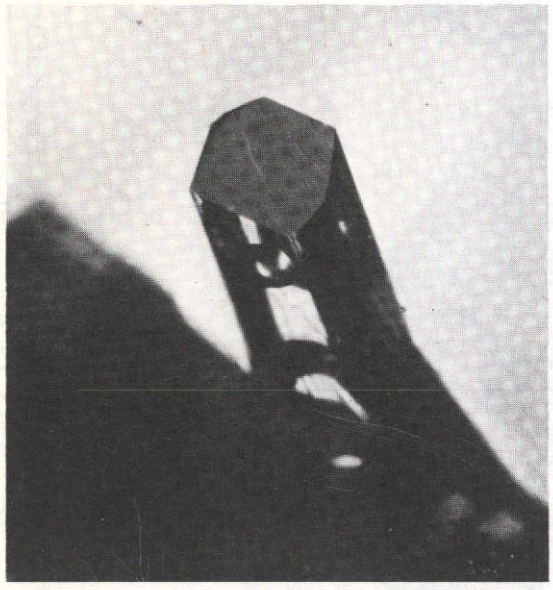

60 X

Figure 20b

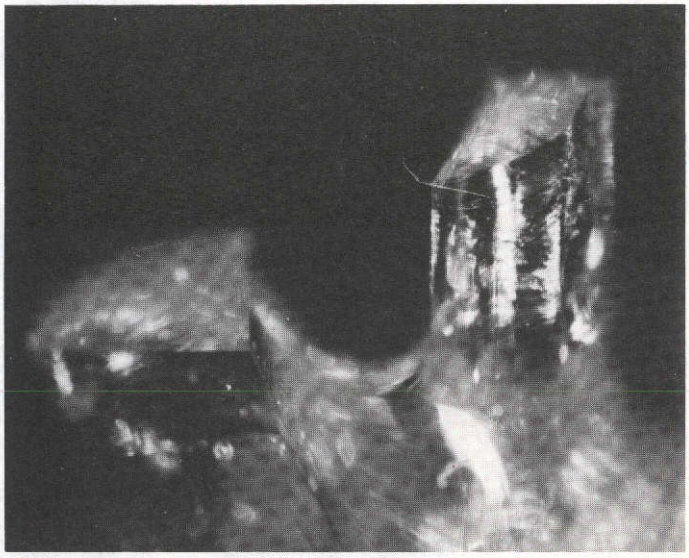

60 X

Figure 20c

TABLE 14. X-RAY DIFFRACTION DATA FOR SEEDED GROWTH OF $Pb_5Ge_3O_{11}$

$Pb_5Ge_3O_{11}$ seed		Literature data[3] $Pb_5Ge_3O_{11}$		FF-74-5		FF-75-2A		FF-103-1A		FF-105-2B dendrites ground up	
d	I/I_o	d	I/I_o	d	I/I_o	d	I/I_o	d	I/I_o	d	I/I_o
4.34	VW	4.439	36	4.4	not meaninful because of weakness of lines						
3.90	VVVW										
3.64	VVW	3.707	9	3.64		3.62					
3.50	VVW	3.561	9					3.50	VVVW	3.57	weak
		3.351	50			3.38	S			3.37	pattern
3.28	W	3.302	15	3.27				3.28	VVW		
3.16	W	3.197	32	3.15		3.10		3.125	W		
								3.07	VW	3.04	
2.91 (Bd)	S	2.949	100	2.92		2.90		2.91 (B)	M		
		2.921									
2.81	W	2.84	23					2.82	VVW		
		2.779	4								
2.42	VVVW	2.494	4			2.36	M			2.37	
		2.442	4								
		2.392	3							2.33	
2.20	VVVW	2.216	8					2.19	VVW		
2.07	M	2.075	19	2.07		2.08		2.06	W	2.06	
2.02	VW	2.031	9								
		2.023	9								
1.98	VVW	1.997	8								
		1.972	4								
1.92	W	1.933	12	1.92							
		1.902	8								
1.86	M	1.880	14	1.87				1.86	W		
		1.800	5								
1.77	W	1.777	5	1.77		1.74		1.77	W	1.76	
1.69	VVW	1.698	5					1.68		1.72	
1.66	VVW	1.675	8	1.64		1.67		1.66	VW	1.64	
		1.652	3								
1.58	VVW	1.626	1	1.57		1.57		1.58	W	1.57	
		1.592	8								
1.56	VVW										
1.515	M			1.52				1.51	W		
				1.46							
1.41	VVW							1.465	VW		
1.40	VVW				1.40	1.40		1.35	VW		
1.355	VVW			1.36		1.36					
1.345	VVW										
1.31	VVW			1.31		1.32		1.31	VW		
1.274	VVW							1.27	VW		
1.19	VVW			1.19				1.21	VVW		
1.17	VVW			1.15				1.17	WW		
1.105	VVW							1.15	VVVW		
1.062	VVW							1.103	VVW		
1.055	VVW							1.064	VVW		

(3) K. Sugii, H. Iwasaki, & S. Miyazawa, Mat. Res. Bull., 6, 503-512, 1971.

From a comparison of diffraction data the following can be concluded:

1) the $Pb_5Ge_3O_{11}$ seed crystal grown at Space Sciences Laboratory may be slightly non-stoichiometric*.

2) somewhat higher crystallinity is present in growths from the glass solvent which includes Al_2O_3.

3) the phase which appears to be present in all growths is $Pb_5Ge_3O_{11}$.

However, the greatest uncertainty in phase identity is for the dendrites of FF-105-2B. The strongest line at 2.94 Å in the pattern reported for $Pb_5Ge_3O_{11}$ is missing from diffraction data for the dendritic growth.

Electron microprobe analysis has been employed in determining the distribution of elements in the growth of composition FF-74-5. There are light and dark colored regions present and Ge is present in large concentrations in the darker areas, but is quite deficient in the light colored portions. There are no data on distribution of boron so that one can't identify the light colored areas as representing glass occlusions but this is probably the case. Pb is found to be uniformly distributed and in large concentrations as expected. The microprobe data is presented in Figure 21.

---

*High quality commercial seeds are not available because of the difficulty in growing $Pb_5Ge_3O_{11}$ from the melt. As reported, the Curie temperature of the seed crystals was in the neighborhood of 177°C.

C-2

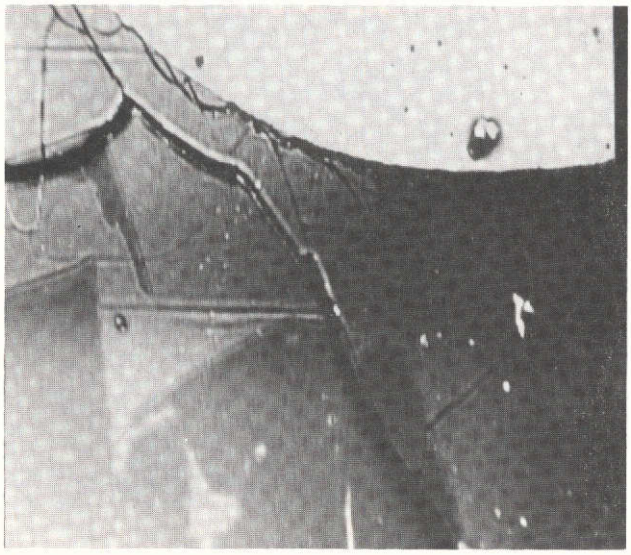

280 X

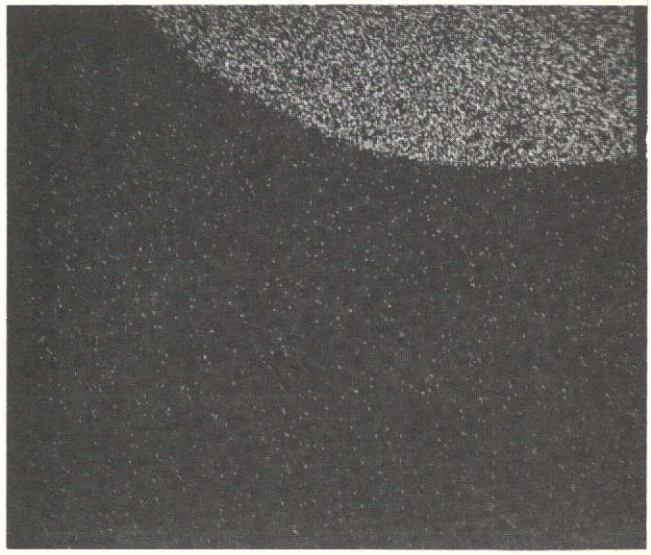

Pt

Pb

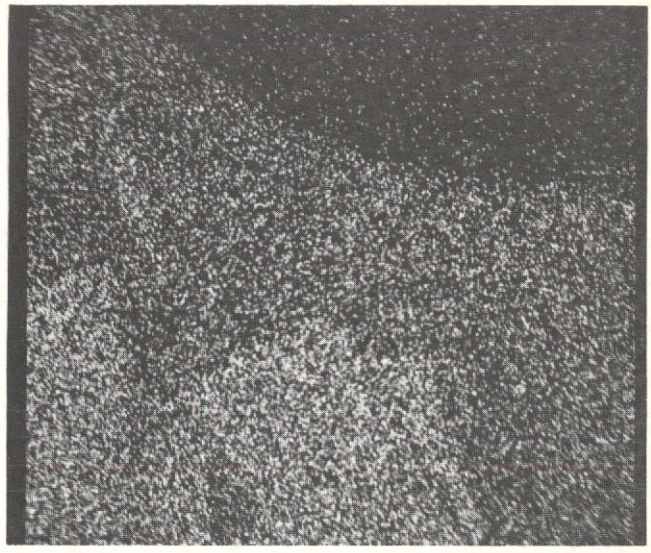

Ge

Figure 21a

Figure 21. Distribution of Elements in Growth of FF-74-5. (Refer to Table 13 for Nucleation and Growth Conditions.)

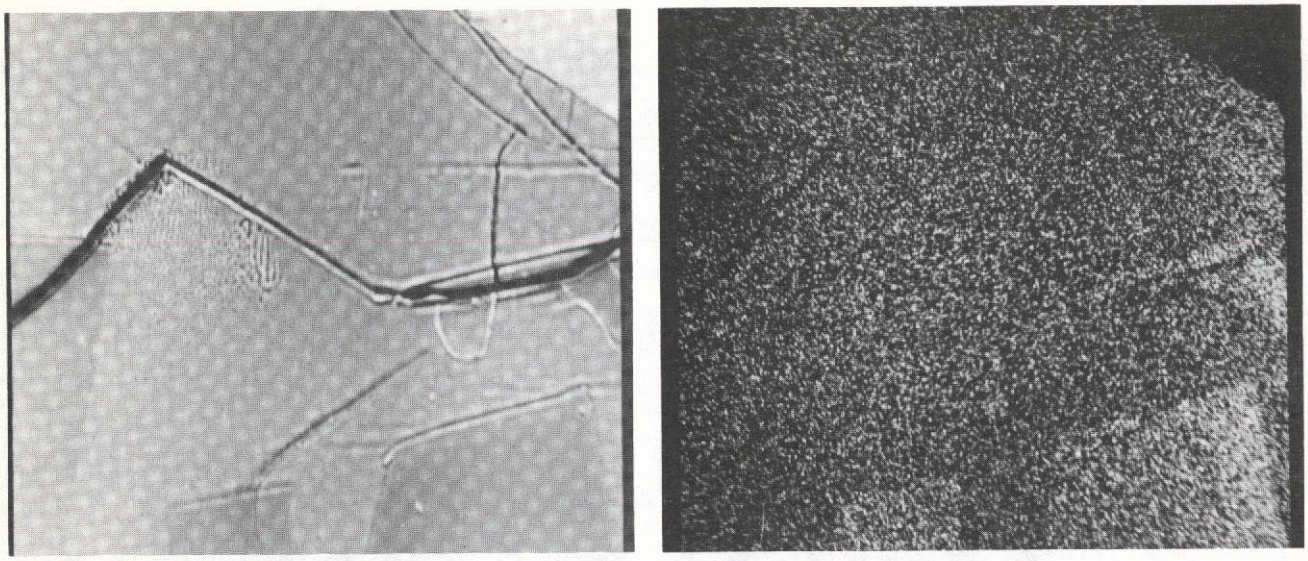

Ge

Figure 21b

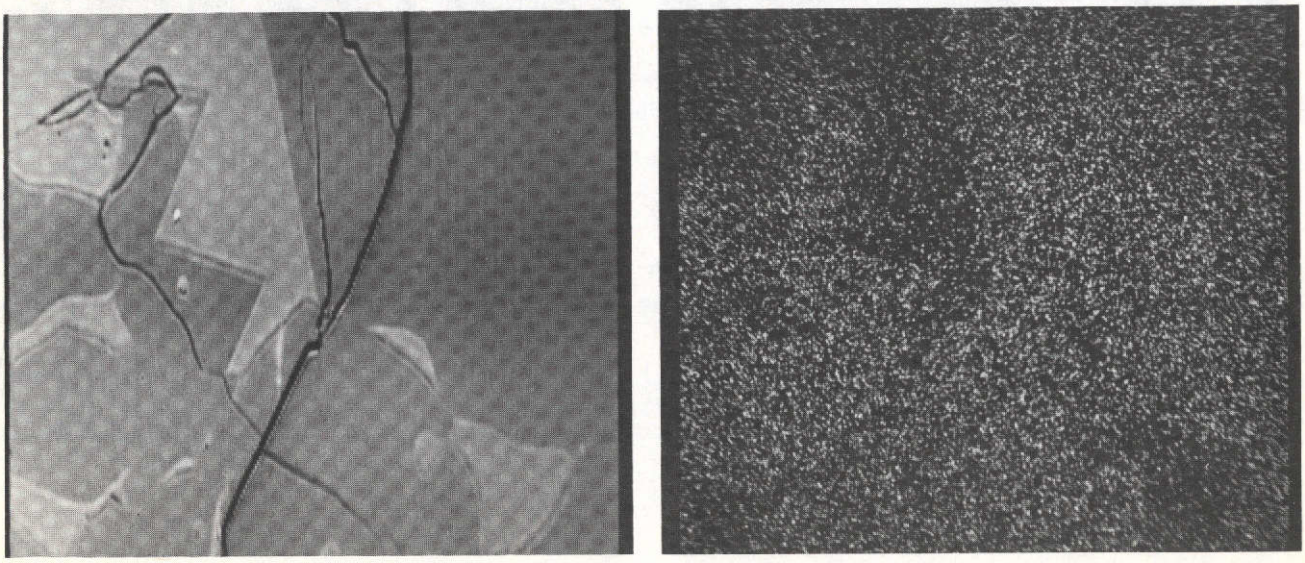

Ge

Figure 21c

280 X

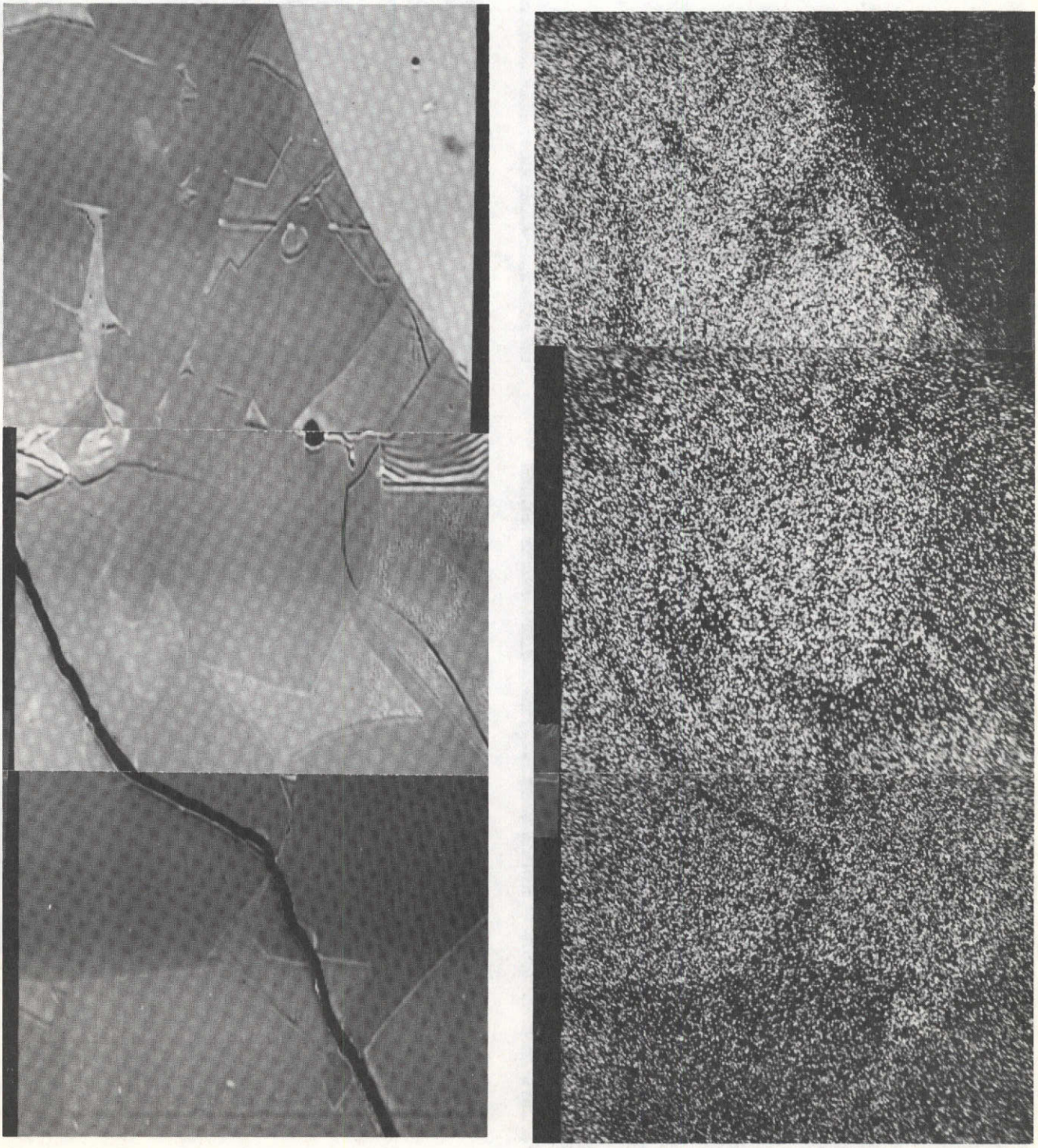

Ge

Figure 21d

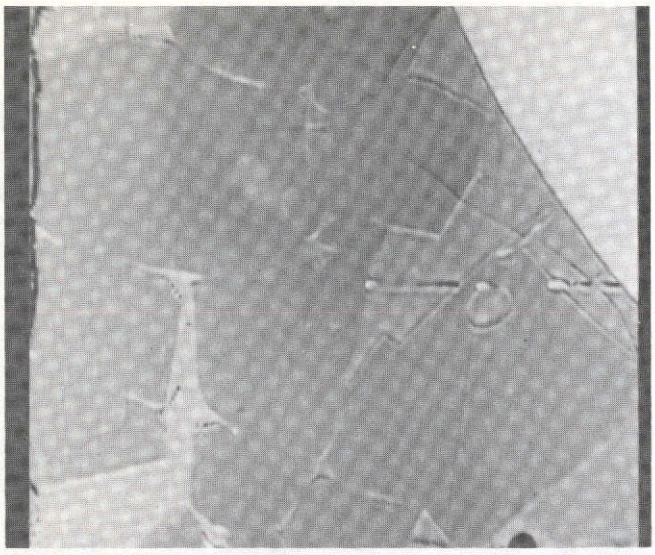

280 X

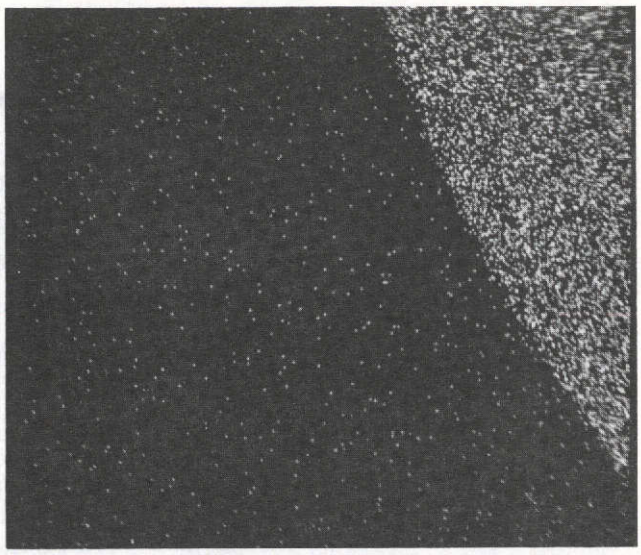

Pt

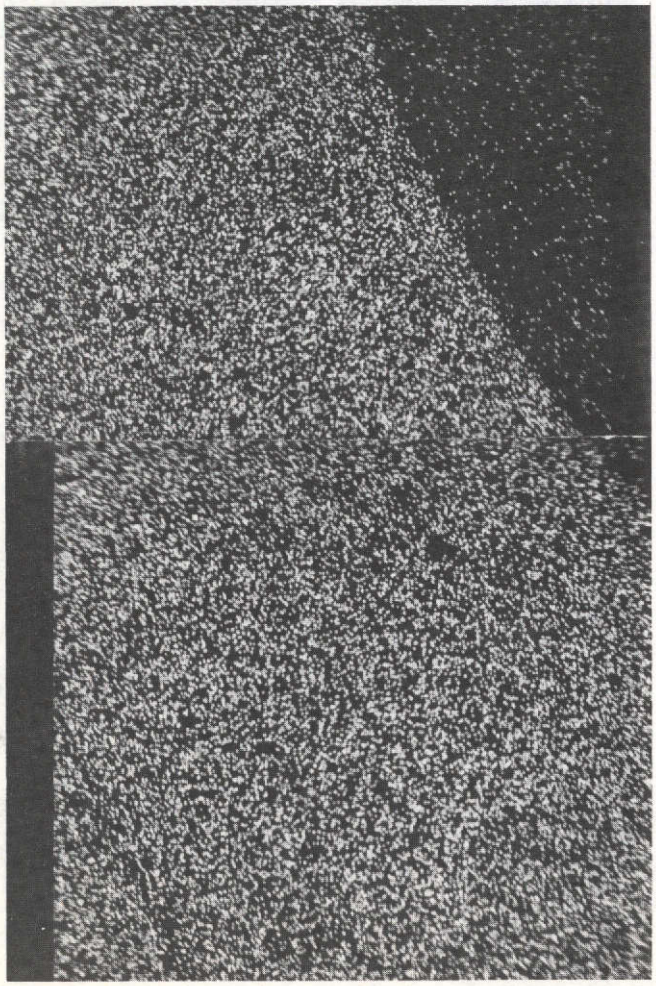

Pb

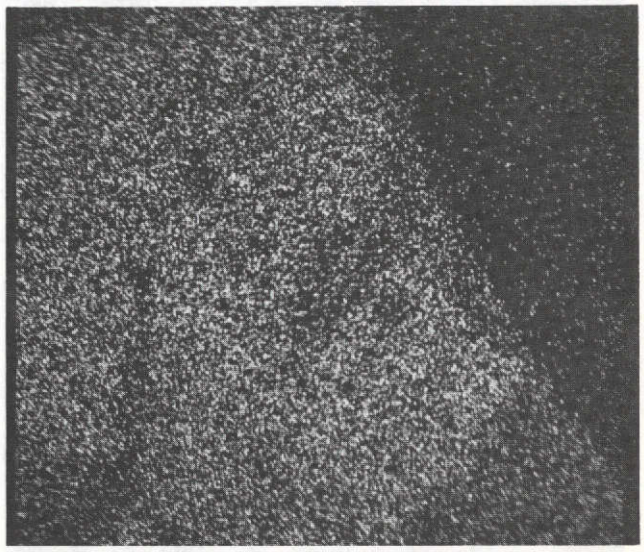

Ge

Figure 21e

However, optical rotation measurements at 6330 Å (He-Ne CW laser) were inconclusive since the crystals were semi-clear and some depolarization of the incident light occurred. A general nulling of the background could be achieved however with a range of values occurring depending on transparency.

C. Conclusions and Recommendations for Future $Pb_5Ge_3O_{11}$ Work

Conclusions and recommendations for future work are:

1) Growth from $PbO \cdot 2B_2O_3$ and $PbO \cdot 2\text{-}xB_2O_3 \cdot xAl_2O_3$ does not produce very crystalline product although greater growth and perhaps a somewhat higher degree of crystallinity results from the use of $PbO \cdot 2\text{-}xB_2O_3 . xAl_2O_3$ as glass solvent.

2) Growth from $PbO \cdot 2B_2O_3$ results in dissolution of seed crystal possibly by reaction with the melt to form a new phase. Subsequent growth then proceeds by means of random nucleation. Al_2O_3 additions apparently stabilize the glass solvent thereby providing conditions suitable for achieving crystal growth nucleated by the seed.

3) More extensive characterization is needed to determine the distribution of glass components in growth, e.g. micrprobe determination of Al as well as the need for emission spectrographic analysis of a portion of growth to determine quantitative measure of glass incorporation. This includes sectioning seed crystal and growth and using Laue techniques to determine if nucleation by seed had occurred.

4) Growth at slower rates and for longer durations might eliminate tendency to form microcrystals. Improvement in quality of seed crystal would be beneficial.

5) Preventing or minimizing the occurrence of constitutional supercooling, which is the most frequent cause of dendritic growth.

D. Preliminary Investigation of Crystal Growth/Viscosity Control Based on $Pb_5Ge_3 - xSi_x0_{11}$ as a Solvent System

The effect of incorporating silica into a glass sytem is to increase the viscosity of the melt in the seeded growth temperature range and decrease the change of viscosity with change in temperature. The result of adding Si to $Pb_5Ge_30_{11}$ in the range extending from $x = o$ to $x \approx 2$ in the series $Pb_5Ge_{3-x}Si_x0_{11}$ is to form a solid solution. The pure silicate end member does not exist.

It has been hypothesized in this study that the solid solution series might eliminate the use of viscous glass solvents containing oxides such as Al_20_3 or B_20_3. These oxides are alien to the solute, may be introduced into the $Pb_5Ge_30_{11}$ growth region and cause property deterioration through the use of the $Pb0 \cdot B_20_3$ or $Pb0 \cdot Al_20_3 \cdot B_20_3$ solvents. In contrast if Si enters the $Pb_5Ge_30_{11}$ lattice, this is beneficial since it has been reported that Si substitution for Ge enhances shorter switching times, lowers operating voltages without loss of spontaneous polarization, and lowers the melting temperature and ferroelectric Curie point [4].

For expedience the glass-ceramic approach was employed with work centering on the compositions $Pb_5Ge_2Si0_{11}$ and $Pb_5Ge_{1.8}Si_{1.2}0_{11}$ as the solutions. While $Pb_5Ge_30_{11}$ required a solvent system such as $Pb0 \cdot 2B_20_3$ (FF-75) to change the temperature-viscosity condition for

(4) W.Eysel, R. W. Wolfe and R. E. Newnham, J. Am. Ceram. Soc. 56 (4) 105 (1973).

extended glass formation, $Pb_5Ge_2Si0_{11}$ easily formed a glass by casting, roller quenching , or fiberizing. The ease of drawing fibers was ascribed to the silicate system. In comparison, roll quenching of $Pb_5Ge_{1.8}Si_{1.2}0_{11}$ resulted in a glassy product, but it was not possible to pull filament. The change of temperature-viscosity curve caused "freezing" in the orifice of the fiber furnace bushing.

In view of the aforementioned results, evaluation was directed at $Pb_5Ge_2Si0_{11}$ as the potential composition of the solution. As shown in Table 15, the differential thermal analysis reactions were found to be very similar to those shown by FF-75; each gave two observable exotherm reactions of crystallization, generally in the same temperature range. The annealing endotherms (glass transition range) were within 10°C of one another.

Crystallization schedules were derived from the DTA profiles and are listed in Table 16. The $Pb_5Ge_2Si0_{11}$ samples were crystallized at 420°C for 3 and 24 hours and 625°C for 1, 1.5, and 3 hours. The melt was also allowed to cool slowly from 750°C in a platinum boat. The samples at 420°C were still transparent, but x-ray diffraction showed some crystallization. This implies that the crystallites are 0.2 microns and less in size. The samples crystallized at 625°C (1 hour)

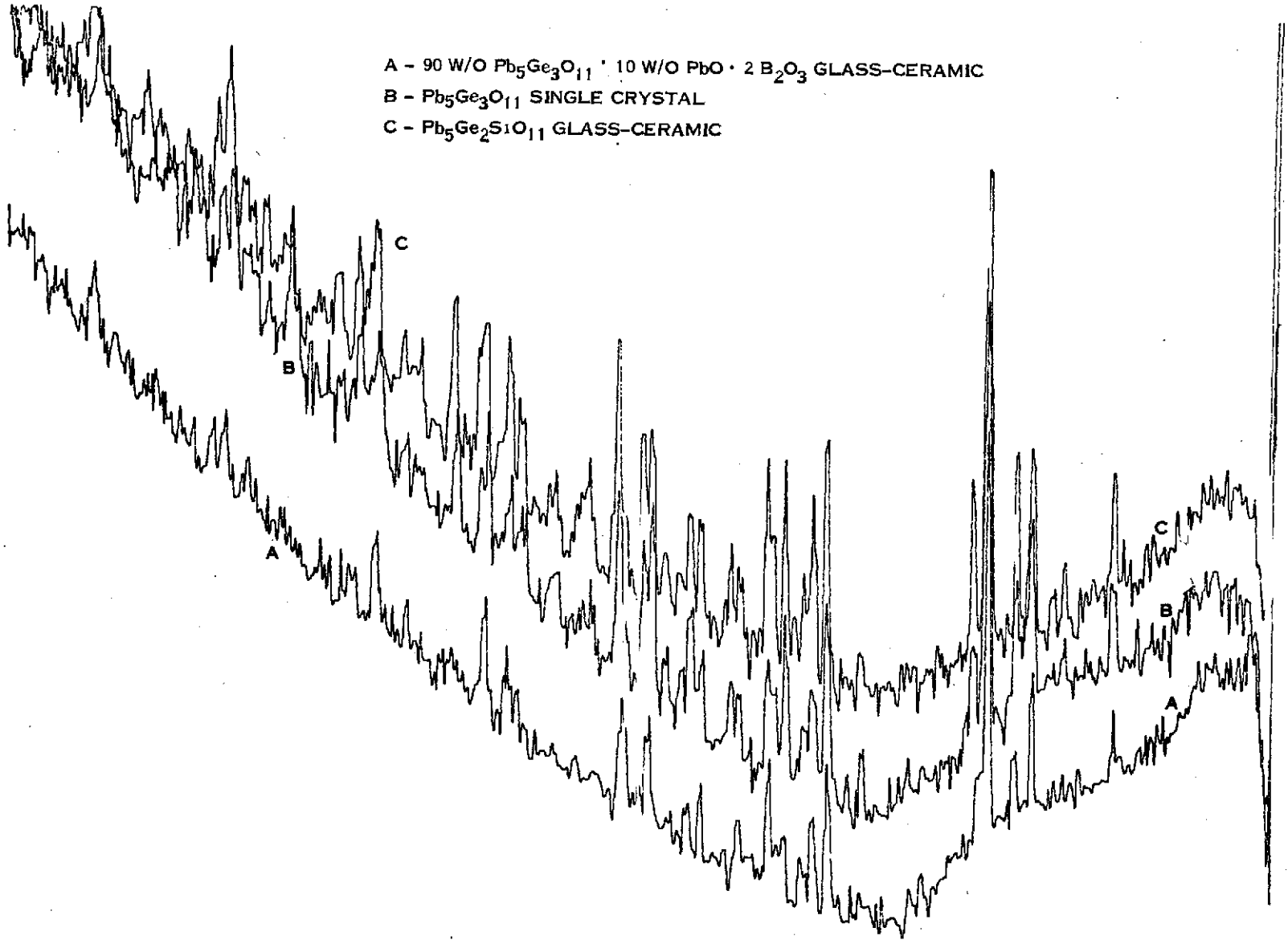

Figure 22. Densitometer Tracings of the Debye-Scherrer X-ray Films for (A) $Pb_5Ge_3O_{11}$ Glass Solvent FF-75 (heat treated 300°C - 3 hrs.; 400°C - 2 hrs.); (B) $Pb_5Ge_3O_{11}$ Single Crystal Grown from Melt; and (C) $Pb_5Ge_2SiO_{11}$ Glass Solvent (heat treated 625°C - 1 hr.).

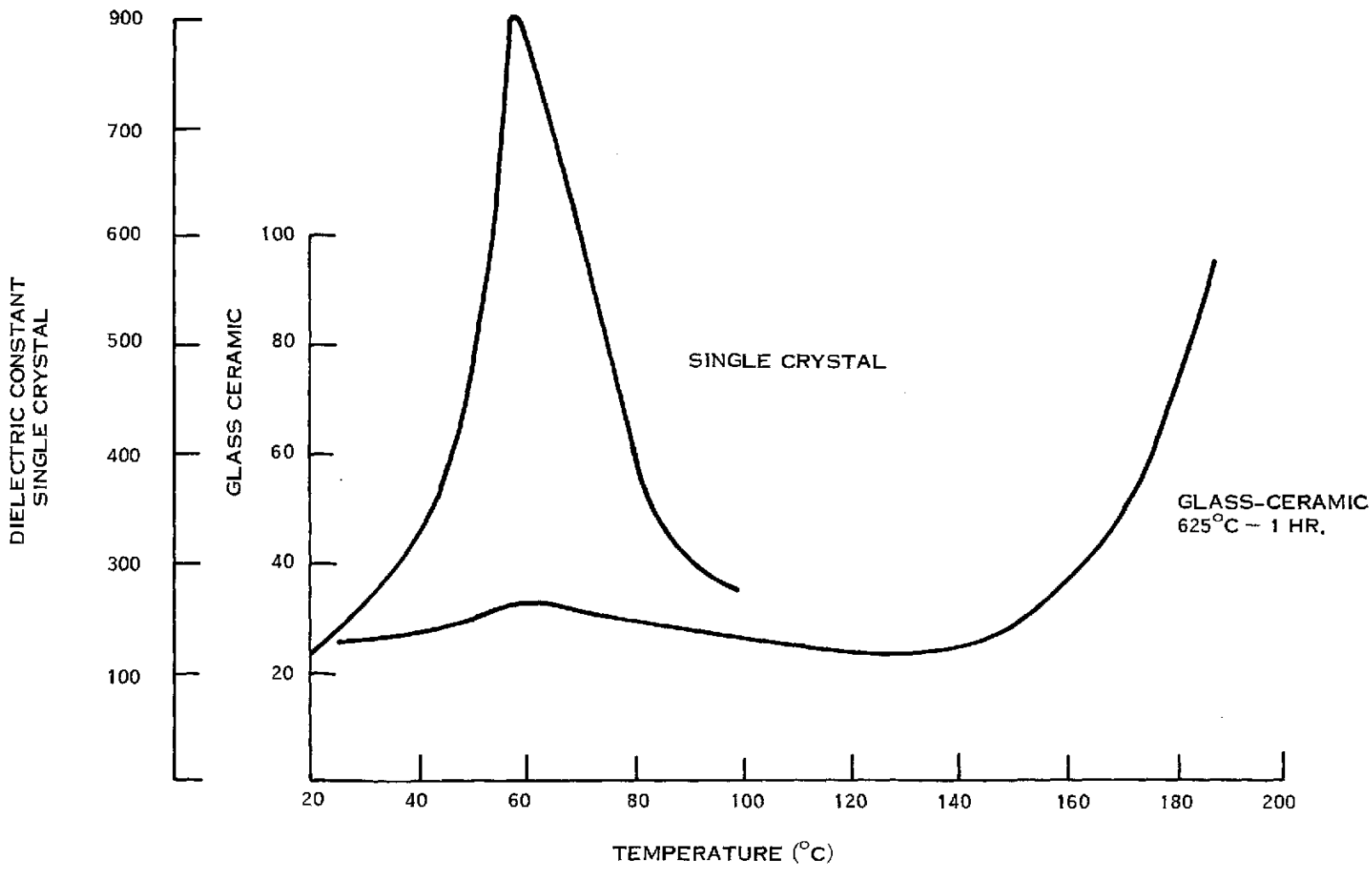

Figure 23. Dielectric-Constant Temperature Profiles at 1kHz of (A) Single Crystal $Pb_5Ge_2Si0_{11}$ and (B) $Pb_5Ge_2Si0_{11}$ Glass Solvent (heat treated 625°C - 1 hr.)

showed a well-developed crystal structure. The major features matched the key peaks of crystallized FF-75 and the melt-grown $Pb_5Ge_3O_{11}$ seed crystals. This can be seen in the densitometer tracings of the Debye-Scherrer films shown in Figure 22.

The dielectric constant profile of the $Pb_5Ge_3O_{11}$ samples crystallized at 625°C for 1 hour showed a Curie temperature at between 58 and 61°C, which corresponds to the 60°C value reported for single crystal $Pb_5Ge_2SiO_{11}$ [5] The profiles are compared in Figure 23 at 1 kHz. Although the room temperature dielectric constant is 25 as compared to 100 for the single crystal, the profiles are similar. The low dielectric constant indicates incomplete crystallization and small crystallite size of 1μ and less.

The Curie temperatures of the dielectric constant-temperature profiles of the crystallized glasses are tabulated in Table 16 as a function of crystallization schedule. Samples crystallized at 420°C showed no Curie point. Samples held at 625°C for longer soak periods showed a decrease in Curie temperature with soak time. This would tend to indicate that a phase conversion is resulting wherein more Si is entering the $Pb_5Ge_3O_{11}$ structure. Using the platinum boat as the bottom electrode, the slowly cooled crystallized melt had a Curie temperature of 52°C.

---

(5) H. Iwasaki, S. Miyazawa, H. Koizumi, K. Sugii, and W. Niizelri, J. Appl. Phys. 43 (12) 4907, December 1972.

The optical-rotation of the glass-ceramics was measured with a He-Ne CW laser at 6330 Å. The transparent glass ceramics (crystallite sizes of 0.2 microns and less) are crystallized in the vicinity of 400°C. Prior to measurement, their transparency was determined from their infra-red spectra. The results are as follows:

$Pb_5Ge_2Si0_{11}$	14 mil ribbon	70% transmission to 5 microns	Cutoff at ≈9 microns
$Pb_5Ge_{1.8}Si_{1.2}0_{11}$	85 mil sample	45% transmission to 4 microns	Cutoff at ≈5 microns

The optical rotation measurements are shown in Table 17. The low temperature crystallized samples showed a very clear null, but little or no optical rotation. The higher temperature samples, which showed a Curie temperature , were completely depolarized. The optical rotation of $Pb_5Ge_30_{11}$ has been reported to decrease from the Si replacement for Ge. This may help to explain the results in part.

In conclusion, the $Pb_5Ge_3Si_20_{11}$ would appear to be the most suitable composition as a $Pb_5(Ge,Si)_30_{11}$ solution for seeded $Pb_5Ge_30_{11}$ growth. While the glass-ceramic approach showed that the correct stoichiometry can be attained (Curie temperature of 58-61°C after 625° after 1 hour), more silicon went into the $Pb_5Ge_30_{11}$ structure with time at high temperature, even in the solid state (as indicated by Curie temperature change at longer soak times at 625°C). This may mean that the Ge/Si distribution will vary

across the growth region on a $Pb_5Ge_3O_{11}$ seed using the $Pb_5Ge_2SiO_{11}$ solution. The first step in future work with the $Pb_5Ge_3O_{11}$ seed/ $Pb_5Ge_2SiO_{11}$ solution system would be determination of this distribution.

TABLE 15

DIFFERENTIAL THERMAL ANALYSIS REACTIONS

IN $Pb_5Ge_2SiO_{11}$ GLASS

Composition	Heating Rate (°C/min.)	Endotherm (°C)	Major Exotherm (°C)	Minor Exotherm (°C)
$Pb_5Ge_2SiO_{11}$	10	340	400	560-570
	20	350	425	560
90 w/o $Pb_5Ge_3O_{11}$ 10 w/o $PbO \cdot 2B_2O_3$ (FF-75)	10	350	450	510

TABLE 16

FERROELECTRIC CURIE TEMPERATURES AS A FUNCTION OF CRYSTALLIZATION SCHEDULE

Composition	Crystallization Schedule	Curie Temperature (°C)
$Pb_5Ge_3O_{11}$ [1]	Single Crystal	177
$Pb_5Ge_2SiO_{11}$ [2]	Single Crystal	60
	420°C, 3 hr. soak	None
	420°C, 24 hr. soak	None
	625°C, 1 hr. soak	58-61
	625°C, 1.5 hr. soak	9
	625°C, 3 hr. soak	-15
	750°C, (cooled in platinum boat)	52
$Pb_5Ge_{1.8}Si_{1.2}O_{11}$ [2]	Single Crystal	18
	600°C, 18 hr. soak	12

1. H. Iwasaki, et al
2. W. Eysel , et al

TABLE 17

SUMMARY OF OPTICAL ROTATION MEASUREMENTS

Composition	Temperature (^{o}C)	Thickness mm	Result
$Pb_5Ge_2Si0_{11}$	625	0.4	no null; depolarized
	450	0.4	no null; depolarized
	420	0.4	no null; depolarized
$Pb_5Ge_{1.8}Si_{1.2}0_{11}$	600	0.4	no null; depolarized
90 w/o $Pb_5Ge_30_{11}$	410	5	null; little if any rotation
10 w/o $Pb0 \cdot 2B_20_3$ (FF-75)	340	5	same
90 w/o $Pb_5Ge_2Si0_{11}$	400	2.1	null; little if any rotation
10 w/o $Pb0 \cdot 0.5Al_20_3 \cdot Si0_2$	440	2.1	no null; depolarized

IV. POTASSIUM TANTALATE-NIOBATE CRYSTAL GROWTH

Crystals with a tantalum to niobium ratio of 0.65/0.35 have a very large quadratic electro-optic effect in the vicinity of room temperature. This makes it especially attractive for applications involving modulation, switching or deflection of light beams. For this purpose sizable crystals of optical quality are required. $K(Ta_{.65}Nb_{.35})O_3$ crystals have been grown by Bonner et al [1] by means of the Kyropoulos method using seed rotation and by Wilcox and Fullmer [2] by Czochralski and floating crystal technique. Such crystals were observed to have defects which included striations, variation in the Ta/Nb ratio and also in K_2O content, milky areas, bubble pipes and large amounts of thermal strain. This material has been selected as a suitable candidate for space processing and studies have been initiated which would lead to growth of crystals in a glass solvent.

A. Solvent Development

An evaluation of potassium silicate glass as a potential solvent for seeded growth of $KTa_{.65}Nb_{.35}O_3$ crystals was begun.

---

(1) W. A. Bonner, E. F. Dearborn and L. G. VanUited, Amer. Ceram. Soc. Bull., 44 (1) 9-11 (1965).

(2) W. R. Wilcox and L. D. Fullmer, J. Am. Ceram. Soc. 49 (8), 415-418 (1966).

Compositions were prepared in which the K_2O to SiO_2 molar ratio was varied including 1:1, 1:1.5, and 1:2 respectively in a fixed 50 w/o KTN - 50 w/o glass formulation. In other preparations the K_2O to SiO_2 ratio was held constant while the overall composition was varied - such that 70 w/o KTN - 30 w/o glass and 50 wt. % KTN - 50 w/o glass were prepared with a $K_2O \cdot SiO_2$ 1:1 ratio while 75 w/o KTN - 25 w/o glass and 50 w/o KTN - 50 w/o glass were formulated with a 1:1.5 molar ratio of K_2O to SiO_2 in the glass.

It was discovered that decreasing the SiO_2 to K_2O molar ratio from 2:1 to 1:1 for a 50 w/o KTN-50 w/o glass resulted in a less refractory batch and the temperature required for melting and roll quenching was reduced from 1300°C to 1100°C. An increase to 70 w/o KTN for a 1:1 K_2O to SiO_2 ratio produced a more refractory composition which did not melt at 1200°C. At a lower ratio of K_2O to SiO_2 of 1:1.5, a 75 w/o KTN 25 w/o glass composition was quite fluid at 1100°C. A solid phase which settled out during pouring of the 75 w/o KTN - 25 w/o $K_2O \cdot 1.5SiO_2$ composition was studied by Debye-Scherrer x-ray diffraction technique. No fit to any of the reported phases in this system could be made. The data is shown in Table 18. The effect of introducing Al_2O_3 into the glass was evaluated. A 50 w/o KTN - 50 w/o $K_2O \cdot 0.2Al_2O_3 \cdot 1.3SiO_2$ composition crystallized at 1300°C and could not be poured as a molten glass.

All the compositions incorporating potassium silicate glass were found to be highly deliquescent.

TABLE 18. X-RAY DIFFRACTION DATA FOR PHASE IN 75 w/o $Ta_{.65}Nb_{.35}O_3$ - 25 w/o $K_2O \cdot 1.5SiO_2$ COMPOSITION

d	I/I_o	d	I/I_o
4.4	VVW	.883	W
3.84	VW	.881	W
3.44	VVVW	.862	W
3.25	VVVVW	.860	W
2.93	S		
2.75	VVW	.835	
2.34	W	.820	
1.94	W-M		
1.89	VVW	.805	M
1.79	W	.803	M
1.74	W		
1.70	VW	.797	W
1.63	M-S	.796	W
1.56	W		
1.50	VVW	.785	
1.48	VVVW	.784	
1.40	VW		
1.38	VW		
1.32	VW		
1.29	VVW		
1.25	VVW		
1.225	VVW		
1.195	W-M		
1.142	W		
1.085	VVW		
1.058	VVW		
1.020	VVW		
.980	VVW		
.972	VVW		
.958	VVVW		
.949	VVVW		
.935	VVVW		
.932	VVW		
.907	VVVW		
.905			
.893	VW		
.891			

V. ROCKET FLIGHT EXPERIMENT

The approach taken in the proposed sounding rocket experiment is in light of the limitations imposed by the short duration of microgravity made available. Crystal growth from a glass solvent is an inherently slow process due to the diffusion of the nutrient being retarded in a highly viscous medium. Prior experience with seeded growth of bismuth germanate crystals revealed that slow cooling at rates as low as $2^{o}C$ per hour does not eliminate incorporation of solvent.

Therefore it was considered expedient to focus on the earliest stages of growth and the nucleation process in assessing the effect of gravity-aided convection on growth from a glass solvent in the absence of a seed crystal. An outline of the proposed sounding rocket experiment which employs a gradient freeze technique is now presented.

The outline typifies investigative work that might be pursued in this area. It illustrates the types of problem that are likely to be met and indicates some of the preliminary ground-based work that would lead to improved evaluation of the feasibility of such rocket-based studies.

TITLE: Fused Solvent Rocket Flight Experiment

OBJECTIVE: Determine nucleation and crystallization characteristics in zero-g of fused solvent systems which are used for seeded crystal growth.

EQUIPMENT: Gradient furnace, heat sink, melt container, glass ingot, thermocouples (6), recorder and instrumentation.

DETERMINE: Nucleation rate (density and distribution of nuclei), crystallite growth rate, the temperature of spontaneous crystallization, crystallization temperature, immiscibility and phase separation and compare with earth-based results.

PROCEDURE: Load capsule, melt frit, and homogenize glass prior to launch.

Launch at maximum temperature.

Bring heat sink in rapidly and use zero-g time for cool-down.

Alternatives:

a) cool slowly
b) several compositions in one system
$Bi_{12}GeO_{20} - 0.75Bi_2O_3 \cdot 0.5Al_2O_3 \cdot B_2O_3$

90 w/o	10 w/o
80	20
70	30
50	50

c) Compare with model solvent of low viscosity such as BiF_3
d) 3 gradients - liquid range and nuclei formation; nucleation or nuclei growth; crystallization or grain growth

Remove glass - crystallized glass bar

Section and characterize.

MEASURE:

a) Glass: Index of refraction and density versus temperature
(determine glass transformation range).
DTA, DSC (determine glass transition temperature
Tg, crystallization temperature-compare with visual)
TEM (immiscibility)
SEM (morphology)
Viscosity vs. temperature

b) Crystalline region: nucleation rate (no nuclei/unit area; distribution)
crystallite size vs. temperature
(which growth eqn. will fit)
Raman spectroscopy (stoichiometry)
Microstructure - SEM, TEM
Crystal structure and phases - X-ray

GROUND-BASED
WORK:

1. Select systems and compositions

2. Experiments and characterization to provide baseline and flow charts.

3. Establish gradients.

4. Capsule design.

5. Furnace design.

6. Characterize capsule and furnace.

7. Procedure for frit and glass homogenization and melting.

8. Flight procedure.

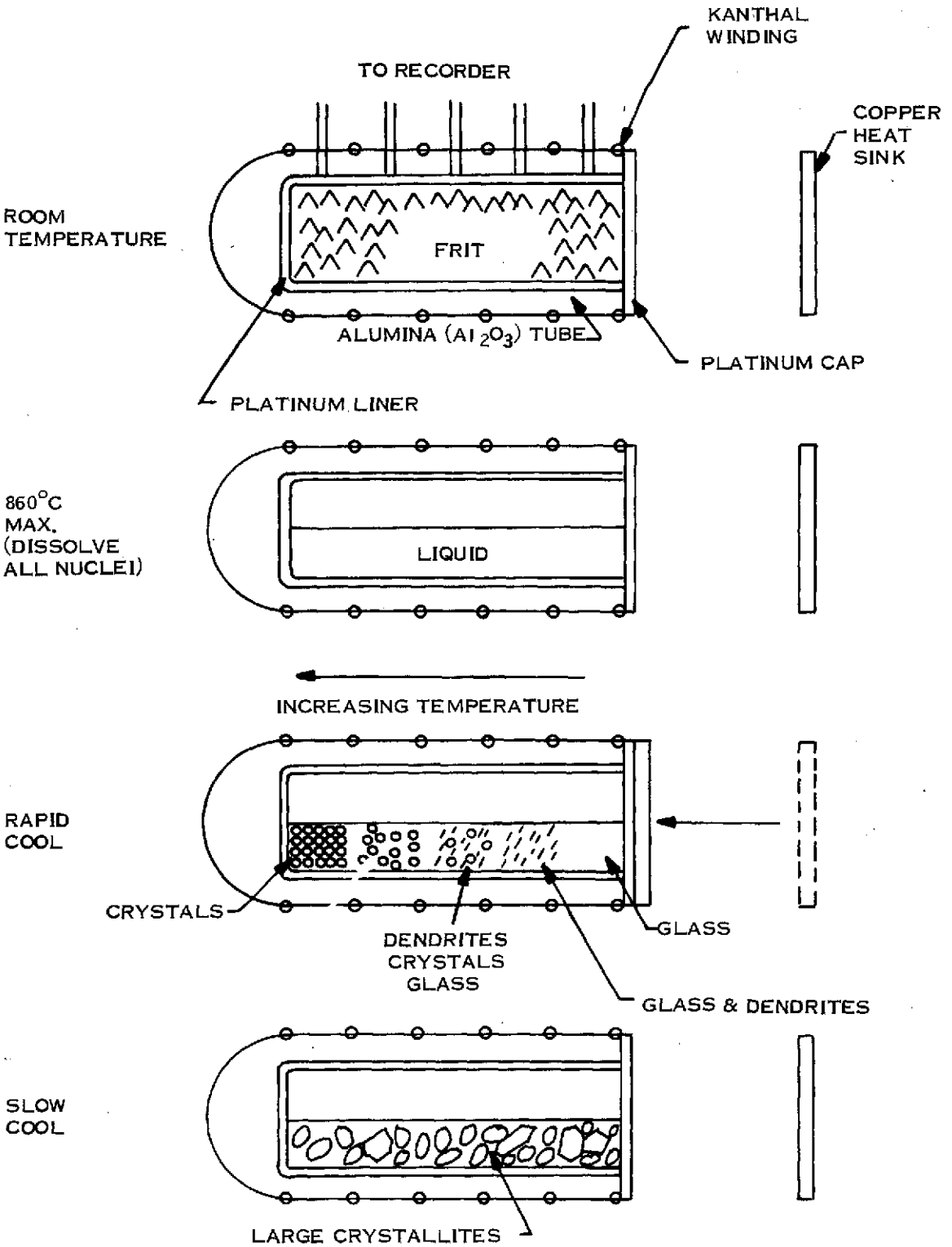

Figure 24. Schematic of Fused Solvent Rocket Flight Experiment.

VI. TRIGLYCINE SULFATE CHARACTERIZATION

A. Introduction

The selection of crystals for growth experiments in orbiting laboratory facilities must be based on at least two criteria:

(1) The crystals must be technologically important.

(2) They must be suitable for illustrating crystal growth principles and for comparing differences between earth-grown and space-grown crystals in a quantitative manner.

A material that meets these criteria is triglycine sulfate (TGS).

Triglycine sulfate is an amino acid salt with the formula

$$NH_3{}^{+}CH_2COOH \cdot NH_3{}^{+}CH_2COO^{-} \cdot NH_3CH_2COOH \cdot SO_4{}^{-2}$$

The material forms highly water-soluble transparent colorless crystals that can be rather easily grown from aqueous solutions. TGS is an important ferroelectric with a Curie temperature of $49^{\circ}C$. It belongs to monoclinic space group $P2_1$ in the ferroelectric phase and changes to $P2_1/m$ with the introduction of a mirror plane in the paraelectric phase. Most of the 1973 report was devoted to a review of the crystal growth of TGS and its characterization.(1)

---

(1) Final Report, Contract NAS 8-28114, June 1973, p. 58.

The main technological application of TGS is in pyroelectric bolometers for use as flat-frequency-response infrared detectors. TGS detectors have the great advantage over electronic detectors in that they operate at room temperature and do not require cryogenic cooling. The detectivity of the best TGS detectors produced so far is on the order of $D^* = 1.3 \times 10^9$ cm $Hz^{1/2}/w$, which is already competitive with other detector systems. The thermodynamic upper limit in detector sensitivity has been calculated to be 1.8×10^{10} for a detector operating at 300 K. There is thus more than an order of magnitude improvement in detector sensitivity to be gained. The present limit appears to be due to crystal imperfections and thus could be improved by introduction of methods for growth of more perfect crystals.

There have been very intensive efforts, mainly in eastern Europe, to produce crystals of a very high degree of perfection and to determine the role of imperfections and impurities on crystal behavior. Much of this has focused on the role of dislocations in pinning domain wall motion with resultant modification of ferroelectric properties. These efforts are summarized in the earlier report.

The application of TGS to infrared bolometry, however, does not make much use of the ferroelectric properties beyond the requirement of a high dielectric constant. Detector elements are slabbed into thin (010)

platelets and are locked in a single domain state either by a poling field or by doping the crystals with alanine, serine or other amino acids. The detectivity, therefore, is not limited by domain wall motion or domain structure, but by the dielectric loss factor which in turn is related to the conductivity of the crystal. A hypothesis, to be tested in this research, is that the loss observed in TGS arises because of sub-microscopic, fluid-filled, volume defects incorporated into the crystals during growth.

Detection of the fluid-filled cavities requires new characterization tools. It was the object of the present project to utilize laser light scattering as a possible technique for doing this. This report describes a series of experiments on volume defect characterization in laboratory-grown triglycine sulfate and the relation of volume defect size and number to the dielectric loss function.

B. Experimental

1. Sources of Crystals

The majority of the crystals studied were grown at Penn State. We chose to use the isothermal evaporation technique, since this requires somewhat less stringent temperature control than other techniques. A slow rate of evaporation was desired to keep growth rates from being excessive, thus a bath temperature of 30°C was chosen. The growth baths used were either 20 liter glass vats or 30 liter stainless steel

tanks filled with water. Temperature control was maintained by a commercial controller that allowed control to a few hundredths of a degree Centigrade. The growth vessels were 400 ml beakers. All growth runs were seeded, but the seeds were not rotated.

Saturated aqueous solutions of TGS were prepared at 35°C. When doped crystals were to be grown, the solution consisted of ten mole percent of dopant to 90% glycine. The warm solutions were gravity filtered into a clean dry beaker using fine mesh filter paper. After filtering, the solutions were cooled slowly to 32°C, covered with a clean watch glass to restrict evaporation, and placed securely in the water bath. The solutions reached equilibrium after 24 to 36 hours and the few crystals at the bottom of the beaker ceased growing. The solutions were then transferred to similar vessels and placed back in the bath. Seed crystals were attached to nylon threads, rinsed with demineralized water to prepare a fresh surface, and hung in the decanted solutions. Evaporation control was achieved only by varying the degree of cover on the growth vessel. Bath temperature for the growth runs was maintained at 30°C and stabilized to less than 0.05°C.

Typical growth runs required periods up to four weeks (Table 19). Good quality crystals from 0.5 to 2.0 cm in long dimension were obtained. The successful runs produced well faceted crystals without veils and without obvious inclusions of solution. Temperature fluctuations

TABLE 19

List of Crystals Used (TGS)

Sample No.	Dopant	Extrapolated Curie Temperature	ϵ_b at 10 kHz 25°C	Growth Conditions
4	Alanine	47.2	130	30.45°C, solution containing 10% of dopant
5	Serine	49.0	141	30.45°C, solution containing 18% of dopant
6	Leucine	50.0	154	30.45°C, solution containing 10% mole leucine
7	None	47.8	73	30.00°C 4 weeks
8	Serine	44.0	85	30.45°C, solution containing 10 mole % of dopant
9	None	47.5	115	30.00°C 4 weeks
10	None	47.8	69	30.00°C 4 weeks
11	None	48.8	80	30.00°C 4 weeks
12	None	46.8	145	Grown by Isomet Corp.
13	Alanine	48.5	345	Grown by Isomet Corp.

apparently produce veiling and some small included bubbles of solution. The principal difficulty was to obtain uniform growth on the seeds. Unless very perfect seed crystals were selected, carefully handled and surface-etched, hollows and voids developed between the seed and the overgrown layers resulting in a highly flawed region around the seed.

All samples for measurement were cleaved from regions of the crystals away from the seed, so that they contained no flaws or inclusions visible to the eye with the aid of a hand lens. The two samples obtained from Isomet Corp. were in the form suitable for measurement when received, and again no flaws were visible.

All the samples used in this study were oriented and cleaved into b platelets, approximately 2 mm thick in the b direction and usually about 5 to 7 mm by 3 to 5 mm in the a and c directions respectively. Triglycine sulfate has an easy cleavage direction perpendicular to the b axis. However, it is not a perfect cleavage and it was thus necessary to polish each of the samples. A right angle polishing block was used, to insure that the b and c faces would be perpendicular, and that the two b faces would be parallel, so that reliable dielectric data could be obtained. Initial rough polishing to obtain a flat face was done on number 400 silicon carbide paper. This was followed by polishing with 1 μ alumina and pure ethanol and finally by polishing with a 0.3 μ alumina with pure ethanol on number 175 tissue paper from Fort Howard Paper Company. After preparation,

crystals were stored in a vacuum desiccator to prevent etching of the surfaces by atmospheric moisture.

2. Light Scattering Measurements

The experimental arrangement used is essentially that of an ultramicroscope, which was originally devised by Vand, Vedam, and Stein[2]. The experimental arrangement used for the present study is shown in Figure 25. It consists of a light source, for which we have chosen a He-Ne laser (12) of average rated output of 2 mW. The laser produces a horizontal parallel beam of red light approximately 1 mm in diameter. A low power lens (9) is needed to spread the laser beam sufficiently to completely fill the rear aperture of the microscope objective (6), because the laser beam itself is too narrow to illuminate the objective evenly. This becomes important if one considers that the use of the full aperture of the objective (6) appreciably reduces the size of the focal spot of the beam on the crystal and consequently increases the intensity of local illumination. The geometry of the light beam near the focal point of the objective is approximately that of a double cone. The angle of this double cone is a function of two variables: the relative position of the low power lens and the power of the microscope objective (6). The position of the low power lens (9) which produces complete filling of the objective by light produces minimum focal spot diameter, but also

(2) V. Vand, K. Vedam, and R. Stein, J. Appl. Phys., 37, 2551-2557 (1966).

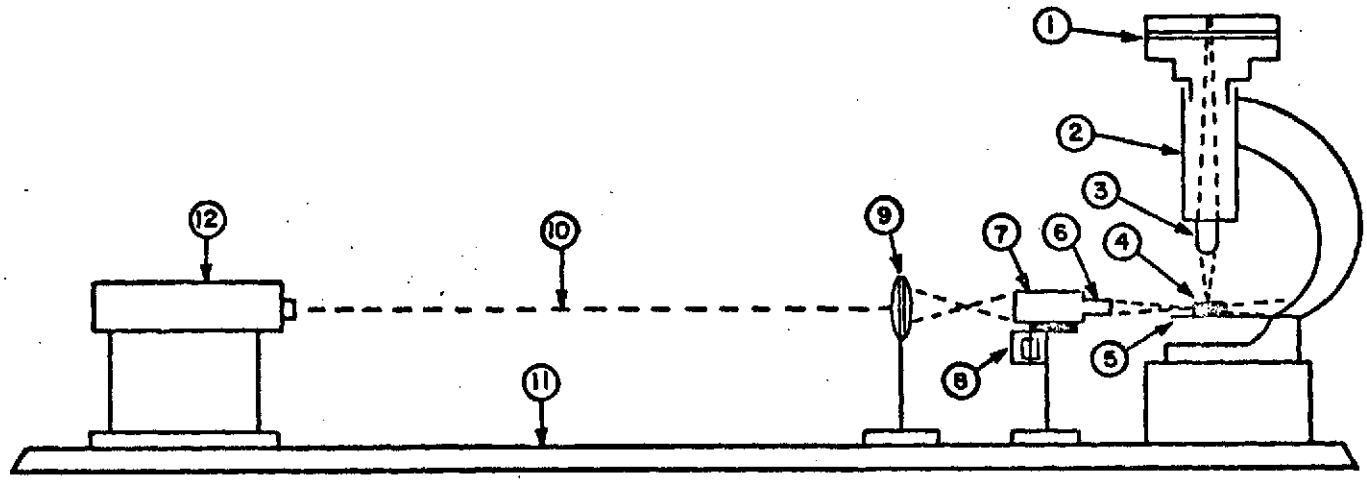

Figure 25. Experimental Arrangements for Laser Light Scattering. (1) Camera (2) Microscope Barrel (3) Objective Lens (4) Crystal (5) Stage (6) Focusing Lens (7) Horizontal Stage (8) Translating Device and Drive Motor (9) Lens (10) Laser Beam (11) Optical Bench (12) 2 mW He-Ne Laser.

maximum cone angle. A compromise is thus necessary, and it was found that a 4x objective combined with a cm distance between the low power lens and the objective gave optimum illumination. This combination of lens position and objective power produced a cone of illumination with a cone angle small enough so that within the field of view of the microscope the geometry of the beam appeared essentially as a horizontal right circular cylinder of 20 μ diameter. The direction of view through the microscope is perpendicular to the direction of the laser beam with a field of view of approximately 2 mm diameter.

This cylinder of light can only illuminate a strip 20 μ wide in the crystal, thus only the defects within this strip are visible in microscope. In order to obtain some information on the distribution of the defects within the field of view of the microscope and consequently throughout the cyrstal, it is desirable to spread this illumination over the horizontal plane on which the microscope is focused. Thus, all the defects within the field of view and also within the focus of the microscope would become visible. This has been accomplished by the use of a translation mechanism (7) with a reciprocating motor drive (8). A horizontal stage was connected to a motor drive through a worm gear and several reduction gears. The direction of travel of the objective (6) on the horizontal stage (7) can be reversed by two limiting microswitches connected to a relay. This produces a reciprocating motion of the objective in a direction perpendicular to both the direction of the laser beam and the direction of view

through the microscope, which results in a scanning motion of the beam in the horizontal plane of the sample on which the microscope is focused.

Therefore, all defects in the field of view in a horizontal plane 20 μ thick will scatter the laser light as the beam sweeps past. A single lens reflex camera (1) is used to integrate these flashes of light in a photograph. The scan time for the beam to traverse this field of view in one direction is 5 sec. The exposure time in all the photographs in this paper were a multiple of the scan time, so that all the defects in the plane would receive equal illumination.

The crystal is placed on the x-y translation stage of the microscope (5). The use of this stage allows one to systematically translate the crystal through the field of view of the microscope, so that it is possible to construct a two-dimensional record of the defects within one horizontal plane. Horizontal planes could be obtained at different heights in the crystal by either adjusting the stage (5) vertically or by changing the vertical position of the 4x objective (6). The latter procedure was used in this study.

All the crystals used in this study were polished on four faces. The two polished vertical faces allowed the beam to enter and leave the crystal with a minimum of diffraction in order to keep the background illumination as low as possible. Two horizontal faces were also polished, so that the crystal could be viewed through either face. In addition, the x-y stage of

the microscope [5] on which the crystal is placed, was painted flat black to maintain a dark background for maximum contrast.

Calibration of the apparatus was made by recording photographs of a polystyrene latex suspension of 880 Å particles in water, and of a microscope scale. The 880 Å particles were visible through the microscope and they were photographed using the same procedure as for the crystals, with the same exposure times.

3. Dielectric Measurement

The measurement of the dielectric properties of the samples necessitated the evaporation of electrodes onto the crystals to insure a good connection to the test equipment. First a layer of chromium, which adheres well to crystal surfaces, was evaporated onto the sample, then a layer of gold, which provides good contact with the platinum fingers of the sample holder, was evaporated on top of the first layer. This was done on both of the 010 faces of the crystal. The sample was then placed between the platinum fingers of a sample holder and immersed in a silicon oil bath. The bath temperature was controlled to within 0.1 °C by means of a suitable controller. The capacitance and dielectric loss data were obtained with the use of a Hewlett-Packard model 4270-A automatic capacitance bridge over a series of temperatures. All measurements were made along the b axis.

C. LIGHT SCATTERING RESULTS

Light scattering from volume defects in the TGS crystals produces the images shown in the series of photographs presented below. The number, size, and shape of defects observed in the light scattering images are strikingly variable and bear little relation to the conditions of crystal growth at the level of control exerted in these experiments.

Sample 10 is typical of the run-of-the-vat crystals. It is of intermediate quality and exhibits the two main types of defects made visible by light scattering. In the lower part of Figure 26 are bright, rather peculiarily shaped images that we associate with volume defects. They tend to be elongate in particular directions. The defects shown in Figure 26 are rather large objects, probably in the fractional micrometer range. They are not visible in ordinary light. In the upper part of the photograph is shown the second kind of light scattering image, whose origin is not known. These may be called "cloudy patches." They appear in a number of photographs and do not appear to be optical artifacts. The crystals are water clear and the beam is carefully centered so that the cloudy patches do not appear to be reflections from the crystal surfaces. There is the possibility that they represent veiled regions consisting of large numbers of volume defects below the resolution limit for single spot scattering, (i.e. below 300 $\mathring{A}$).

There is a tremendous variability between growth runs conducted under what appear to be identical conditions. Samples 7 and 11 in Figure 27

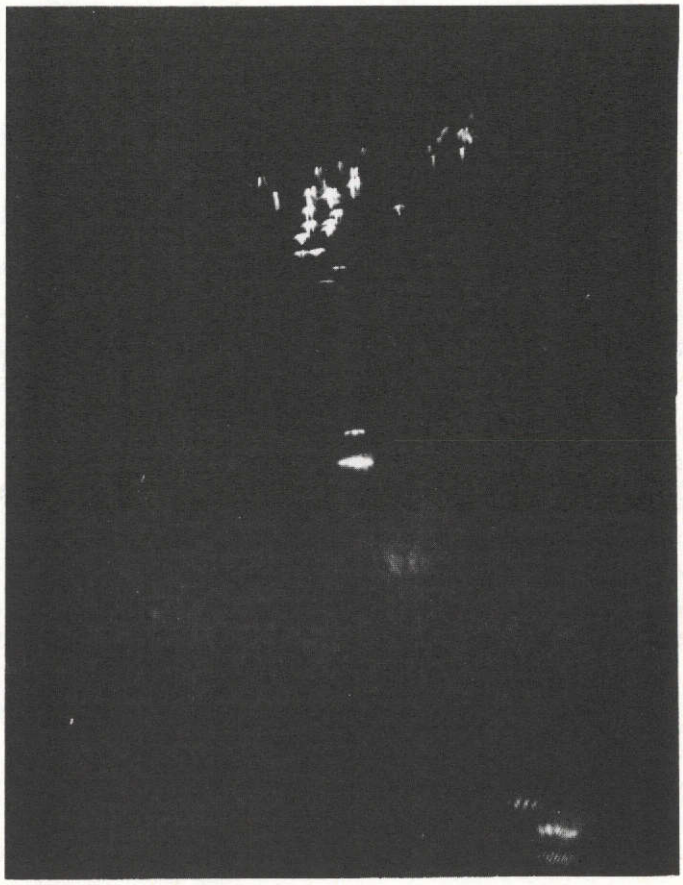

Figure 26. Light Scattering Images in Triglycine Sulfate Sample 10.

Fig. 27a

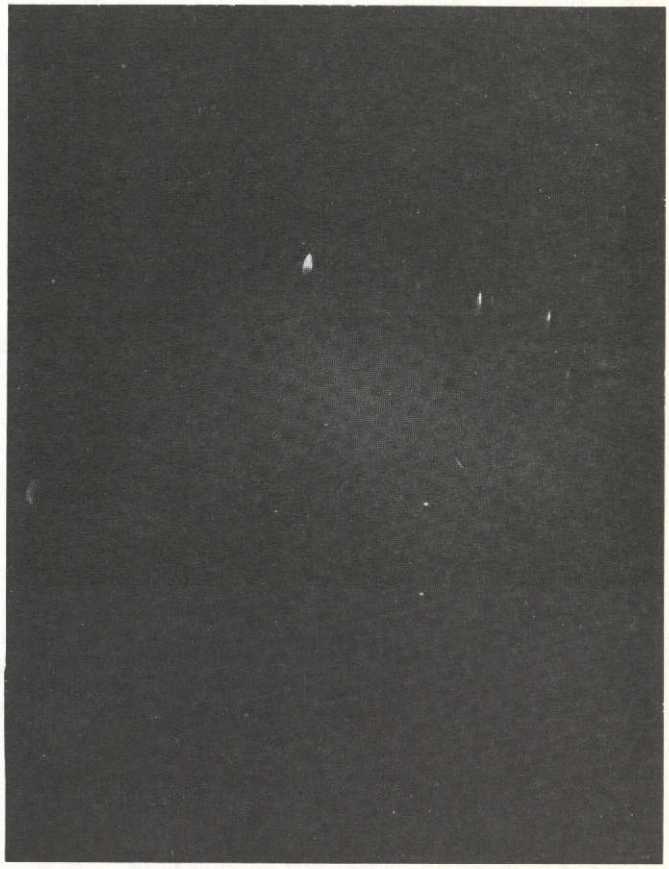

Fig. 27b

Figure 27. Light Scattering Images in Triglycine Sulfate Samples: (a) 7 and (b) 11.

appear to be identical conditions. Samples 7 and 11 in Figure 27 offer a comparison. Both of these crystals were grown in the same vat under conditions of temperature and concentration as nearly identical as possible. Sample 11 appears to have fewer volume defects than Sample 10 and those that appear are much smaller. The spots shown in Figure 27 are at about the lower limit of resolution of our scattering apparatus and by comparison with the latex spheres would appear to be in the size range of 500 to 1000 Å. Sample 7 also has fewer volume defects but several cloudy patches are well developed.

No scattering measurements were made on crystals that were visibly flawed. Several samples of a serine-doped TGS crystal (Figure 28) give the approximate threshold for visible observation. These crystals appeared transparent and unflawed under microscopic examination. Sample 5 shows a line of voids in the micrometer size range as well as a large cloudy patch. The alignment of volume defects is clearly visible in Sample 8 and other patches and bright regions appear. Crystals that show more imperfections than these in the light scattering photographs also appeared flawed under visual examination.

The data are not sufficiently conclusive to determine whether or not the amino acid-doped crystals are less perfect than undoped TGS. The evidence that we have suggests that it is more difficult to obtain near-perfect doped crystals. The two best amino acid-doped crystals appear in Figure 29. Leucine-doped TGS (sample 6) is largely free of volume

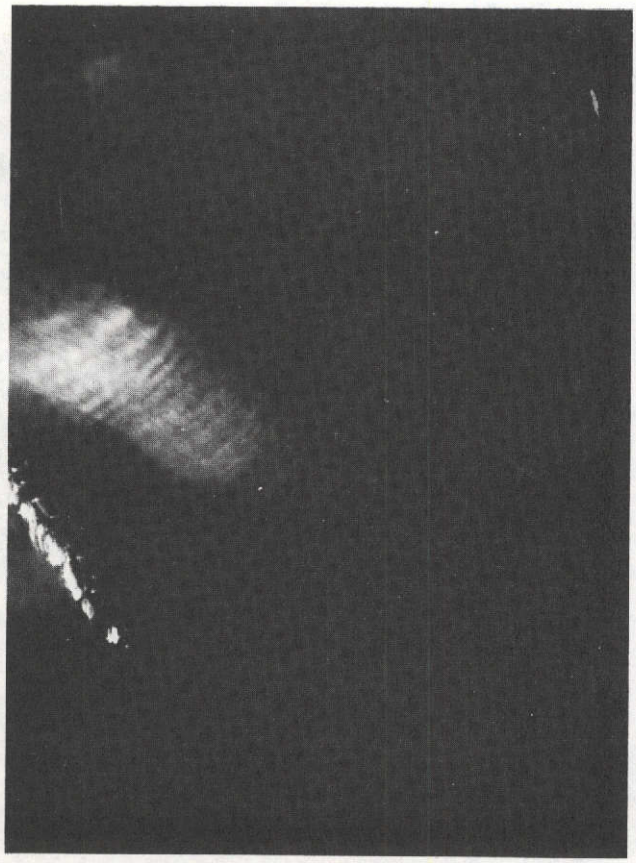

Fig. 28a

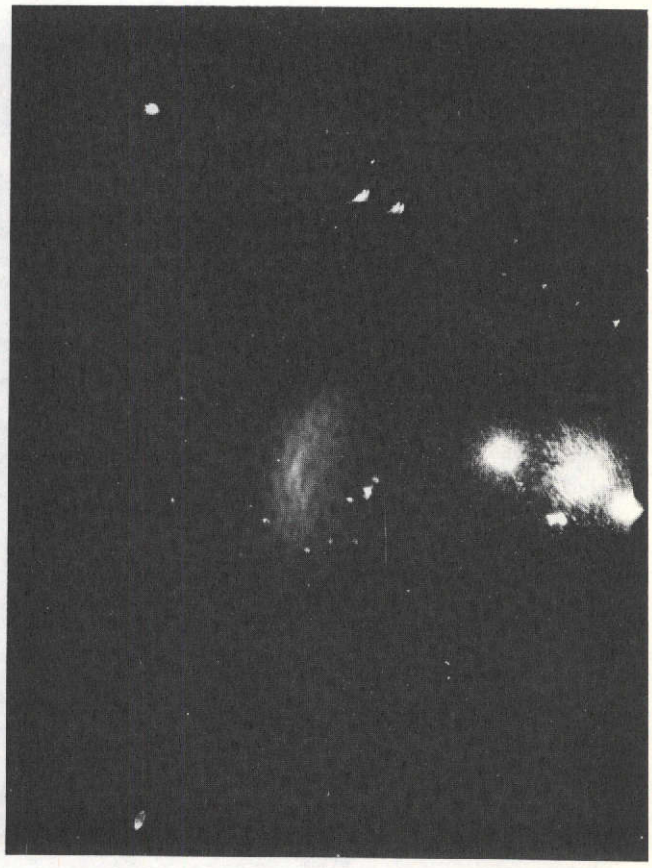

Fig. 28b

Figure 28. Light Scattering Images in Serine-doped Triglycine Sulfate Crystals (a) 5 and (b) 8.

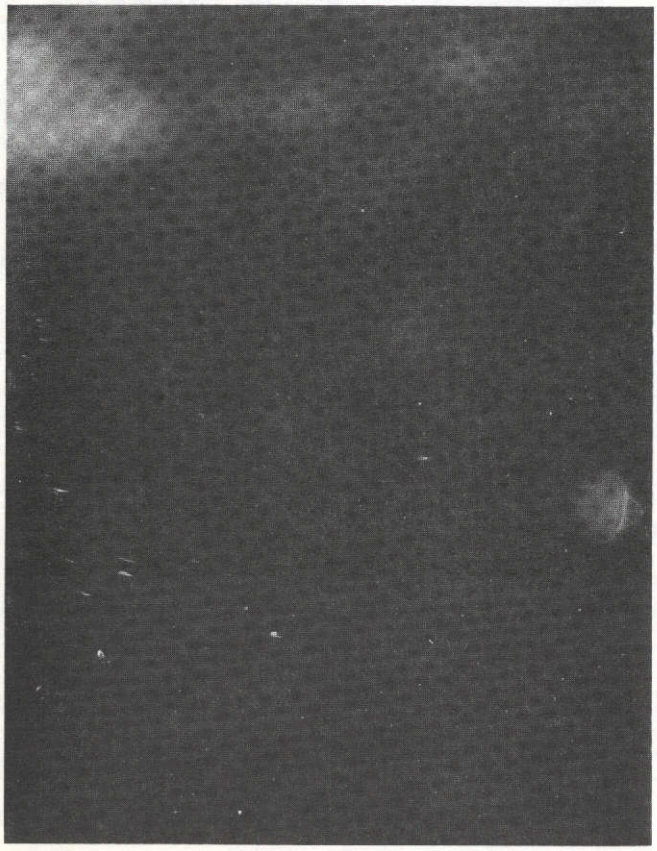

Fig. 29a

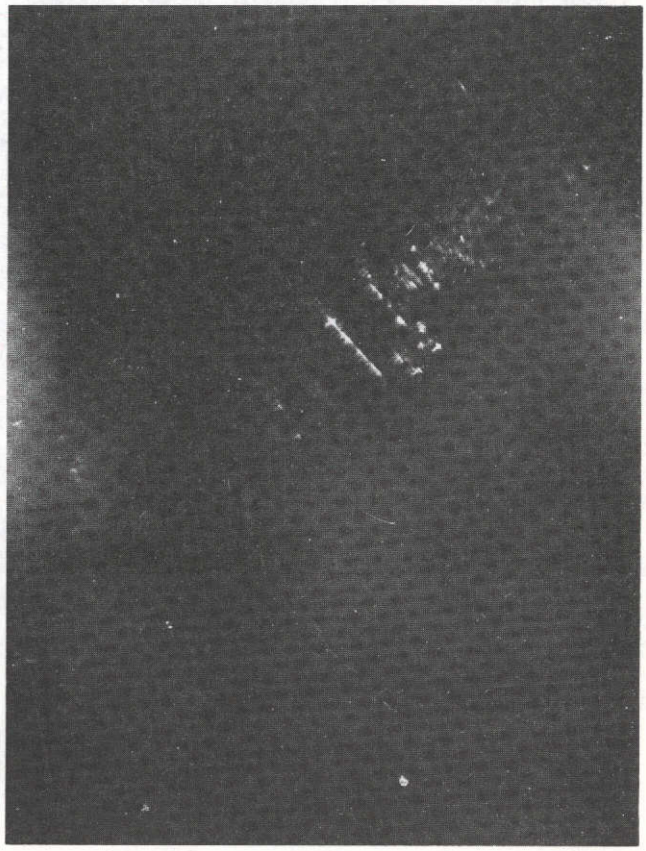

Fig. 29b

Figure 29. Light Scattering Images in (a) Leucine-doped TGS Sample 6 and (b) Alanine-doped TGS Sample 4.

defects and those that are present are very small but large regions of cloudy patches appear. The alanine-doped crystal (sample 4) has an irregular distribution of intermediate sized volume defects arranged in linear patterns.

The distribution of volume defects through as-grown crystals is very non-uniform. This point is illustrated in Figure 30 where four different regions of sample 9 are displayed. Sample 9 is a moderately defective crystal and the individual voids are of substantial size. They tend to be concentrated in local regions so that in the upper two photographs, for example, there are regions where the concentration of volume defects is very great, separated by nearly perfect regions. This property creates problems for the dielectric measurements. Since the measuring electrodes sample a much larger volume of the crystal than does the laser beam, it is necessary to compare the same regions of the crystal. The electrodes for sample 9 were placed directly over the regions shown in the upper two photographs so that this measurement should be characteristic of a crystal with a high concentration of fairly large voids.

There is some value in comparing the crystals grown in this laboratory from small growth vats with crystals grown in other laboratories. We were fortunate in being able to obtain two crystals grown by the Isomet Corp. for use in device application. These were kindly supplied by Dr. Joseph F. Balascio at Isomet. One Isomet crystal was pure TGS, the other was doped with alanine. Both were water-clear and visually perfect.

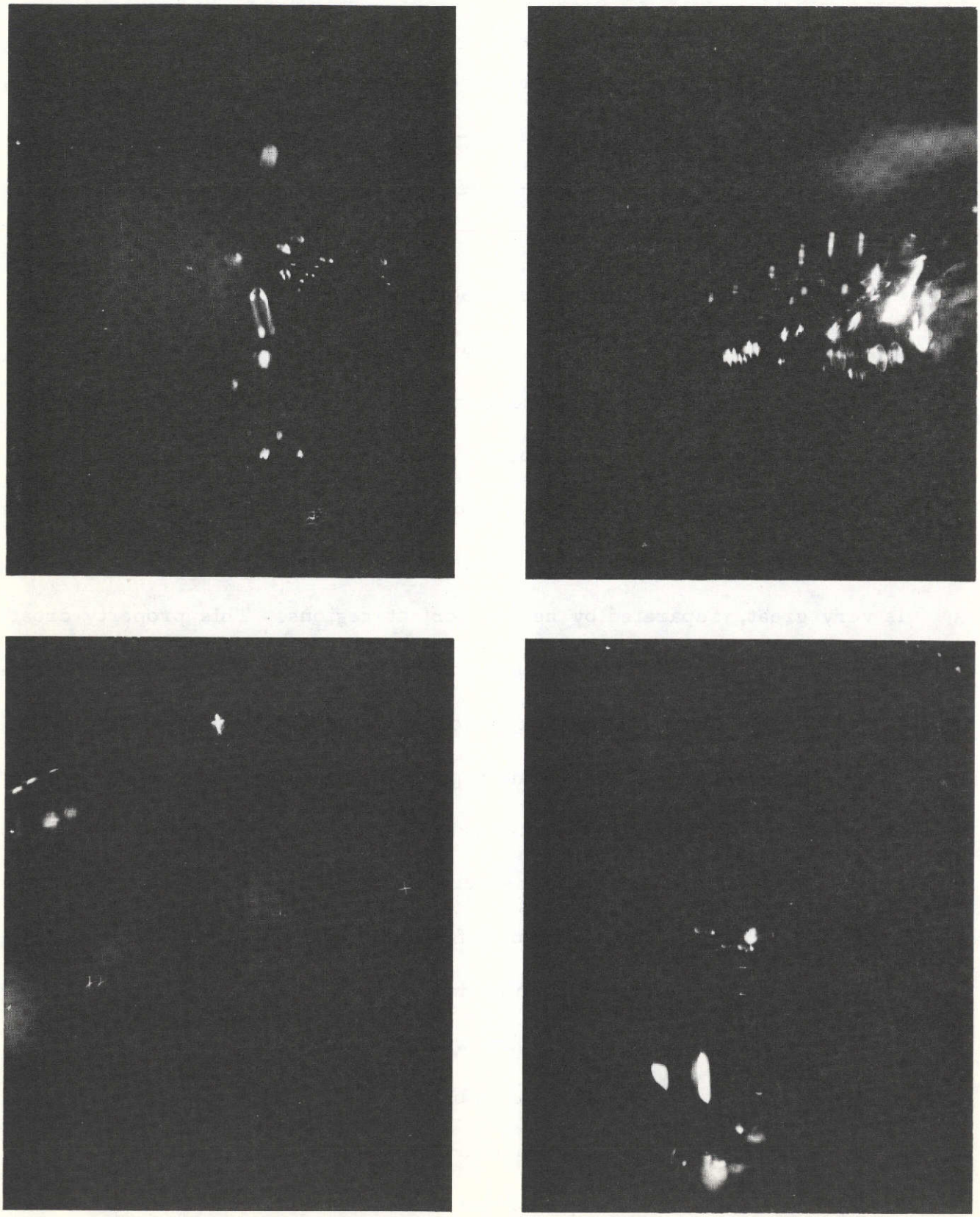

Figure 30. Light Scattering Images in TGS Sample 9.

Four regions of the alanine-doped Isomet crystal are shown in Figure 31. The crystal is free of the large voids illustrated in the previous photographs but still contains a large number of smaller imperfections. These appear to span a range of sizes and are distributed through most of the crystal. It appears that here again the amino-acid doped crystals are less perfect than the undoped crystals.

Two regions of the Isomet TGS crystal are shown in Figure 32. The center of the crystal is one of the most perfect observed in the entire set of samples. There are a few very small imperfections that appear to be randomly distributed. A very faint cloudy patch appears covering part of the field of view. The density, size, and distribution of imperfections of sample 12 are quite comparable to sample 11, a TGS crystal grown in this laboratory. Figure 32b shows the region near the corner of the Isomet TGS crystal. Here a well defined region of higher void concentration occurs in the upper right hand side of the photograph.

The main results of the light scattering experiments may be summarized as follows:

(i) At least two types of imperfections become visible in the scattering photographs: (a) Isolated spots of varying size and often elongated in particular crystallographic directions which we associate with volume imperfections. (b) Cloudy patches with ill-defined boundaries, much larger than the spots and with little resolved detail. The origin of the cloudy patches is not known with certainty.

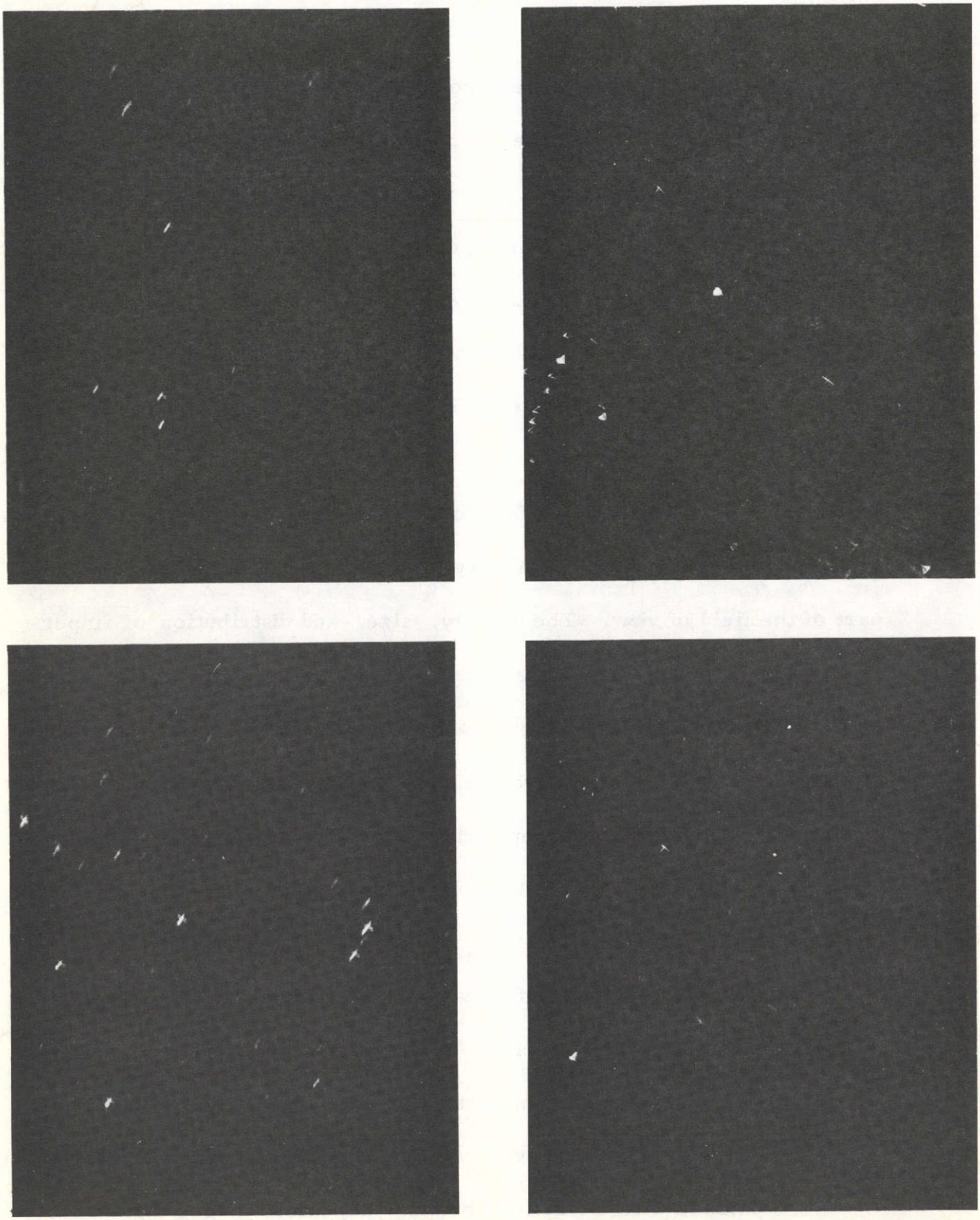

Figure 31. Light Scattering Images in Alanine-doped Isomet Crystal - Sample 13.

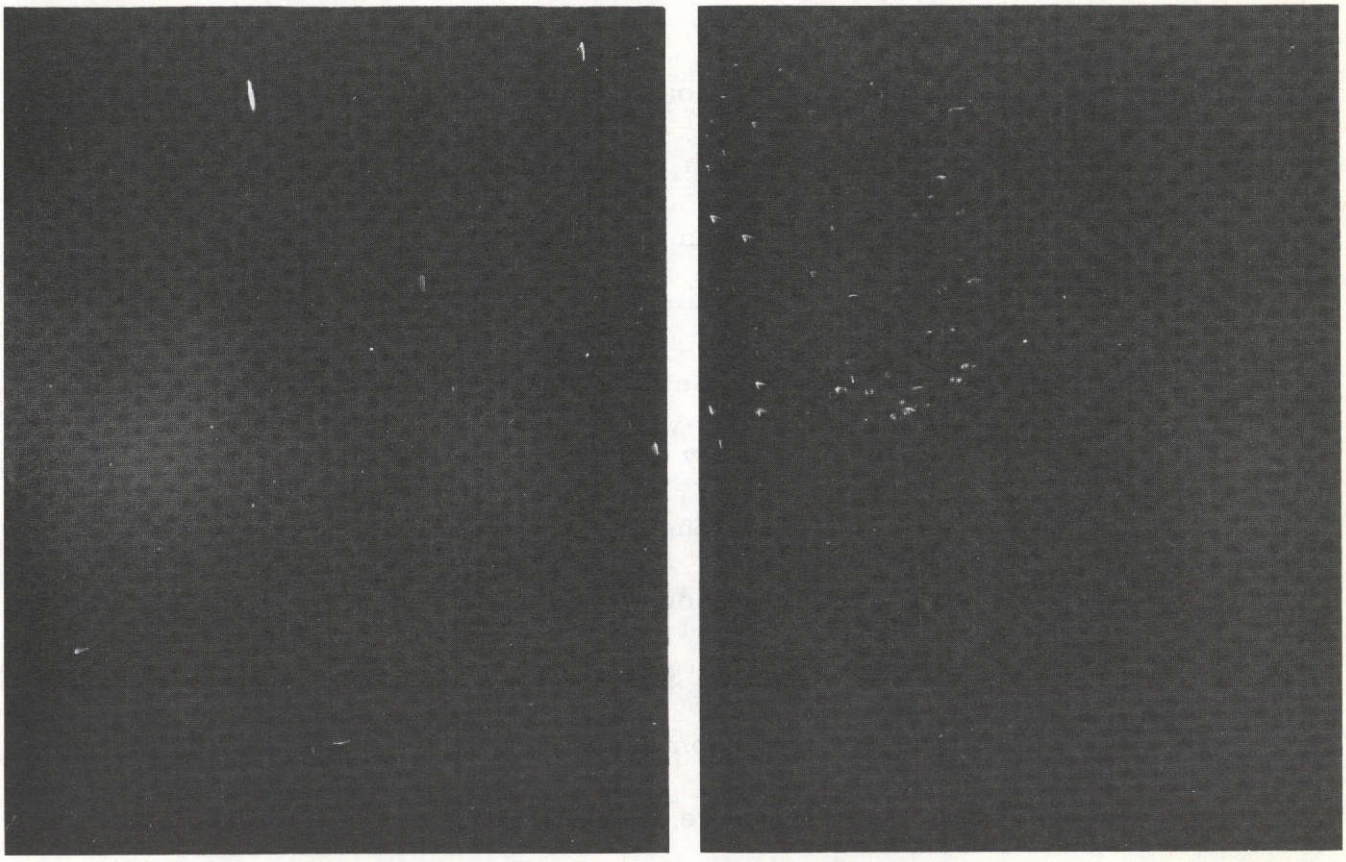

A B

Figure 32. Light Scattering Images in Isomet TGS-Sample 12.

(ii) Crystals grown from the same equipment, under identical conditions, exhibit a wide range of imperfection size and concentration. It is clear that the utmost effort at controlling growth conditions must be made if meaningful comparisons between earth-grown and space-grown crystals are to be made.

(iii) The distribution of defects within the volume of a crystal is not uniform. Highly defective regions can be found surrounded by regions that are nearly perfect. A few crystals show a homogeneous distribution of imperfections but most do not. In general, the more perfect crystals are also the most homogeneous.

(iv) There is a very large range in the size of the volume defects. Those just below the threshold for visual detection are in the range of one to five micrometers. They scale downward to the lower limit of resolution of the scattering experiment, 300 to 500 $\mathring{A}$. There is no reason not to suspect that still smaller voids exist in the two decades of dimension separating the smallest observable voids from the size of the unit cell. The most perfect crystals do not have fewer voids but rather have smaller ones.

D. DIELECTRIC MEASUREMENT RESULTS

Because the Curie temperature is so close to room temperature, dielectric properties change rapidly with temperature. A single temperature measurement of dielectric constant and dielectric loss would not be particularly meaningful. Therefore dielectric properties were measured at intervals of one to five degrees over the entire temperature range of interest, 25 to 75°C. All measurements were made on (010) plates, so that all reported properties refer to the components of the dielectric tensor in which the applied field is in the b crystallographic direction.

1. Dielectric Constant

The real part of the dielectric constant is plotted as a reciprocal against temperature for the undoped crystals (Figure 33) and for the amino acid-doped crystals (Figure 34). This technique produces a straight line plot both above and below the Curie temperature and by extrapolating to zero (corresponding to the temperature at which the ideal dielectric constant would go to infinity) a value for the Curie temperature may be obtained. The Curie temperatures for the various crystals and the numerical value for the dielectric constant at 25° are tabulated in Table 19.

As many previous workers have observed, the dielectric constant varies quite a bit from one crystal to the next. The spread in slopes for the doped crystals is much larger than for the undoped crystals

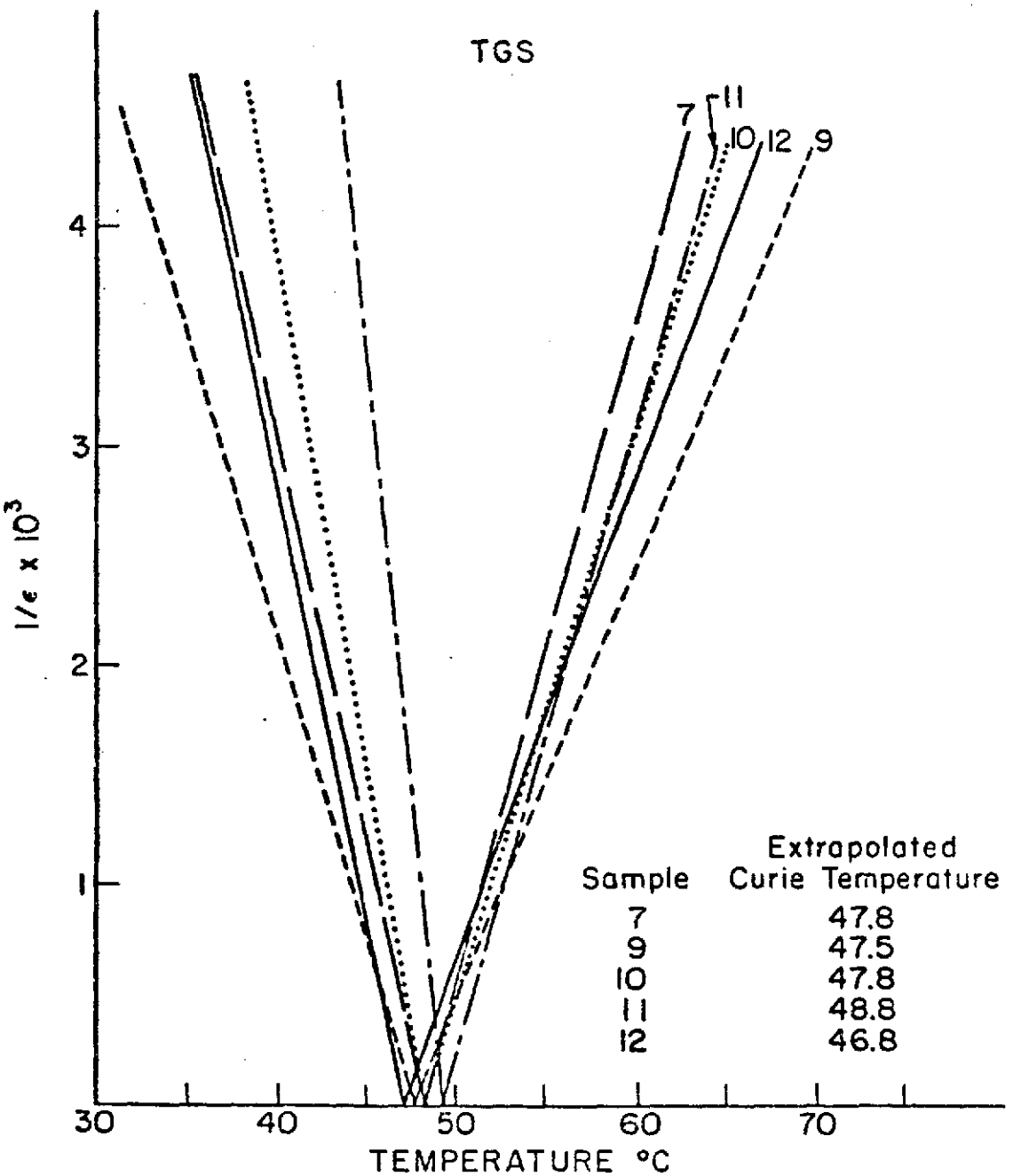

Figure 33. Real Part of the Dielectric Constant for Undoped TGS Crystals as a Function of Temperature

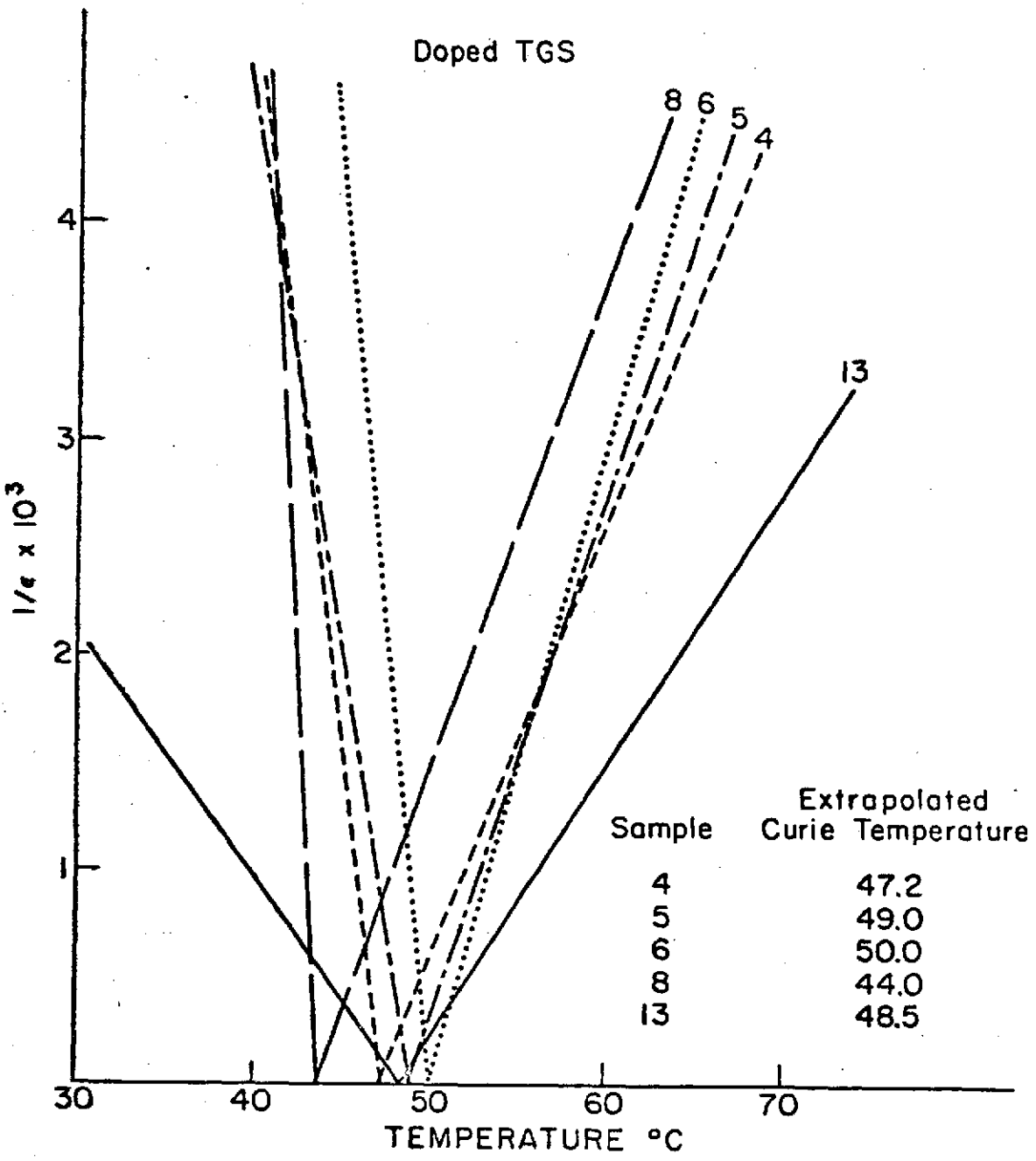

Figure 34. Real Part of the Dielectric Constant for Amino-acid Doped TGS Crystals as a Function of Temperature

as is the spread in Curie temperatures. There is no obvious correlation between either the slope of the curve or the Curie temperature and the perfection of the crystal as determined from the light scattering experiments. It is true that sample 7 at one end of the range is one of our most perfect crystals and sample 9 at the other end of the range is one of the imperfect. But sample 12 which falls close to sample 9 is the highly perfect Isomet crystal. Samples 10 and 11 for which the dielectric curves are nearly superimposed are widely different in perfection. The data for the doped crystals reinforce this conclusion. It is apparent that the widely varying behavior is a function of the presence of the amino acid dopants. The uptake of the second amino acid in the TGS crystals may or may not be uniform, but it appears that there is a considerable influence on domain formation and motion as the temperature is changed.

2. Dielectric Loss

The complex part of the dielectric constant is of most importance because the dielectric loss is the limiting factor on device performance of infrared bolometers. The dielectric loss expressed as the logarithm of the loss tangent as a function of temperature is shown in Figures 35 and 36. The loss increases by two to three orders of magnitude below the Curie temperature, and there is about an order of magnitude variation between the samples of undoped TGS and two orders of magnitude between the samples of doped TGS. The loss in the ferroelectric region is

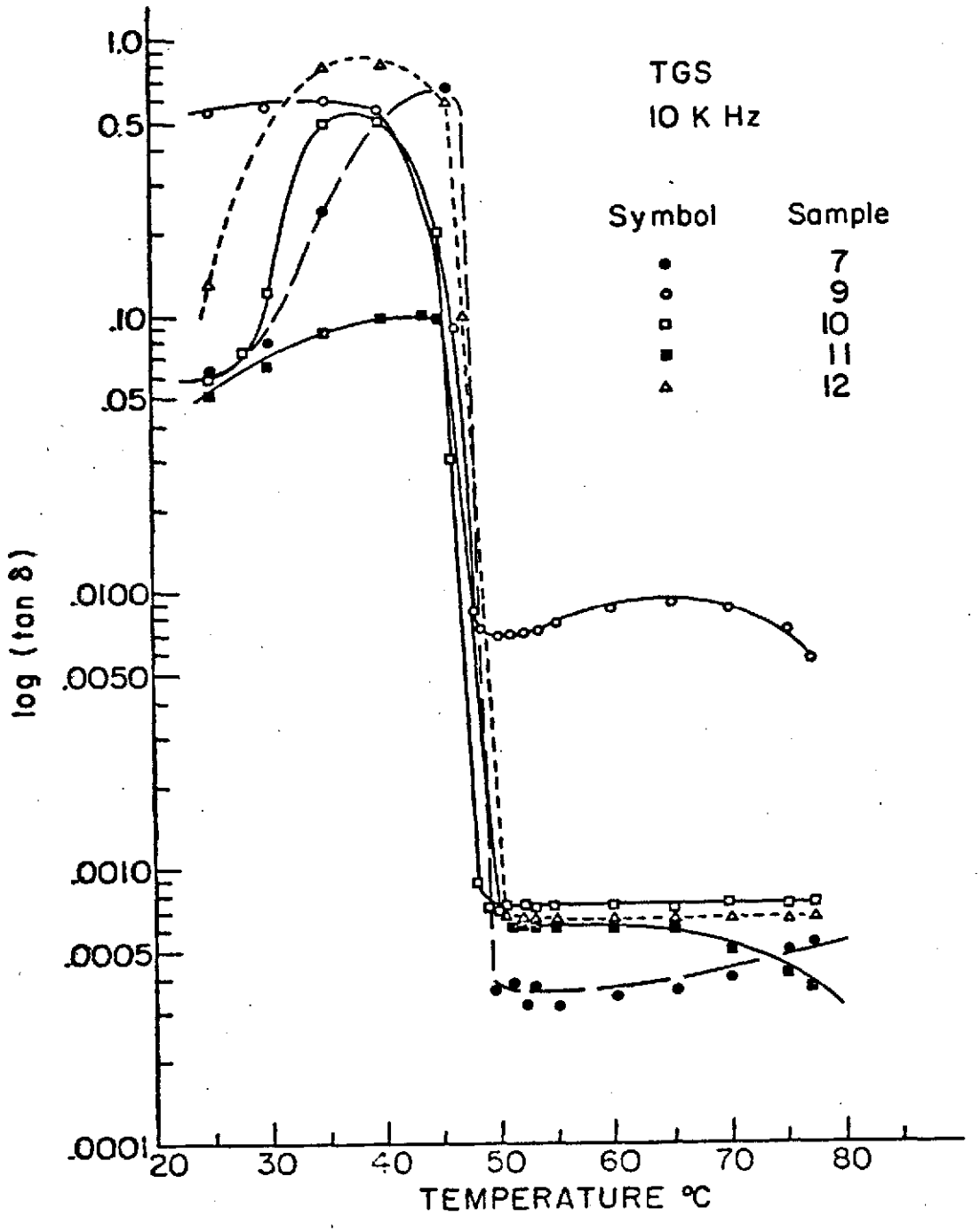

Figure 35. Loss Tangent for Undoped TGS Crystals as a Function of Temperature

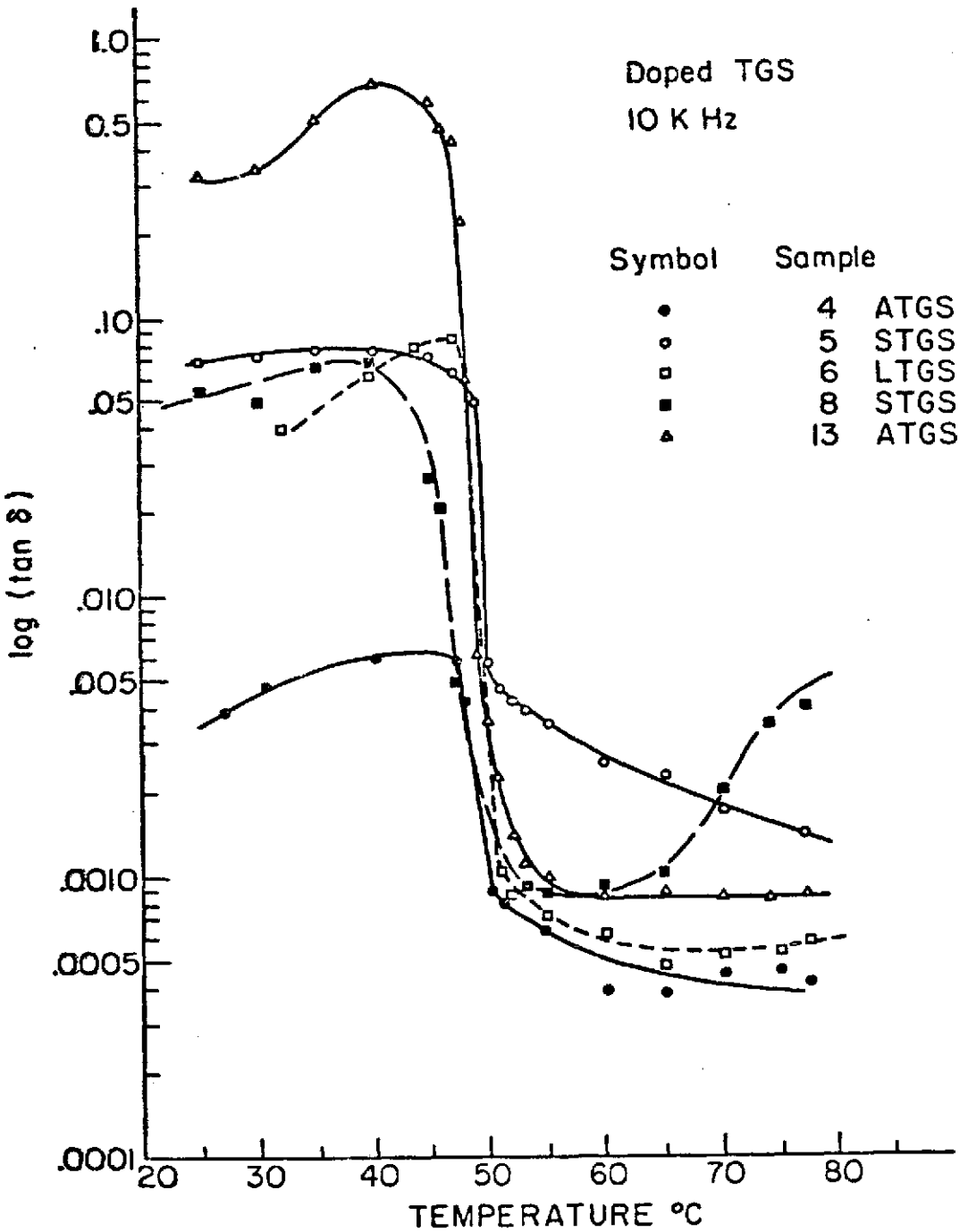

Figure 36. Loss Tangent for Amino Acid-doped TGS Crystals as a Function of Temperature

a complex function of temperature with maxima in some curves and other complex behavior. For the most part, except for two of the doped crystals, the loss tends to be more or less independent of temperature in the paraelectric region, although there is still a considerable variation from one sample to the next.

It appears that the best comparison between the dielectric loss and the presence of volume defects can be made from data in the paraelectric region. Consider the undoped TGS crystals. Samples 7 and 11 are the two best crystals grown in our laboratory. Sample 11 does indeed have the lowest measured loss in the ferroelectric region but sample 7 goes through a maximum near the Curie temperature before descending to the same loss level at lower temperature. Both samples 7 and 11 appear as the lowest loss specimens in the paraelectric region. Or consider the two serine-doped crystals, samples 5 and 8. According to the photographs in Figure 28, these are the most highly damaged crystals for which data were reported. Yet the highest loss in the ferroelectric region is obtained from sample 13, the rather more perfect Isomet crystal. In the paraelectric region, samples 5 and 8 are unquestionably the most lossy.

Sample 9 is by far the most lossy undoped TGS crystal in the paraelectric region. The electrodes on sample 9 were rather carefully placed directly over the patch of large volume defects illustrated in Figure 30. Sample 9, on the other hand, does not stand out from the other samples in the ferroelectric region.

If, as we suspect, the contribution of the volume defects to the loss mechanism is a simple absorption of energy by solution-filled cavities then indeed the loss should remain in the paraelectric region. The increased loss below the Curie temperature contains contributions from domain walls and detailed interpretation is much more difficult.

E. SUMMARY AND CONCLUSIONS

Use of laser light scattering ultramicroscopy provides a useful tool for the characterization of volume defects in transparent triglycine sulfate single crystals. Volume defects in the size range of 500 Å to 5 μm can be observed. These defects are not generally visible to ordinary optical examination.

Crystals grown by similar techniques tend to vary greatly in perfection. Volume defects are often concentrated in local regions. Increasing perfection appears to be more a matter of a decreasing size of volume defects rather than a decrease in their number. No crystals were observed to be entirely free of scattering centers.

As expected, the dielectric properties of the ten samples exhibited a great spread in values. The spread was greater for the amino acid-doped crystals than for the undoped crystals. There is at least a qualitative correlation between the dielectric loss as measured in the paraelectric temperature region with the size and number of volume imperfections. Variations in the real part of the dielectric constant do not correlate well with volume defects.

The main problem in developing a correlation between volume defects and dielectric properties is in comparing the same sampling volume, since most crystals are internally heterogeneous.

Because of the large variability in both defect distribution and in dielectric properties, a valid comparison between crystals grown in an orbiting laboratory facility and crystals grown in an earth-bound laboratory would require enough measurements for statistical techniques to be applied. This is necessary to separate the crystal-to-crystal variation from the laboratory-to-laboratory variation.

VII. REQUIREMENTS FOR SPACE SOLUTION CRYSTAL GROWTH EXPERIMENTS

A. Scope of Experiment Definition

During the past two years effort, experimental studies were conducted to define the variables needed to design a zero-gravity crystal growth experiment. High and low temperature solution growth were investigated. Studies were conducted for the growth of lithium niobate ($LiNbO_3$), potassium sodium niobate ($K_{0.5}Na_{0.5}NbO_3$), bismuth germanate ($Bi_{12}GeO_{20}$), and lead germanate ($Pb_5Ge_3O_{11}$) from fused solvents. Studies were also conducted on the growth of triglycine sulfate $(NH_2CH_2COOH)_3 \cdot H_2SO_4$ from aqueous solutions.

During these studies, emphasis was placed on definition of the growth parameters and characterization of the resultant products. The variables included:

1. Definition of the solvent system
2. Determining the temperature and thermal control requirements
3. Determining the solubility characteristics
4. Determining the need for any mechanical apparatus such as introducing a seed crystal.

B. Fused Solvent Growth

During the first year of study and into the second we restricted the study to growth conditions which were within the capabilities of the M518 Skylab crystal-growth furnace. This meant designing crystal growth experiments around temperatures of 1000°C and less. Solvent definition became critical since their compositions had to be capable of reducing the growth of high temperature crystals such as lithium niobate and potassium sodium niobate to less than 1000°C, and, concurrently, be chemically compatible with these materials as solutes in a growth solution.

Bismuth germanate and lead germanate were identified as crystals which could benefit technically and economically from growth in space. Since their melting points were, respectively 935°C and 750°C, they became the foremost candidates for study within the M518 furnace temperature restriction.

During the second year, under Task 3, an experimental study on ceramic oxide crystals needing solution temperatures higher than 1000°C was initiated. This class of materials needs to be evaluated since the Shuttle-Space Lab. capabilities will not be as restricted as those of Skylab. Potassium tantalum niobate ($K(Ta_{.65}Nb_{.35})O_3$) was chosen as the crystal for study. At this point, in view of what has been learned from the use of common-cation binary solvents containing Al_2O_3 additions, it is recommended that lithium niobate be re-examined for Shuttle Spacelab growth at temperatures exceeding 1000°C.

The experiment which to date is practical for a space flight is the slow cooling of $Bi_{12}GeO_{20}$ from a seeded fused solvent. It is described in detail in Table 20. Further work is required on defining the requirements for $LiNbO_3$ and $Pb_5Ge_3O_{11}$. The best conditions to date are also listed in Table 20.

C. Benefits of Growing Bismuth Germanate from Fused Solvents in Space

If the comparison of the $Bi_{12}GeO_{20}$ single crystal regions grown from the seeded low viscosity melt and high viscosity glass solvent is an indication of what improvement can be expected from growth in space by slow diffusion, then a space flight experiment of the growth of $Bi_{12}GeO_{20}$ from a viscous fused solvent will be a step forward in the growth of more perfect crystals for surface wave acoustic devices. Due primarily to its low acoustic velocity (lowest of all crystals currently used for SWA devices) and high coupling factors, bismuth germanate has many potential device applications. Its low velocity allows longer delay times to be achieved in a smaller package. Its high coupling factors mean low insertion loss; thus, high efficiency acoustic delay lines and other signal-processing devices are practical. The elimination of the growth striations would mean larger crystal area for interdigitated electrode delineation. A higher surface quality would improve the yield and feasibility

TABLE 20

EXPERIMENTAL REQUIREMENTS FOR SOLUTION CRYSTAL GROWTH FROM FUSED SOLVENTS IN SPACE

1. $Bi_{12}Ge0_{20}$

Solvent system:	$0.75Bi_2O_3 \cdot 0.5Al_2O_3 \cdot B_2O_3$
Growth composition	80 w/o $Bi_{12}Ge0_{20}$ solute
	20 w/o $0.75Bi_2O_3 \cdot 0.5Al_2O_3 \cdot B_2O_3$
Temperature Range	$795^oC \longrightarrow 767^oC$
Slow cooling rate:	2^o to 0.2^oC/hr.
Seed:	1/10 x 1/10 x 1/2 inch $Bi_{12}Ge0_{20}$, (110) growth direction
	Preheat at 805^o - 810^oC prior to insertion
Weight of Charge:	100 gms
Weight of Growth:	5 gms
Equipment:	Furnace, autotransformer (supplied with stabilized current) and programmed cam regulating system with motor drive. Automatic seed insertion and withdrawal equipment (with platinum wire clamps and support attached to external pressure activated plunger; 50^oC sealable platinum crucibles.
Difficulty:	Attain lowest rate of cool with temperature control. Length of time (6 days) at lowest rate.

2. $Pb_5Ge_3O_{11}$

Solvent system:	$PbO \cdot 0.2Al_2O_3 \cdot 1.8B_2O_3$
Growth composition:	87 w/o $Pb_5Ge_3O_{11}$ 13 w/o $PbO \cdot 0.2Al_2O_3 \cdot 1.8B_2O_3$
Temperature range:	624° $600^{\circ}C$
Slow cooling rate:	2° to $0.2^{\circ}C$/hr.
Seed:	Obtain* high quality, stoichiometric seeds. Preheat 10-15°C above insertion temperature.
Equipment:	Furnace, autotransformer (supplied with stabilized current), and programmed cam regulating system with motor drive. Automatic seed insertion and withdrawal equipment (with platinum wire clamps and support attached to external pressure activated plunger; 50 cc sealable platinum crucible).
Difficulties:	Seed* procurement. Determine minimum, slow rate of cool. Determine length of time. Lead-oxide toxicity (lead oxide reaction with the platinum with reduction of metallic lead has not been observed).

*Seed crystals not commercially available at present time; preparation described pp. 145-152, Final Report, NAS 8-28114, June 1973.

3. $LiNbO_3$ (< 1000°C growth)

Solvent:	$Li_2O \cdot 2SiO_2$
Growth Composition:	40 w/o $LiNbO_3$ - 60 w/o $Li_2O \cdot 2SiO_2$
Temperature Range:	1000°C ——→ 980°C (cool and hold)
Slow Cooling Rate:	10°C** to 0.2°C per minute.
Seed:	$LiNbO_3$
	1/10 x 1/10 x 1/2 inch seed
	Preheat at 10-15°C before insertion
Equipment:	Furnace, autotransformer (supplied with stabilized current) and programmed cam regulating system with motor drive. Automatic seed insertion and withdrawal equipment (with platinum wire clamps and support attached to external pressure activated plunger; 50 cc sealable platinum crucible).
Difficulties:	Determine minimum slow rate. Determine length of time. Growth very slow. Determine ternary $Li_2O \cdot Al_2O_3 \cdot SiO_2$ solvent for higher temperature growth.

** has not been optimized

of high frequency devices since the spacings of the interdigitated electrodes approaches the size of surface defects on earth processed crystals.

It can be inferred from the ground based results with $Bi_{12}GeO_{20}$, that with a chemically-balanced solvent, we should be able to grow more perfect crystals of other surface wave acoustic compositions in space such as lithium niobate. Lithium niobate has the highest coupling constant of known SWA crystals.

D. A Comparison of Bulk Oxide Crystals with Thin Films for Electronic Device Applications

There is a current difference of opinion and rationalization as to where ceramic oxide bulk single crystals and thin film structures fit relative to the production of electronic devices. High volume production of electronic devices makes use of thin film technology because of the ease of producing circuits at low cost. However, for low volume, specialty applications where superior performance is required, such as in surface wave acoustic or electrooptic devices, the ceramic bulk oxide single crystals are used because of their unique inherent properties. These crystals have been researched and produced for many years but, with the exception of quartz, none have received the concentrated effort which has gone into the development of bulk semiconductors. The growing of the oxidic crystals or new oxide compositions which may be identified in the future in the low-g environment of space may be a means to markedly improve the quality to the extent that space processing may become economically viable. In view of this a comparison of the mechanism of the propagation and generation of elastic waves along the surfaces of bulk single crystals and thin films, as well as a comparison of bulk crystals and dielectric thin films for modulation in optical fiber transmission systems is in order.

The leading bulk single crystal materials for surface wave acoustic devices are the piezoelectric bismuth germanate and lithium niobate compositions. Each of these crystals has material parameters which make it

unique under certain conditions. For example, $LiNbO_3$ has the highest electromechanical coupling coefficient and bismuth germanate has the lowest acoustic velocity. Film structures consist of non-piezoelectric substrate materials such as sapphire or spinel which support deposited thin piezoelectric films of polycrystalline zinc oxide or aluminum nitride.

Theoretically it was predicted in 1971 that a thin film of zinc oxide (ZnO) deposited on a substrate such as sapphire would exhibit a relatively large electro-mechanical coupling coefficient for surface acoustic waves.[1] Since that time a number of investigators have been attempting to verify this prediction experimentally. The ZnO films that have been studied have been polycrystalline rather than single crystal; it is assumed in the theory that they are single-crystal. The measured electromechanical coupling coefficient has been typically about one half as large as the theoretical value, and this has been attributed to imperfect orientation of the crystallites in the polycrystalline films. F. S. Hickernell and J. W. Brewer in 1972 suggested that sputtered zinc oxide crystals can be obtained whose quality approaches closely that of single crystal zinc oxide [2]. However, A. J. Baker and co-investigators examined several ZnO films obtained from several different

---

1. L. P. Solie, Appl. Phys. Letters, Vol. 18, pp. 111-112, (February 1971)
2. F. S. Hickernell and J. W. Brewer, Appl. Phys. Letters, Vol. 21, pp. 389-91, (October 1972).

laboratories and found striking differences in film structure and coupling factor for films obtained using different deposition techniques and different sputtering parameters [3].

According to Dr. S. W. Tehon of the General Electric Company Electronics Laboratory, in general there is no evidence at present of any film which will provide the coupling between the electrical and acoustic signals that can be obtained with bulk single crystals. The piezoelectric films for surface wave acoustic devices have generally been polycrystalline, consisting of cyrstallites whose piezoelectric (unique or "c" axis) axes have lined up perpendicular to the substrate during nucleation. Thus the condition for effective coupling wherein the piezoelectric axis is parallel to the direction of wave propagation does not exist. Crystals which have intrinsically high coupling in bulk form generally will not couple with the surface waves in film form, which results in acoustic insertion loss. (Refer to Footnotes 1 and

---

3. A. J. Baker, R. E. Lee, F. S. Hickernell, C. B. Willingham, and T. M. Reeder, pp. 202-205, 1972, Ultrasonics Symposium Proceedings (IEEE Publication Catalog No. 72-CHO 708-854).

Footnote 1: The deposition of epitaxial layers of zinc oxide on single crystal sapphire substrates by chemical vapor transport resulted in ordered deposits of rather poor crystallinity and textured appearance (Appl. Phys. Letters, Vol. 16, pp. 439-441, 1970). Epitaxial layers of zinc oxide were briefly described for electrooptic waveguide deflectors where the c axis was in the plane of the waveguide (Appl. Phys. Letters, Vol. 23, pp. 176-177, 1973). It was not clear if the parallel optic axis corresponds to the piezoelectric axis which is essential for acoustic wave coupling.

Footnote 2: For any one given crystal structure the mechanisms may be quite complex. A simple generalization of the preferred axis of orientation cannot be made to apply to all crystal classes.

According to Dr. Tehon, Dr. N. Foster at Bell Telephone Laboratories minimized the effect by applying a high electric field parallel to the substrate surface during growth. He got the unique or "c" axis to tilt several degrees off perpendicular with the applied field in polycrystalline films, thus obtaining better control of coupling. This experiment, however, was conducted in the days of microacoustic waves when geometries were different from those of surface acoustic wave devices and there was interest in generating shear waves.

It is expected that poor coupling would result also if epitaxial films of bismuth germanate or lithium niobate were deposited unless the films had the required crystallographic-axis orientations. In the case of lithium niobate, the films would be required to have the Y-Z orientation, which gives the highest coupling available in single crystals. While the coupling is not as strong in bismuth germanate, this crystal has the advantage of low acoustic velocity and films would be required to have the X direction as the unique axis. (See Footnote 3). The satisfactory deposition of epitaxial thin films of bismuth germanate has not been reported. Deposits of $Bi_{12}GeO_{20}$ on $Bi_{12}GeO_{20}$, sapphire, spinel, quartz and MgO were polycrystalline; in attempts to vapor grow $Bi_{12}GeO_{20}$ the reaction of the deposit with substrates and reactor parts is observed and remains a major obstacle to growing the material in single crystal

---

Foot note 3: The Y-X orientation is a crystal whose face is perpendicular to the Y-axis. The device is oriented on the face so that the generated wave will travel in the direction of the Z axis in the face (perpendicular to the Y).

forms.[4] The growth of single crystal $LiNbO_3$ films by sputtering or epitaxial-growth-by-melting has been reported for guided optical wave technology; however, insufficiencies have been reported in the quality of the films. These films are reported in the integrated optical circuit discussion.

The high acoustic wave velocity in aluminum nitride and sapphire is the basis for a high surface wave velocity device which means that the metal fingers deposited on the aluminum nitride transducer are farther apart for the same frequency, or permit higher frequency at the same spacing as compared to $LiNbO_3$. With normal photolithography, the range of operation can be extended to 1GHz. (The optical resolution with lithium niobate gives an upper range of 500 MHz due to the lower velocity in the crystal.) The limitation of this device lies in the thin film structure. Because the transducer loss is high, the restriction of lower electromechanical coupling coefficient is introduced. Therefore, according to Dr. Tehon, for low loss we want the strong coupling which we have in bulk $LiNbO_3$ crystal, particularly the Y-Z orientation.

---

(4) V. J. Silvertri, T. O. Sedgwick, and J. B. Laudermann, J. Crystal Growth, 20, pp. 165-168 (1973).

Footnote 3: The Y-Z orientation is a crystal whose face is perpendicular to the Y-axis. The device is oriented on the face so that the generated wave will travel in the direction of the Z axis in the face (perpendicular to the Y).

This means that thin films cannot operate with any reasonable bandwidth in the zero insertion loss region. However, bulk crystals can operate as a band pass filter, or even as a delay line, uniformly over a frequency range. We can have zero transducer loss for a narrow bandwidth up to a moderately wide bandwidth. The maximum percent bandwidth available is proportional to k^2, where k is the coupling constant. $Bi_{12}GeO_{20}$ has low loss at bandwidths up to 10%. In the range of zero insertion loss, as bandwidth increases for different crystals according to k, it becomes widest for $LiNbO_3$. Thin films which display low coupling coefficient can provide zero insertion loss, but only for small bandwidths.

The growing interest in fiber optical communication systems, as well as the prospect of making efficient inexpensive optical devices, have stimulated interest in modulators, deflectors and switches for integrated optics [5]. The method and approach to the modulation of optical signals is highly dependent upon the optical source used. The semiconductor sources - the light-emitting diode (LED), the superluminescent diode (SLD), and the injection laser - can all be directly modulated at high speed by variation of the pumping current. On the other hand, the Nd:YAG laser requires an external modulator.

---

(5) P. K. Tien, Appl. Opt. 10, 2395 (1971).

An external optical modulator can be either the reactive type or absorptive type [6]. They can be either the bulk crystal form in which the optical beam is freely propagating or the waveguide form where the optical beam is confined in a guiding structure as in a thin film. The reactive-type modulator in bulk form has received the most attention, since many materials exist that can be used in this type of modulator. The field-induced interactions upon which the reactive-type modulator depend for their function are the electrooptic the acoustooptic and the magnetooptic effects. The electrooptic effect in high-speed light modulators has been the most widely exploited. Among the many electrooptic materials that have been investigated for modulators, lithium niobate and lithium tantalate emerged as the most practical and useful in the 0.4 to 4 micron wavelength range.

The limited range of optical transparency of present day magnetooptic materials has hampered the application of the magnetooptic effect for light modulators. Only moderate attention has been given to the acoustooptic effect. Very little work has been done on the absorptive-type modulator.

For thin film waveguides, waveguiding layers of $LiNbO_3$ and $LiTaO_3$ produced by out-diffusion techniques or in single crystal form have been reported. The crystallinity and optical quality of the crystal films produced by sputtering or epitaxial growth by melting are not sufficiently good for

---

(6) S. E. Miller, T. Li, and E. A. J. Marcatile, Proc. of the IEEE, 61, pp. 1703-1751 (1973).

active devices [7, 8]. The out-diffusion technique appears to be more attractive for producing $LiNbO_3$ and $LiTaO_3$ optical waveguides of high quality since the crystallinity of the guiding layer is scarcely influenced during the diffusion process [9]. Both techniques require high quality bulk crystals of $LiTaO_3$ or $LiNbO_3$ as substrates.

Thin amorphous dielectric films can also guide. Films of $BaSiO_3$ and Ta_2O_5 have been investigated [10, 11] Recent work was reported on several amorphous films, including amorphous $LiNbO_3$; a definite trend that would enable prediction of useful waveguiding compounds was not found.

The argument for single crystal films versus bulk crystals also enters into whether or not optical storage of digital data can make an impact at the high capacity end of computer storage [13]. Major breakthroughs will be required in all subsystems of optical storage including storage media, deflectors, sensors, etc. Bulk crystals of Fe-doped $LiNbO_3$ [14] and strontium barium niobate ($Sr_{0.75}Ba_{0.25}Nb_1O_6$) [15] are leading contenders for holographic storage in the form of thick phase-volume holograms in crystals

---

(7) S. Fukunishi, N. Uchida, S. Miyazawa, and J. Noda, Appl. Phys. Lett. 24, p. 924 (1974).

(8) J. Noda, N. Uchida, and T. Saku, Appl. Phys. Lett., 25, p. 131 (1974).

(9) I. P. Kaminow and J. R. Carruthers, Appl. Phys. Lett., 22, p. 326 (1973).

(10) J. E. Goell, Appl. Opt. 12, p. 737 (1973).

(11) D. H. Hensler, J.D. Cuthbert, R.J. Martin, and P. K. Tien, Appl. Opt., 10, p. 1037 (1971).

(12) R. H. Deitch, E. J. West, T. G. Giallorenzi and J. F. Weller, Appl. Opt., 13, p. 712 (1974).

(13) E. S. Barrekette, Appl. Opt., 13, p. 799 (1974).

(14) D. L. Staebler and W. Phillips, Appl. Opt., 13, p. 788 (1974).

(15) J. B. Thaxter and M. Kestigian, Appl. Opts., 13, p. 913 (1974).

via the optical damage effect.

The competing technology of magnetic bubbles utilize single crystal garnet films deposited from solution on other garnet crystals by liquid phase epitaxy.[16] However, the amorphous rare earth-transition metal alloys show potential as a class of bubble domain materials [17] that require considerable less preparation than conventional single crystal garnets when deposited as thin films by sputtering or evaporation [13]. Use of these materials may lead to lower per bit prices of magnetic bubble memories.

In summary, for low volume, specialty applications such as surface wave acoustic devices the superior intrinsic properties of $LiNbO_3$ and $Bi_{12}GeO_{20}$ call for the use of bulk crystals rather than polycrystalline films. Effective coupling of the acoustic and electrical signals has not been attained in film structures wherein the surface wave is propagated parallel to the surface of the substrate while the piezoelectric axis of the film is perpendicular to the substrate. Reported epitaxial deposits of $Bi_{12}GeO_{20}$ have been polycrystalline.

Interest in optical waveguiding layers for fiber optical communication systems has stimulated the growth of thin single crystal $LiNbO_3$ films on bulk $LiTaO_3$ or $LiNbO_3$ bulk crystals by sputtering or epitaxial growth. Much

---

(16) H. J. Levinstein, J. W. Nelson, and L. J. Varnerin, Bell Lab. Record, 51, p. 208 (1973).

(17) P. Chauddari, J. J. Cuomo, and R. J. Gambin, IBM & Res. Devel., 17, p. 66 (1973).

improvement is required in the quality and crystallinity of the films before they will surpass the reactive-type $LiNbO_3$ modulator in bulk crystal form. It has been pointed out that out-diffusion techniques rather than single crystal film growth results in much improvement in the quality of $LiNbO_3$ optical waveguides since the crystallinity of waveguide layer is scarcely influenced during the diffusion process.

Thus, surface wave acoustic devices and optical waveguides, as well as external modulators, will call for bulk crystals as substrates. However, the properties of these crystals should be markedly further improved over the present state-of-the-art if effective devices are to be produced. To this end, it appears that space grown piezoelectric and electrooptic crystals offer significant promise of meeting these demands.

E. Aqueous Solution Growth

During the past two years, triglycine sulfate was studied within the hardware confinements expected in an Apollo or Skylab mission. The requirements for a space flight experiment by slow cooling are detailed in Table 21. Growth by isothermal evaporation in space does not appear to be practical unless specially designed equipment is built. The details and difficulties are also outlined in Table 21.

TABLE 21

EXPERIMENTAL REQUIREMENTS FOR CRYSTAL GROWTH

FROM AQUEOUS SOLUTIONS IN SPACE

1. Triglycine Sulfate (slow cool)

Solvent:	Demineralized water
Solution: *	Saturated solutions of multiple recrystallized triglycine sulfate crystals at 40°C (40-42 gms TGS/100 cc H_2O) should yield growth of 15 gms per 100 cc H_2O at 25°C.
Equipment:	An insulated aluminum box (5 x 10 x 10 cm) having a window in the front face to view crystal growth. Transparent growth cell with a capacity of 50 ml of aqueous solution. Typically a cell would be 7 cm x 3 cm x 2.5 cm deep. Side-view mirror 7 cm x 2.5 cm. Time, temperature, and power indicators. Heater built into base or rear wall of growth cell. Programmable temperature regulating system. Hasselblad camera. A special tripod about one foot long will be provided which mounts to the box and contains two Hasselblad lens extension tubes to which the lens and camera body attach. Lighting required. Moire pattern grid (5 lines/min.)
Time/ Temperature Schedule:	(1) Heat solution to 50°C and allow time for solution of solute; (2) cool at about 0.2°C/hr. during nucleation and the first few hours (e.g. 4) of growth; (3) cooling rate of 0.5°C for 10-15 hours; and (4) final cool (unpowered) to ambient.

Seed: One or more stainless steel pins at the center of the cell provide nucleation sites. The pin is cooled by attaching it to a 1/8 inch diameter aluminum or copper rod which extends out of the heated growth cell into the cooler atmosphere.

Power Requirements: Approximately 8 watts heater power.

Difficulties: Handling procedure required for removal of crystals from the growth solution and packing.

Acidic nature of the solution.

Controlled conditions important to seed crystals; avoid redissolution and spurious nucleation.

*Solution preparation will be ground-based work. Commercial triglycine sulfate crystals, such as were used for the preparation of the solutions for growth by slow cooling, can be purchased or TGS crystals can be prepared as follows. Solutions of glycine in water and sulfuric acid in water are prepared with volumes corresponding to the 3:1 stoichiometric ratio. Typically the sulfuric acid solution is about 50% by weight H_2SO_4 in H_2O. The sulfuric acid is poured into a hot solution of glycine and the mixture stirred and allowed to cool. Crystals of TGS precipitate out on cooling. These can be filtered off, redissolved in ultrapure water, and again recrystallized. Usually two or three recrystallizations are carried out to obtain a material of suitable purity. (Discussed in detail on pp. 68-70 of the Final Report for the first year of effort).

2. Triglycine Sulfate (Slow Isothermal Evaporation)

Solvent: Demineralized water

Solution:* Saturated solutions of multiple recrystallized triglycine sulfate crystals at 35°C (34-35 gms TGS/100 cc H_2O)

Equipment: A closed evaporation system would allow growth temperatures to be kept above the ferroelectric Curie temperature. This temperature regime results in too rapid evaporation rates with the open system.

Temperature controller to control to within $\pm$ .01°C

Seed insertion apparatus.

Temperature: 30°C (to keep growth rates from being excessive unless a closed system is used).

Time: Up to 4 weeks.

Seeds: TGS crystals attached to thin nylon rods, and suspended in the solution. The rods are attached to external, pressure-activated plungers, for controlled insertion and withdrawal of the seeds.

Difficulties: Required time period of growth.

Capacity of closed system for large solution content (up to 400 cc).

Temperature and evaporation control.

Acidic nature of solution.

Procedure for removal of crystals from growth solution and packing.

*Ground-based saturated solutions are prepared at 35°C. The warm solutions are gravity-filtered into a clean, dry beaker using fine mesh filter paper. After filtering, the solutions are cooled to 32°C, covered with a clean watch glass to prevent evaporation, and placed securely in a water bath controlled at 30°C to a few tenths of a degree centigrade. Typically the solutions are placed in 400 cc "no lip" beakers which are placed in 20 liter glass vats filled with water. The solutions should reach equilibrium after 24 to 36 hours.